N° Ordre...../FT/UMBB/2024

PEOPLE'S DEMOCRATIC REPUBLIC OF ALGERIA

MINISTRY OF HIGHER EDUCATION AND SCIENTIFIC RESEARCH

UNIVERSITY M'HAMED BOUGARA OF BOUMERDES

Faculty of Technology

Doctoral Thesis

Presented by:

Fatima BENNIA

Submitted for the Fulfilment of the Requirements of the **DOCTORAT-LMD** degree in

Field: Electronics

Specialty: Instrumentation

Contribution to improving the efficiency of a wireless power transfer system using artificial intelligence techniques

Jury members:

Mohammed	AMMAR	Professor	Univ. Boumerdes	President
Aimad	BOUDOUDA	MCA	Univ. Boumerdes	Supervisor
Fares	NAFA	MCA	Univ. Jijel	Co-supervisor
Hamza	AKROUM	MCA	Univ. Boumerdes	Examiner
Noureddine	MESSAOUDI	Professor	Univ. Boumerdes	Examiner
Ahcene	BOUZIDA	Professor	Univ. Bouira	Examiner

Academic Year : 2024/2025

بسم الله الرحمن الرحيم

{ يَرْفَعِ اللَّهُ الَّذِينَ آمَنُوا مِنكُمْ وَالَّذِينَ أُوتُوا الْعِلْمَ دَرَجَاتٍ }

سورة المجادلة – الآية11

اللهم إني أحمدك وأشكرك على نعمة العلم، وأستعين بك على أن أستخدمه فيما يرضيك وينفع الناس

ACKNOWLEDGEMENTS

First and foremost, I would like to thank my supervisor, Dr. BOUDOUDA Aimad, for his constant support, availability, invaluable advice, and real human qualities. I also extend my gratitude to Dr. NAFA Fares for co-directing this work.

My sincere thanks go to Pr. LEONARDO Sandrolini, and Dr. MATTIA Simonazzi from Bologna University, Department of Electrical, Electronic, and Information Engineering 'Guglielmo Marconi', Italy, for accommodating me in their Laboratory (Laboratorio di Compatibilit à Electromagnetic (LACEM)). I am deeply grateful to Mr. Paolo Guglielmi, Professor at the Polytechnic University of Turin, for his warm welcome and sound advice during my stay in Italy.

I would also like to thank Dr. AIBACHE Abderrezak, Pr. MERAIHI Yassine and all the members of the Telecommunication Systems Laboratory, Electronics Department at the Institute of Electrical and Electronic Engineering, UMBB, especially Pr. CHALLAL Mouloud and Dr. DEHMAS Mokrane for their assistance.

I extend my gratitude to the jury members, particularly Pr. AMMAR Mohammed, who served as President, and Professors MESSAOUDI Noureddine, BOUZIDA Ahcene, and Dr AKROUM Hamza for accepting to review my thesis and providing valuable feedback.

I wish to express my sincere gratitude to my colleagues at the University of Boumerdes for their invaluable support and guidance throughout my research journey.

I would like to thank my father, HARIR Amar, and my biological parents, BENNIA Akli and HARIR Sadia, may their souls rest in peace, and my second mother, LOUNI Dahbia, for their countless efforts and continuous encouragement throughout my academic career and life.

My heartfelt thanks go to my brothers Mohamed, Hamid, Hamza, Ali , Ilyas, Rabah, Billal and my sisters Nadjia, Faroudja and Noura. Special thanks to my sisters-in law Ouardia, Nawel, Zakia, Doha, Sandra, and my brothers-in law Lounes, Hamid, and Nabil. And aunt B. Malika. And uncle H. Menouar , H. Kader, B. Amar, and their wife.

I am also grateful to Mr. KECIBA Mohamed, a biomedical instrumentation engineer, for his help and support throughout this thesis work.

Finally, I thank my friends MOUSSAOUI Siham, FARES Belynda, AZZOUGUI Safia, LATERI Hibatallah, and MOUSSAOUI Soraya for their daily support.

ملخص

تقنية نقل لاسلكي للطاقة (WPT) هي طريقة ثورية لتشغيل الأجهزة بدون أسلاك مادية، وقد تم إقتراحها في هذه الأطروحة لتوفير الطاقة للأجهزة القابلة للزرع الحيوي. تتمثل قيود التصميم الرئيسية في تحقيق أقصى قدر من كفاءة النقل مع الحفاظ على صغر حجم الغرسة بما يكفي لتكون مناسبة لجسم الشخص الحي. ويُعد نقل لاسلكي للطاقة بالاقتران الرنيني المغناطيسي (MRCWPT)، الذي يستخدم أزواجاً من ملفات الحث في الدوائر الخارجية ودوائر الزرع، طريقة تم بحثها بنشاط لهذا النوع من نقل الطاقة.

وعليه فإن الهدف من هذه الأطروحة هو تصميم وتحسين ملف استقبال WPT عالي الكفاءة لنقل الطاقة المغناطيسية للتطبيقات الطبية الحيوية. تقليديًا، غالبًا ما يستغرق تحسين أنظمة WPT استنادًا إلى المعادلات الرياضية أو النماذج العددية وقتًا طويلاً وقد لا ينتج عنه تصميمات مثالية. ولمعالجة هذه القيود، تقدم هذه الأطروحة نهجًا جديدًا يدمج نموذج التعلم الآلي مع الأساليب الإرشاد الذاتي للتصميم والتحسين.

ويتمثل الهدف الأساسي في زيادة كفاءة النقل إلى أقصى حد لملف قابل للزرع بأبعاد 20 مم ومسافة نقل تبلغ 30 مم، يعمل بتردد 13.56 ميجاهرتز. ولتحقيق هذا الهدف، تم تحديد أولاً المعلمات الهندسية للملف التي تؤثر بشكل كبير على كفاءة نظام نقل لاسلكي للطاقة للزرع. ثم تم إنشاء شبكة عصبية اصطناعية قائمة على نموذج (ANN) وتدريبها على مجموعة بيانات شاملة تم إنشاؤها من خلال محاكاة طريقة العناصر المحدودة (FEM). يتنبأ هذا النموذج بالكفاءة بناءً على معلمات الملف الهندسي، مما يلغي الحاجة إلى حسابات معقدة. وفي وقت لاحق، تم استخدام خوارزميتي الإرشاد الذاتي للمجال :الخوارزمية الجينية (GA) وخوارزمية التحسين الذئبي (COA)، للعثور على المعلمات المثلى التي تزيد من الكفاءة.

يُظهر نموذج الشبكة العصبية الاصطناعية المقترح دقة استثنائية تتجاوز 97%. علاوةً على ذلك، يعزز نهج تصميم ملف WPT كفاءة النقل بنسبة تصل إلى 76% مع تخفيض زمن المعالجة بشكل كبير مقارنةً بالطرق التقليدية.

الكلمات الرئيسية: *نقل لاسلكي للطاقة؛ اقتران الرنين المغنطيسي ؛ تصميم الملف؛ الشبكات العصبية؛ خوارزميات* الإرشاد الذاتي ؛ *الزرع الطبي الحيوي.*

Abstract

Wireless Power Transfer (WPT) technology is an innovative method for powering devices without physical wires, which has been used here to provide power to bioimplantable devices. The main design constraints are to achieve maximum transfer efficiency while keeping the implant size small enough to be suitable for the living subject's body. Magnetic Resonant Coupling Wireless Power Transfer (MRCWPT), which uses pairs of inductor coils in the external and implant circuits, is a method actively researched for this type of power transmission.

The objective of this thesis is to design and optimize a high-efficiency WPT receiving coil for biomedical applications. Traditionally, optimizing WPT systems based on mathematical equations or numerical models is often time-consuming and may not yield optimal designs. To address these limitations, this thesis introduces a novel approach that integrates a machine-learning model with metaheuristic methods for design and optimization.

The primary goal is to maximize the transfer efficiency for an implantable coil with dimensions of 20 mm and a transfer distance of 30 mm, operating at a frequency of 13.56 MHz. To achieve this goal, we firstly identified the critical geometric coil parameters that significantly influence the WPT system's efficiency. A model-based Artificial Neural Network (ANN) was then constructed and trained on a comprehensive dataset generated through Finite Element Method (FEM) simulations. This model predicts efficiency based on geometric coil parameters, eliminating the need for complex calculations. Subsequently, two metaheuristic algorithms: the Genetic Algorithm (GA) and the Coyote Optimization Algorithm (COA), were employed to find the optimal parameters that maximize efficiency.

The proposed ANN model demonstrates exceptional accuracy, exceeding 97%. Furthermore, this WPT coil design approach significantly enhances transfer efficiency by up to 76% while drastically reducing computation time compared to conventional methods.

Keywords: *wireless power transfer; magnetic resonant coupling; coil design; neural networks; metaheuristic algorithms; biomedical implants.*

Résumé

La technologie de transfert d'énergie sans fil (WPT) est une méthode innovante pour alimenter des appareils sans fils, utilisée pour fournir de l'énergie à des dispositifs bio-implantables. Cependant, la contrainte majeure pour de telles techniques est de maximiser l'efficacité du transfert tout en gardant la taille de l'implant suffisamment petite pour être adaptée au corps du sujet vivant. En effet, le transfert d'énergie sans fil par couplage résonant magnétique (MRCWPT), qui utilise des paires de bobines inductrices dans les circuits externes et implantables, est une méthode activement recherchée pour ce type de transmission d'énergie.

Ainsi, l'objectif de cette thèse est de concevoir et d'optimiser une bobine réceptrice WPT à haute efficacité pour des applications biomédicales. Traditionnellement, l'optimisation des systèmes WPT basée sur des équations mathématiques ou des modèles numériques est souvent lente et peut ne pas produire des conceptions optimales. Pour surmonter ces limitations, cette thèse propose une approche novatrice intégrant un modèle d'apprentissage automatique avec des méthodes métaheuristiques pour la conception et l'optimisation.

Le but principal est de maximiser l'efficacité du transfert pour une bobine implantable de dimensions 20 mm et une distance de transfert de 30 mm, opérant à une fréquence de 13,56 MHz. Pour atteindre cet objectif, nous avons d'abord identifié les paramètres géométriques critiques des bobines qui influencent de manière significative l'efficacité du système WPT. Un modèle basé sur le réseau de neurones artificiels (ANN) est ensuite construit et entraîné sur un ensemble de données généré par des simulations utilisant la méthode des éléments finis (FEM). Ce modèle ainsi conçu, permet la prédication de l'efficacité en fonction des paramètres géométriques des bobines, et évite tout besoin de calculs complexes. Ensuite, deux algorithmes métaheuristiques: l'algorithme génétique (GA) et l'algorithme d'optimisation par coyote (COA), ont été impliqués pour trouver les paramètres optimaux maximisant l'efficacité.

Les résultats obtenu à base de ce modèle ANN, démontre une précision exceptionnelle, dépassant 97%. De plus, cette approche de conception de bobine WPT améliore considérablement l'efficacité du transfert pour atteindre une valeur de 76% tout en réduisant drastiquement le temps de calcul par rapport aux méthodes conventionnelles.

Mots clés : *Transfert de puissance sans fil; couplage par résonance magnétique; conception de bobines; réseaux neuronaux; algorithmes méta-heuristiques; implants biomédicaux*

TABLE OF CONTENTS

LIST OF FIGURES

Chapter 2 An overview of wireless power transfer

Chapter 3 Modeling of a resonant inductive wireless power transfer

Chapter 4 Coil design for high efficiency wireless power transfer

Chapter 5 Optimization of wireless power transfer using artificial intelligence

LIST OF TABLES

ABBREVIATIONS

AC	Alternating Current
AI	Artificial Intelligence
AMD	Age-Related Macular Degeneration
ANN	Artificial Neural Network
CNNs	Convolutional Neural Network
COA	Coyote Optimization Algorithm
CPT	Capacitive Power Transfer System
DC	Direct Current
EMP	Electromagnetic Pulse
ESCS	Spinal Cord Stimulation
EVs	Powering Electric Vehicles
FEM	The Use Of Finite Element Method
FNN	Feed-Forward Neural Network
GA	Genetic Algorithm
GPUs	Highly Parallelized Graphics Processing Units
HILPBs	High-Intensity Laser Power Beam Systems
IMDs	Implantable Medical Devices
IoT	Internet Of Things
IPT	Inductive Power Transfer System.
IP	Iterative Procedure
LED	Light Emitting Diode
LPT	Laser Power Transfer
ML	Machine Learning
MLP	The Multilayer Perceptron
MPT	Microwave Power Transfer
MR-WPT	Magnetic Resonance Wireless Power Transfer
MSE	Mean Squared Error
NSGA-II	No-Dominated Sorting Genetic Algorithm II
PMA	Power Matters Alliance
PP	Parallel-Parallel Topologies.
PPMs	Implanted Permanent Pacemakers
PS	Parallel-Series Topologies.
PSO	Particle Swarm Optimization
PTE	Power Transfer Efficiency
RP	Retinitis Pigmentosa
Rx	Receviver Coil
SML	Supervised Machine Learning
SP	The Series-Parallel
SP	Series-Parallel Topologies.
SS	Series-Series Topologies.
SVM	Support Vector Machines
Tx	Transmitter Coil
UAVs	Unmanned Aerial Vehicles
USML	Unsupervised Machine Learning
WPC	Wireless Power Consortium
A4WP	Alliance for Wireless Power
WPT	Wireless Power Transfer

SYMBOLS

μ	The permeability constant
μ_r	The relative permeability
ρ_c	The resistivity of the conductor
η_1	The efficiency of primary side
η_2	The efficiency of the secondary side
η	The power transfer efficiency
δ	The depth of skin
δ1	The alpha impact
δ2	The group effect
ω	The group that adjusts least to the environment than young ones
φ	The group of coyote that adjusts less to the group size
θ	The constant that varies with the shape of the coil and is empirically
C_{T1}	The resonance capacitor transmitting coil
C_{T2}	The resonance capacitor receiving coil
D	The task dimension
din_T	The inner diameter of primary coil
din_R	The inner diameter of secondary coil
$dout_T$	The outer diameter of primary coil
$dout_R$	The outer diameter of secondary coil
d_{TR}	The transfer distance
$E(\gamma)$	The elliptic integrals of the second order
f	The operating frequency
f_0	The fixed frequency
I_1	The currents flowing in the transmitting coils
I_2	The currents flowing in the receiving coils
K	The coupling coefficient
$k(\gamma)$	The elliptic integrals of the first order
lb	The lower bound
lc	The length of the conductor
L_1	The inductances of the transmitting coils
L_2	The inductances of receiving coil
m	The number of examples in the data
M_{12}	The mutual inductance between the two coils
N	The number of features
N_T	The number of turns of primary coil
N_R	The number of turns of secondary coil
N_{pop}	The number of Population
N_{it}	The number of iterations
N_{var}	The number of variables
p_{sc}	The probabilities of scattering
p_{ac}	The probabilities of association,
Q_T,	The uality factors of the primary
Q_R	The uality factors of the secondary coils
Qi standard	The global standard for wireless charging
r_j	The random variable taking values between 0 and 1
R^2	The coefficient of determination
R_1	The resistances the transmitting coils
R_2	The resistances the transmitting coils
R_L	The equivalent AC load resistance
R_{dc}	The represents the DC resistance

S_T	The spacing between the turns of primary coil
S_R	The spacing between the turns of secondary coil
t_c	The thickness of the conductor
ub	The upper bound
V_1	The sinusoidal voltage
W_T	The width of conductor of primary coil
W_R	The width of conductor of secondary coil
X	The features of data
Y	The target variable of data
Z_1	The equivalent impedance on the transmitter side
Z_2	The equivalent impedance on the receiver side
Z_T	The total impedance
Z_R	The reflected impedance at the transmitter side

Introduction

Chapter 1

1.1. Background and motivation

In today's world, technology is crucial to comfort and lifestyle. We rely on sophisticated electronic devices, such as implanted medical devices, electric cars, drones, and smart phones. These devices require a stable and reliable power source. Traditionally, these devices are powered through wired connections or built-in batteries. However, using wires limits mobility and flexibility, while built-in batteries have a limited lifespan and require periodic replacements, leading to financial burdens, patient surgeries, and potential mission failures. Fortunately, WPT technology offers a more convenient and reliable solution to these challenges. By eliminating cables and batteries, wireless power transfer (WPT) reduces associated problems and provides seamless charging for electronic devices.

This thesis proposes a new approach based on artificial intelligence to optimize the power transfer efficiency (PTE) to increase power transfer while also reducing latency and cost in the manufacturing process.

In inductively coupled WPT systems, the power transfer efficiency depends on factors such as the coil quality factor (Q) and coupling coefficient (K) [1]. These factors are directly related to the power transfer efficiency and are fundamentally connected to the geometric characteristics of the coils. The geometric characteristics of the coils are among the most important criteria for determining efficiency. Therefore, optimizing the geometric parameters of the coils is crucial for achieving higher efficiency [2]. Additionally, the choice of frequency, such as 6.78 MHz or 13.56 MHz, affects system advantages like size, weight, and long-distance transmission capabilities [3]. When dealing with frequencies in the MHz

range, accurately representing the coils using mathematical expressions for lumped elements becomes challenging due to factors such as proximity, skin effects, and other hidden sources

of loss, including resistance (R), self-inductance (L), mutual inductance (M), and capacitance (C), which determine the quality factor Q and coupling coefficient K of the coils [4].

The use of finite element method (FEM) solvers, namely Ansys Maxwell and COMSOL, has emerged as a promising approach for optimizing coil design in high-frequency scenarios. This method facilitates a more precise and realistic calculation of the parameters associated with the system. . However, the design optimization process based on FEM simulations requires a substantial amount of time to calculate the parameters and determine the best design [5]. To address this issue, machine learning has recently emerged as a promising approach for designing and optimizing electromagnetic devices. With machine learning models, the design process can be accelerated significantly. Recently, there is a growing interest in utilizing machine learning to design WPT systems [6].

[7] Published the first comprehensive research paper on artificial neural networks (ANNs) for optimizing (WPT) systems. Their review covers a wide range of aspects related to WPT optimization, including system design, coil design, and power control. The authors thoroughly examined various techniques, providing a comparative analysis while addressing the challenges and constraints associated with employing ANN methodologies in this field. Initially, machine learning techniques were used to predict parameters and performance metrics, such as the quality factor and coupling coefficient, for coil design in WPT systems [4, 8-11]. [4, 8, 9] characterized the quality factor in spiral coil designs for high-frequency WPT systems using machine learning. The proposed approach used a feed-forward neural network (FNN) to predict the quality factor, which is a critical parameter in coil design optimization for WPT systems. The proposed approach achieved an impressive accuracy exceeding 98%, and the coil design method notably reduced the computation time, resulting in decreased analysis complexity. Moreover, the authors recently presented a cutting-edge design method based on machine learning for spiral coils in WPT systems operating at high frequencies. This innovative method offers superior performance, with significant computational time savings [8].

A novel approach has recently emerged to farther expedite the design process, explore the design space more efficiently, and reduce the computation time. This approach combines machine learning techniques with metaheuristic methods [3, 12-14]. [12] Proposed a computational approach for WPT link design optimization that considers electromagnetic compatibility. They used a neural network-based genetic algorithm to minimize the field

signature around each design while maintaining high efficiency. This process significantly reduced the computational time by nearly 90%. Another notable work is by [3], who proposed a fused helical-spiral coil design using combined neural networks and genetic algorithms. The proposed approach used a neural network to predict the initial coil structure, and a genetic algorithm was applied to optimize the design for maximum power transfer efficiency. This method reduced the computational time by more than 90%. [13] Proposed a fast design optimization method for dynamic inductive power transfer systems. The proposed approach combines an ANN and a GA to optimize the system design. The results show that the proposed approach significantly improves system efficiency compared to conventional methods. In their study, [14] proposed an optimal design approach for a tram wireless power charging system using a machine learning regression model associated with the No dominated Sorting Genetic Algorithm II (NSGA-II). The proposed approach achieved high efficiency in terms of the coupling coefficient and coil shape.

Most of the papers above focused on predicting the coupling coefficient and quality factor to calculate the efficiency, extending the design process's time. This thesis proposes a new design optimization approach for WPT systems by leveraging the power of machine learning (ML) and metaheuristic methods. Instead of first calculating the coupling coefficient and quality factor to estimate the efficiency, we predict the efficiency of the WPT system directly, and then we use metaheuristic algorithms to find the optimal coil parameters to maximize the transfer efficiency.

1.2. Thesis objective and approach

As mentioned in the previous section, improving the transfer efficiency is one of the major technical challenges in WPT. Therefore, this research proposes a new design optimization approach based on machine learning (ML) combined with metaheuristic methods. The approach involves developing and training a machine learning model using artificial neural networks (ANNs) to predict WPT efficiency based on geometric coil parameters. Additionally, metaheuristic algorithms, such as the genetic algorithm (GA) and coyote optimization algorithm (COA), are employed to identify optimal parameters and achieve maximum efficiency. Compared with classical methods the new approach aims to enhance power transfer efficiency and reduce computation time. This research covers the scope of emerging WPT technology which is applied to medical implants or other implementations where there are

constraints on the receiving coil. Specifically, the, following issues will be discussed in this thesis:

- ❖ We intend to establish a step-by-step design process for modeling the coils essential to the power transfer system. This process aims to automate the design of a WPT system based on predefined design constraints and application requirements.

- ❖ Our research will conduct an in-depth analytical investigation of the parameters of WPT coils and their impact on efficiency. This analysis aims to optimize the physical specifications of the coils to maximize the power transfer efficiency. We will validate our findings through simulations using finite element methods (FEMs).

- ❖ We utilize a parametric model generated through the finite element method (FEM) to calculate efficiency as design parameters vary. By collecting a substantial dataset of 33,210 designs, we support machine learning techniques for accurate predictions of the WPT system's efficiency. This approach eliminates the need for complex mathematical equations and significantly reduces computational time during the optimization process.

1.3. Contributions

The main contributions of this thesis are summarized as follows:

- Direct efficiency prediction: The proposed approach based on machine learning can predict WPT system efficiency directly, eliminating the need to predict the coupling coefficient and quality factor. This eliminates the need for complex mathematical equations and reduces the computation time for the design and optimization of the WPT system.
- Exploration of medical applications: The proposed approach explores, for the first time, the design challenges of WPT systems for medical applications, particularly for powering implantable medical devices.
- Innovative optimization algorithm: For the first time, we introduce the use of the coyote optimization algorithm to determine the optimal geometric parameters of a WPT system.

1.4. Thesis Outline

The thesis is organized into five chapters, as follows:

Chapter 1: Introduces the background, motivation, and objectives of the research and the contribution of the thesis.

Chapter 2: An overview of wireless power transfer

We Introduce WPT fundamentals and discuss WPT methods. A range of WPT applications is briefly explained, with particular attention given to WPT for biomedical implants, and the literature concerning WPT systems in this area is reviewed.

Chapter 3: Modeling of a resonant inductive wireless power transfer

The operating principle of inductively coupled WPT systems is discussed, and a detailed theoretical framework for analytical modeling of WPT systems is provided. Then, a thorough analysis is conducted to identify the key geometrical parameters influencing the WPT efficiency. Other performance metrics such as the quality factor and coupling coefficient are also explained in this chapter.

Chapter 4: Coil design and optimization for high efficiency wireless power transfer

This chapter presents the optimization of the geometric parameters of circular spiral coils with a planar shape, designed for a series-parallel (SP) inductive coupling WPT system specifically for biomedical applications. To achieve this, we propose two approaches. First, an analytical approach implementing either iterative or metaheuristic optimization methods is proposed. Second, a numerical approach called the GA-FEM is used. The GA-FEM integrates the finite element method with a genetic algorithm, allowing accurate WPT efficiency calculations via coil design.

Chapter 5: Artificial intelligence based optimization techniques for WPT systems

This chapter presents a novel approach for optimizing resonant inductively coupled spiral coils to maximize the transfer efficiency of WPT system. First, we train an artificial neural network (ANN) model to accurately predict the efficiency of a WPT system based on its geometric parameters, using a big dataset generated through 3D finite element method (FEM) simulations. Second, we combine the trained ANN model with metaheuristic algorithms (GA and COA) to efficiently determine the optimal coil design that maximizes the transfer efficiency.

Chapter 6: Conclusion and future work

In this chapter, the thesis aims and outcomes are summarized. We also cite future works to advance WPT technology and our publications resulting from this research.

An overview of wireless power transfer

Chapter 2

2.1. Introduction

Wireless power transfer (WPT) has gained significant attention due to its potential applications in various fields, such as electric vehicles, biomedical implants, and consumer electronics. This chapter provides an overview of the basics and methods of WPT and explores its applications in different domains. Additionally, we review previous studies on WPT in implanted biomedical devices.

2.2. History of wireless power transfer

Based on the literature reviewed [15-24], the history of wireless power transfer can be broadly divided into three distinct eras. The initial era commenced with H.C. Rsted's discovery that an electric current flowing through a metallic conductor produces a magnetic field surrounding it. James Clerk Maxwell demonstrated how electric and magnetic fields are created, laying the foundation for the principles of electromagnetism. Subsequently, in 1888, H.R. Hertz constructed a setup using induction coils linked to an alternating current generator, which enabled the transmission of electricity to a receiving coil over a short distance, thereby proving the existence of electromagnetic waves.

The era in question was significantly shaped by the endeavors of Nikola Tesla, particularly in his pioneering work with WPT for practical use. In 1896, Tesla took a monumental stride in transferring energy across vast distances, culminating in the wireless transmission of a radio-frequency signal over a remarkable distance of approximately 50 km.

By 1899, he furthered his experiments by wirelessly transferring an exceptionally high voltage, which proved powerful enough to supply electrical energy to 200 light bulbs and drive an

electric motor more than 40 kilometers away. Despite the major achievements of his experiments, the high voltage involved resulted in the creation of electric arcs that posed a significant risk to those nearby. Among Tesla's most prominent visions was the construction of the Wardenclyffe Tower, referred to in Figure 2.1, with the ambitious goal of wirelessly conveying power through the ionosphere. However, the technological and fiscal constraints of the time ultimately hindered the practical realization of Tesla's concepts.

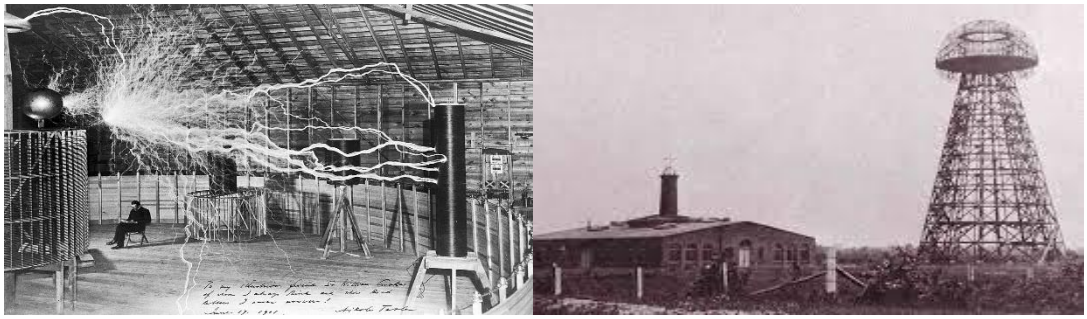

(a) (b)

Figure 2.1: Illustrations of the main wireless energy transfer systems: a) Nikola Tesla in his Colorado Laboratory, b) Wardenclyffe.

The third era of WPT development began following World War II when dedicated researchers managed to generate considerable quantities of power at microwave frequencies using parabolic reflectors. This era saw the application of WPT in various fields. In 1961, John Schuder proposed the concept of a transcutaneous energy transfer system. William C. Brown reached an important landmark in 1964 by wirelessly transmitting power to an aircraft Figure 2.2. The year 1969 marked the start of WPT technology utilizing magnetic induction. The 1980s experienced a significant proliferation of magnetic induction WPT systems in domestic appliances, altering our conventional use of electricity. In the latter part of the 1990s, SONY led the way with the innovation of the 'FeliCa' wireless integrated circuit card.

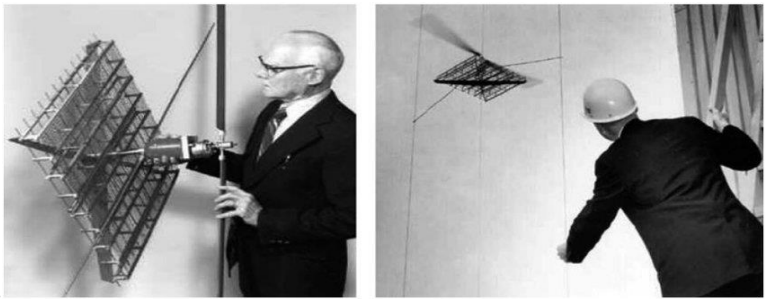

Figure 2.2: W. C. Brown's microwave-powered airplane.

Notable progress occurred when a group of researchers at MIT (Figure 2.3) discovered resonant coupling in WPT in 2006, laying the groundwork for new technological prospects. By 2007, this team had achieved the milestone of successfully transmitting power over long distances.

Figure 2.3: MIT team experimentally demonstrating WPT.

Research is currently being conducted to refine systems for transmitting and receiving power through magnetic induction, which is emerging as a particularly auspicious field. To facilitate widespread interoperability, consortia have been established to standardize these technologies and ensure their compatibility across various devices, laying a foundation for the seamless integration of future WPT. The movement towards standardization began with the inception of the Qi standard, introduced by the Wireless Power Consortium (WPC) in 2009 [25], complemented by the development of the Rezence standard by the Alliance for Wireless Power (A4WP), and the Power Matters Alliance (PMA) standard, which predominantly adhered to North America, and was slated for unification in 2015 [26]. The industry consensus is leaning towards the idea that it is far more advantageous for manufacturers to produce mutually compatible systems, rather than continuing to develop and market proprietary technologies that are limited in their scale and reach. This strategy is expected to not only enhance consumer accessibility but also drive progress within the industry itself.

2.3. Wireless power transfer technologies

Generally, the WPT concept presented in Figure 2.4 is based on transmitting electrical energy from a power source to a receiving device “receiver” for charging batteries without needing

tangible connections such as wires or cables. Despite the straightforward nature of its description, WPT is a sophisticated process that consists of three main steps [27]:

- AC or DC electrical power is provided to a high-frequency converter. The role of this converter is to transform the initial electrical input into a much higher frequency output and then feed it to the transmitting apparatus.
- Subsequently, the electromagnetic energy propagates from the transmitter toward the receiving structure.
- Upon arrival, the receiver captures the radiated electromagnetic energy, typically as an alternating voltage. It then employs a rectifier to convert this energy into direct current (DC). The rectifier is an electronic component tasked with the $conversion of AC into DC, ultimately supplying power to an electrical load.

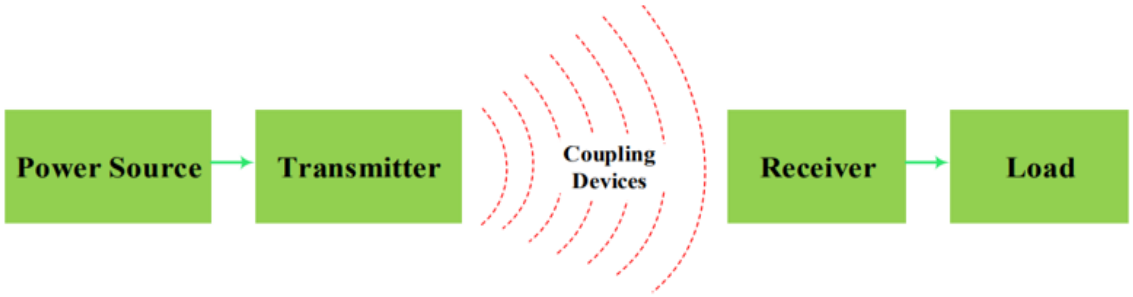

Figure 2.4: Schematic block diagram of the WPT system.

2.4. Types of wireless power transfer

This section discusses various methods of WPT, categorizing this technology into two main segments based on their operational proximity, which includes near and far fields. Predominantly utilized in low-power applications, inductive coupling is the most prevalent method. An alternative technique, magnetic resonance coupling, is used for higher power demands and characteristically sustains transmission distances ranging from a few millimeters to several meters. Far-field methods extend to microwave and laser transmission techniques, which are potent enough to transfer several kilowatts of energy. The diagram in Figure 2.5 is designed to highlight WPT technologies [28].

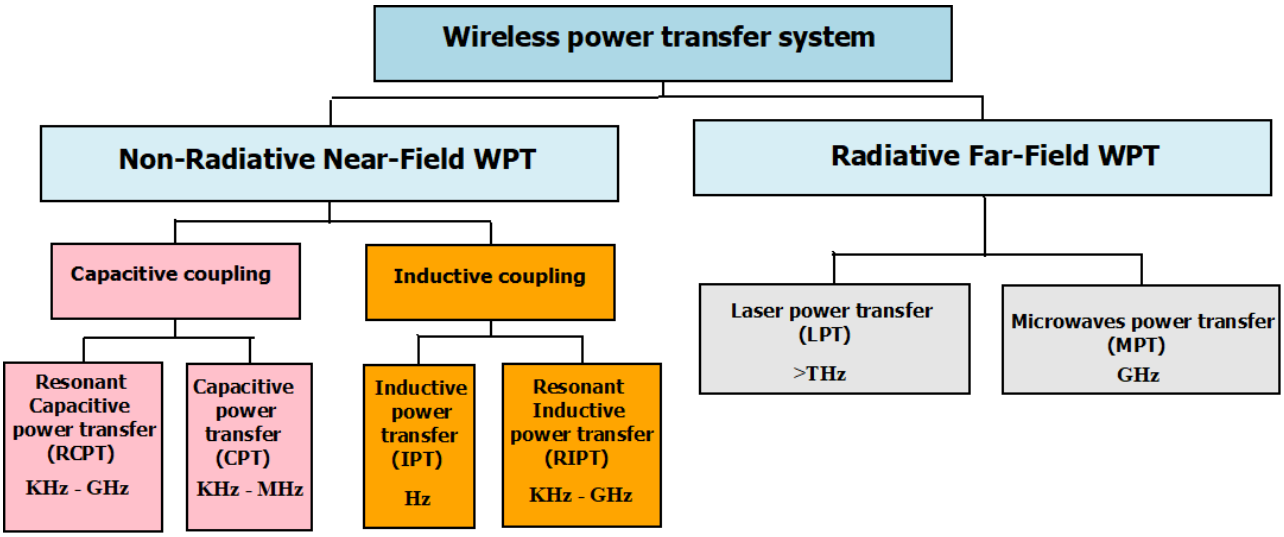

Figure 2.5: Wireless power transfer techniques.

2.4.1. Radiative Far-Field WPT

2.4.1.1. Microwave Power Transfer (MPT)

Wireless power transfer via microwaves represents the leading technique for energy transmission across extensive distances, known as far-field regions, as shown in Figure 2.6. This method leverages electromagnetic waves within the microwave spectrum, ranging from 1 GHz to an upper limit of 1000 GHz. A fundamental aspect of long-distance power conveyance in both microwave and optical systems is the utilization of antennas with a high degree of directivity [29].

The process begins with the generation of high-frequency electromagnetic waves by a microwave power source. Following this step, the transmitter unit transforms the electric power harnessed from the microwave generator into microwaves in the form of radio waves. These waves then traverse through a coax to a waveguide adapter, leading them further to a waveguide circulator. The circulator functions to isolate the microwave source, thus safeguarding against any frequency detuning. After this, a tuner along with a directional coupler is utilized, the latter's role being to segregate the waves based on the direction they are propagating, thereafter projecting them into the open space. Culminating the process, the receiving end apparatus receives the microwave signals, converting them back into usable electrical power. Specifically, the terminal translates microwave energy into direct current (DC) power [30]. MPT systems are engineered with specificity for their intended applications and necessitate meticulous design alongside rigorous examination to guarantee their secure and efficacious functionality. It is of

paramount importance to verify that such systems do not exert any undue interference upon the surrounding electronic apparatus. The applications of microwave power transfer are prevalent in diverse fields, encompassing radar systems, microwave heating appliances such as ovens, electromagnetic pulse (EMP) weaponry, and wirelessly powered aircraft [31].

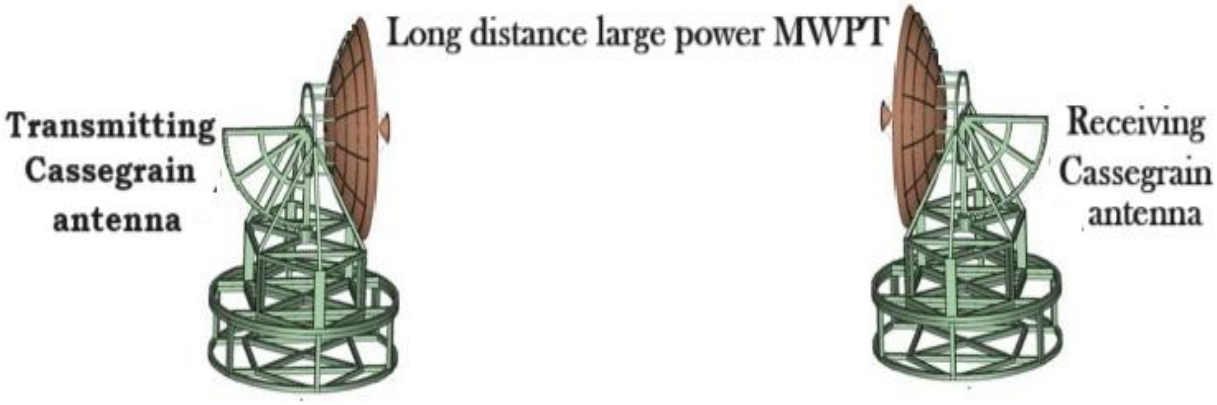

Figure 2.6: Microwave power transfer.

2.4.1.2. Laser Power Transfer (LPT)

LPT stands out as one of the most promising contenders in the realm of WPT technologies. Despite its potential, it is still a relatively inexperienced technology and faces several hurdles that must be surmounted before it can achieve widespread implementation. In the case of high-intensity laser power beam systems (HILPBs), the typical transmission range extends to several hundred meters, with comparatively modest efficiency levels. As illustrated schematically in Figure 2.7, a HILPB system operates by transforming electrical energy derived from a power source into a laser beam. This laser beam is projected towards the destination device. A photovoltaic cell or a designated receiver, positioned at the receiving end, captures the laser beam. It then harnesses the beam's energy and translates it into electric power that can be utilized. This mechanism mirrors that of solar panels, which convert sunlight into electricity; however, the HILPB system substitutes sunlight with intense laser beams to serve as the source of energy [32]. Ongoing research within this domain continues, and it is anticipated that laser power transfer (LPT) will assume an increasingly integral role in the field of WPT. As stated by the Russian Academy of Cosmonautics, it is foreseen that LPTs will be deployed for the energization of sophisticated satellites and military vehicles [33].

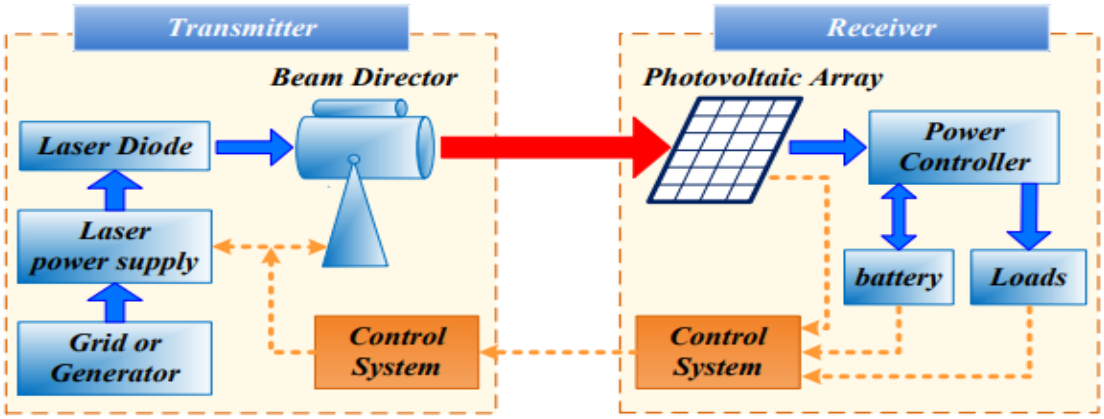

Figure 2.7: Block diagrams of the HILPB system.

2.4.2. Non-Radiative Near-Field WPT

2.4.2.1. Capacitive Power Transfer (CPT)

A capacitive power transfer system (CPT) converts electrical power between the transmitter and receiver using the principle of capacitive coupling, as shown in Figure 2.8. This principle revolves around the transfer of electric charge across two entities that are separated by an intervening substrate that could be air, water, or even an insulator such as wood. In instances where the plates are a mere millimeters to centimeters apart, the CPT harnesses high-frequency electric fields. There are three notable benefits to the CPT technology: it allows for minimal eddy-current losses, it is characterized by relatively inexpensive costs and lightweight components, and it provides exceptional performance even under conditions of misalignment. Within a CPT arrangement, a capacitor coupler typically referred to as a unipolar structure, is composed of at least two metallic plates; one of these plates functions as the transmitter and is located on the primary side, while the other plate operates as the power receiver on the secondary side.

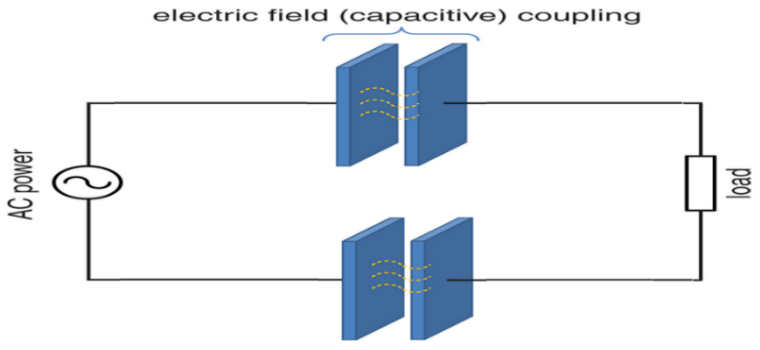

Figure 2.8: Capacitive power transfer (CPT) system.

The electrical current flows to the load via the mutual capacitance established between these plates. To ensure the completion of the electrical circuit, there must be a conductive route through which the current can percolate back to the primary side [34].

Integrating a compensation circuit constitutes one of the most efficacious strategies for augmenting the performance of a CPT system, as shown in Figure 2.9. This approach aims to generate an electric field that is in harmonious resonance with the grid, thereby achieving a heightened voltage on the transmitter plate(s). An elevated voltage results in a robust electric field, which is potent enough to facilitate capacitive charging. Moreover, this enhancement also contributes to doubling the feasible transmission distance [35].

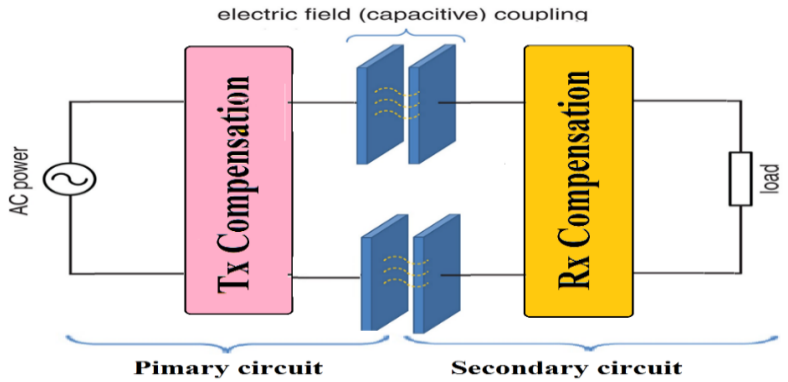

Figure 2.9: CPT system configuration with a resonator circuit.

2.4.2.2. Inductive power transfer (IPT)

Inductive coupling is based on the physical principle of magnetic induction between two coils [36]. Wireless inductive power transfer occurs when a transmitting coil generates a varying magnetic field near a receiving coil, as shown in Figure 2.10. These two coils will couple magnetically and exchange a magnetic flux, generating a voltage at the terminals of the receiving coil. This voltage will then cause a current to flow through the receiver coil, which, once rectified, will be used to power the battery of an electronic device [37].

The frequency of application of such systems is generally between 50 and 500 kHz, and the separation distance between the transmitting and receiving coils is typically between a few millimeters and a few centimeters [38].

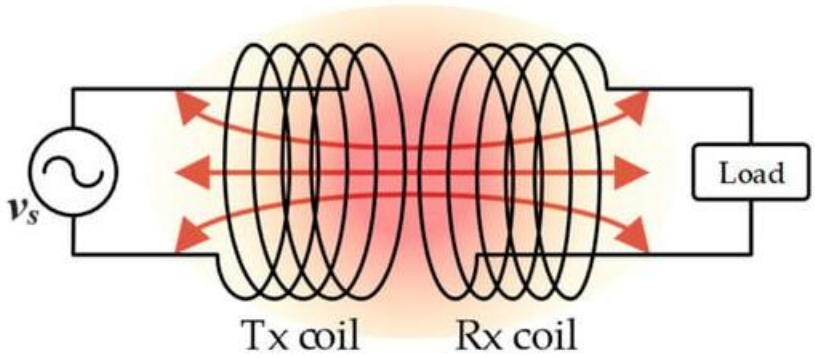

Figure 2.10: Inductive coupling wireless power transfer

WPT systems using inductive coupling are sensitive to the reduction in magnetic coupling that can occur when the coil is too far apart. This results in either a decrease in power efficiency (the transmitter will need to supply more power to provide the same power to the receiver) or a reduction in power to the receiver (the transmitter supplies a fixed power and moves further away from the receiver, resulting in a reduction in the power available to recharge the battery). The advantages of inductive magnetic coupling are its ease of implementation, low system complexity, and energy efficiency, which can be significant when the inductive transmitting and receiving antennas are close [39].

2.4.3. Advantages and disadvantages of different WPT techniques

A summary of the advantages and disadvantages of different WPT technologies is presented in Table 2.1 [39-41]

Table 2.1: Advantages and disadvantages of WPT systems.

WPT technologies type		Advantages	Disadvantages
Near Field	Capacitive	• Offers Medium power transfer (several kilowatts). • Power transfer is possible through metallic objects. • Cheap because it relies on aluminum plates for power transfer. • Suitable for air gaps up to 10 cm. • Restricted electric field: shielding is not needed for EMI control.	• Power transfer capabilities depend upon the gap between the transmitter and receiver. • Parasitic capacitance forms. • Efficiency is approximately 70 -80%.

	Inductive	• Implementation is simple. • Galvanic isolation provided. • Simple control. • High efficiency in the low air gap (Typically less than a coil diameter). • Safe operation compared to resonant mode. • Bidirectional power transfer is possible.	• A short air gap of a few millimeters to centimeters. • EMI shielding is needed. • Very low efficiency at larger air gaps. • Heating effect in the presence of metal objects. • Tight alignment is needed between the transmitter and receiver to achieve good efficiency.
	Resonance	• Offers high power transfer compared to other methods. • Commercialized technology for EV charging. • Able to transfer power in misaligned conditions. • Provides galvanic isolation. • Bi-directional power transfer is possible.	• The cost of the system increases with power. • Extremely sensitive to the obstacles in between coupler coils. (Especially the metallic ones). • Shielding is needed for EMI.
Far-field	Micro Wave	• Power can be transferred up to several km. • Dynamic power transfer is possible (for moving loads). • Possible to transfer power up to several kilowatts. • Higher efficiency achieved at beam forming. • Compatibility with the existing communication system.	• Low efficiency compared to inductive and capacitive methods. • Very difficult to implement. • Unidirectional power flow. • Unsafe for living things when exposed to the microwave beam. • The size of the antennas increases when power transfer capability increases.
	Optical	• The effective gap in km. • Dynamic power transfer is possible (for moving loads). • Capacity to transfer several kilowatts of power. • The transmitter size is small compared to MPT.	• Low efficiency (approximately 20% depends upon the air gap). • Unidirectional power flow. • Difficult to operate. • No obstacles are allowed in the wag of the light beam. • Unsafe operation for living beings, if exposed to radiation.

2.5. Applications of wireless power transfer

WPT has gained significant traction in high-power and low-power applications due to its exceptional flexibility, position-free operation, and movability. WPT plays a pivotal role in powering electric vehicles (EVs) in high-power applications, offering convenient and efficient charging without physical connectors or cables. Additionally, WPT has extensive utility in diverse low-power applications, including portable consumer electronics such as smartphones, tablets, and wireless headphones. Moreover, WPT technology has revolutionized healthcare by facilitating the wireless charging of implantable medical devices (IMDs), such as pacemakers, neuro-stimulators, and hearing aids, thereby eliminating frequent battery replacements. Furthermore, WPT enables wireless charging of drone batteries, extending flight durations and simplifying the charging process for uncrewed aerial vehicles (drones) [42].

Even in challenging underwater environments, WPT has shown promise in enabling efficient and reliable charging of underwater electronic devices, including sensors and underwater robots. The versatility and wide-ranging applications of WPT have demonstrated its potential to revolutionize power delivery across various industries [43]. Wireless power transmission applications are summarized as follows:

2.5.1. Consumer electronics

With the growing popularity of smart home devices and cordless appliances, WPT technologies becoming mainstream in consumer electronics , as shown in Figure 2.11. Wireless power allows for more seamless, convenient experiences for users. To operate domestic appliances, motors, heaters, and other systems require several kilowatts of power. Future wireless products such as LED TVs may require more than 2kW of power. Portable device charging requires approximately 1-20W. Products used in houses, especially in the kitchen, must meet strict safety standards by limiting the intensity, frequency, and other aspects of electromagnetic radiation and fields employed in wireless applications[44].

Figure 2.11: Wireless power transfer for consumer electronics.

The transmission distance is typically short; it requires only 10 cm to enable high-efficiency power transfer between couplers or coils. While ensuring safety and electromagnetic compatibility, consumer wireless power solutions will likely be optimized for necessary power levels, component selection within practical frequency ranges, and short transmission distances to enable compact, convenient product designs [45].

2.5.2. Electric vehicles

Electric vehicles have large batteries with a relatively limited range, which must be recharged. In 2008, the Canadian company Bombardier presented a system that enables electric vehicles such as trams, buses, and Lorries to be recharged while in operation and when stationary, using the power transfer principle by induction. Figure 2.12 shows the wireless recharging of an electric vehicle. Currently, studies are underway to construct stretches of roads equipped with antennas that will enable the batteries of all-electric cars to be charged while in motion [27].

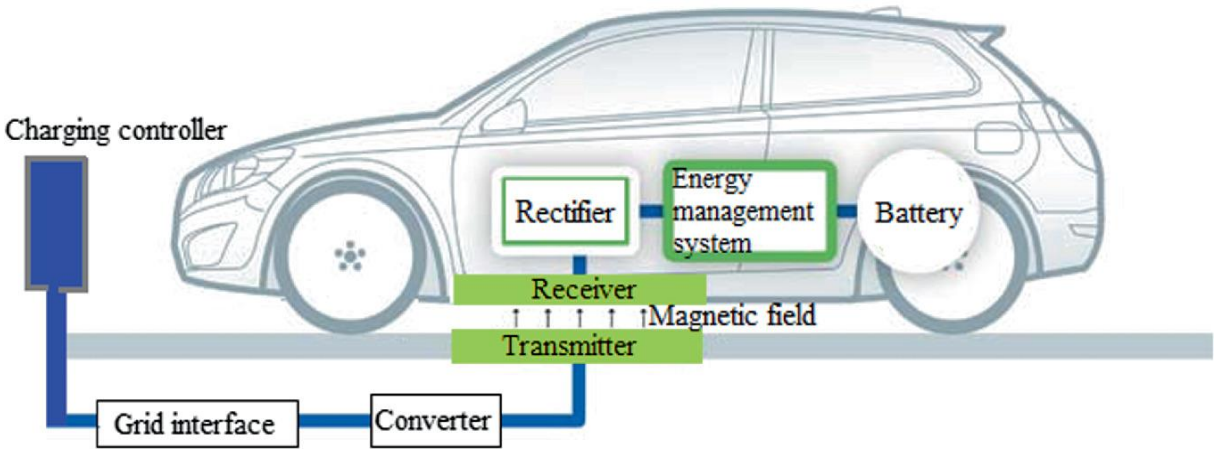

Figure 2.12: The wireless power transfer (WPT) system for electric vehicles (EVs).

2.5.3. Industrial automation

Recent technological advancements have paved the way for using mobile robots in hazardous environments , as shown in Figure 2.13, where they can undertake remote inspections and interventions.

Figure 2.13:Industrial automation application of WPT:(a) Husky, (b) ANYmal, (c) CARMA 2, (d) Corin, (e) Phantom Pro 4, (f) Matrice 600 Pro, (g) AVEXIS, (h) BlueROV.

However, these robots often require long-lasting batteries to ensure extended operation. With the advent of WPT, the need for batteries or wired power can be eliminated, revolutionizing the way these robots are charged [46]. WPT enables robots to receive power without the constraints of traditional battery systems or wired connections. By employing this technology, robots can

be charged during the execution of their intended processes. This flexibility allows for continuous operation without interruptions for battery replacements or the limitations of wired power sources [47].

2.5.4. Aerospace and defense

WPT systems play a crucial role in the advancement of aerospace and defense: WPT for unmanned aerial vehicles (UAVs), spacecraft, and military applications, enabling a remote power supply and reducing reliance on physical connectors [48].

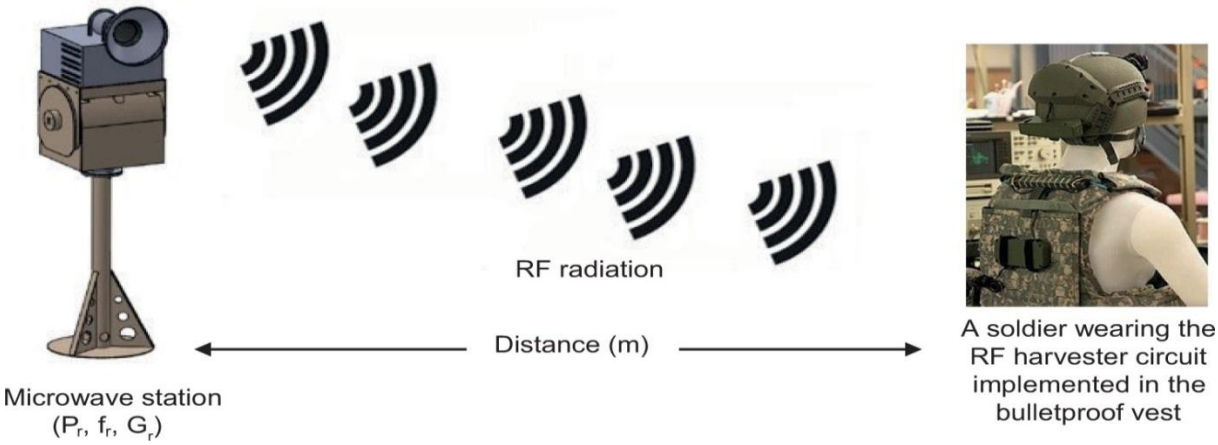

Figure 2.14: The topology of a wireless energy transmission system on a battlefield.

2.5.5. Biomedical devices

Extensive research efforts have been dedicated to healthcare, particularly in the medical applications of health monitoring and treating dysfunctional organs. Over the past few decades, remarkable progress has been made in developing implantable medical devices (IMDs) with the necessary functionality and packaging for successful biological implantation. One of the essential technologies that have contributed to the development of IMDs is WPT. This technology allows power transmission through the air and multilayer tissue, facilitating the functionality of biomedical implants. WPT methods can be classified into near-field and far-field methods based on the operating frequency and the distance between the transmitter and receiver [24]. In the case of lossy dielectric materials such as skin, fat, and muscle, far-field waves experience significant path loss due to high energy absorption [35]. Additionally, the use of higher-frequency waves in far-field transmission, while potentially more harmful to the human body, is subject to strict limitations imposed by standard regulations due to the increased energy absorption in human tissue. These considerations highlight the challenges and trade-offs

involved in designing and implementing WPT systems for biomedical implants. The field of power transfer must arbitrage between achieving efficient power transfer and ensuring the safety and well-being of the human body [49].

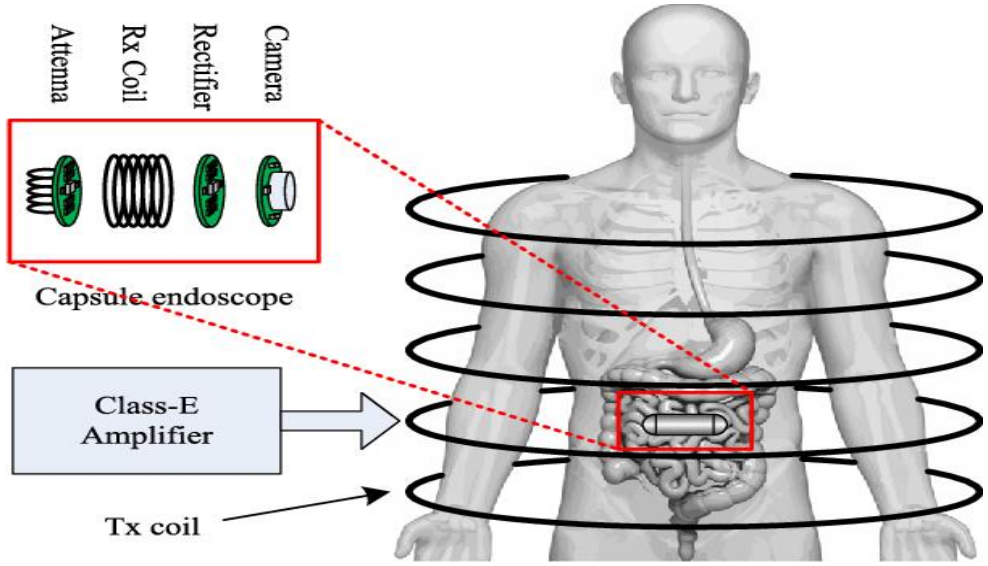

Figure 2.15: The WPT system for capsule endoscopy.

IMDs (implantable medical devices) that can be recharged and powered wirelessly have received considerable attention due to their ability to improve patient quality of life, which we can classify into three applications [50].

2.5.5.1. Nerve stimulation

Stimulation of the nerves is an effective method for alleviating the adverse effects of neurodegeneration. Although they are of different types, as shown in Figure 2.16, they all require an initial electrical input and follow electrical waves or light illumination. According to nerve category, nerve stimulation can be divided into three types: deep brain stimulation is a therapy that aims to ameliorate the impacts of neurodegeneration, which can cause neuronal death and a series of diseases such as Alzheimer's disease, Parkinson's disease, and amyotrophic lateral sclerosis [51]. Peripheral stimulation, such as Vagus Nerve Stimulation, is similar to cortical stimulation in that it aims to rehabilitate dysfunctional limbs and sensors. Finally, retinal nerve stimulation and retinal prostheses are widely adopted and promising therapies for eye-handicapped patients suffering from degenerative conditions of the outer retina, such as age-related macular degeneration (AMD) and retinitis pigmentosa (RP).

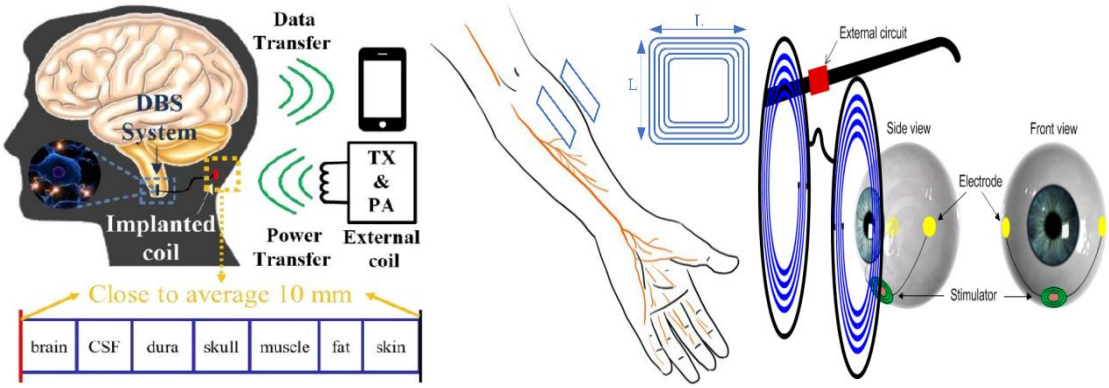

Figure 2.16: The WPT system for different nerve stimulations.

2.5.5.2. Spinal cord stimulation

Spinal cord stimulation (ESCS) has emerged as an established and effective treatment for chronic pain relief, with expanding applications in various neurological conditions. Previous studies have explored the impact of the ESCS on motor performance. Regrettably, current stimulator devices possess technical limitations such as voltage, waveform, and frequency, which hinder their application.

Figure 2.17: The WPT system for spinal cord stimulation.

A notable advancement in this field is the integration of wireless charging capability into implantable stimulators, which offers significant improvements, as shown in Figure 2.17. WPT technology has considerable benefits, eliminating invasive battery replacement or recharging procedures in traditional stimulator devices. With wireless charging, physical connections and

direct contact with the implantable device are no longer necessary. This provides patients with a safer and more convenient charging method [52].

2.5.5.3. Assistant devices

Assistant devices are implanted chargers designed to increase the operating duration. Biomedical implants , as shown in Figure 2.18. The charging component of these devices is separate from that of biomedical appliances. As medical devices move during operation, the charging coil remains fixed in a nearby area, ensuring relative efficiency. Among the assistant devices, implanted permanent pacemakers (PPMs) are the most notable. Presently, users of these devices have to undergo regular pacemaker replacement surgeries due to the depletion of the pacemaker's battery within 5-10 years. Although PPMs have been proven to decrease deaths in various patient populations, surgery still poses risks for PPM users. This is especially important considering that most users are elderly. Furthermore, replacement surgery for PPMs is also financially burdensome [53]. WPT technology may mitigate some of these complications, such as eliminating battery replacement surgery.

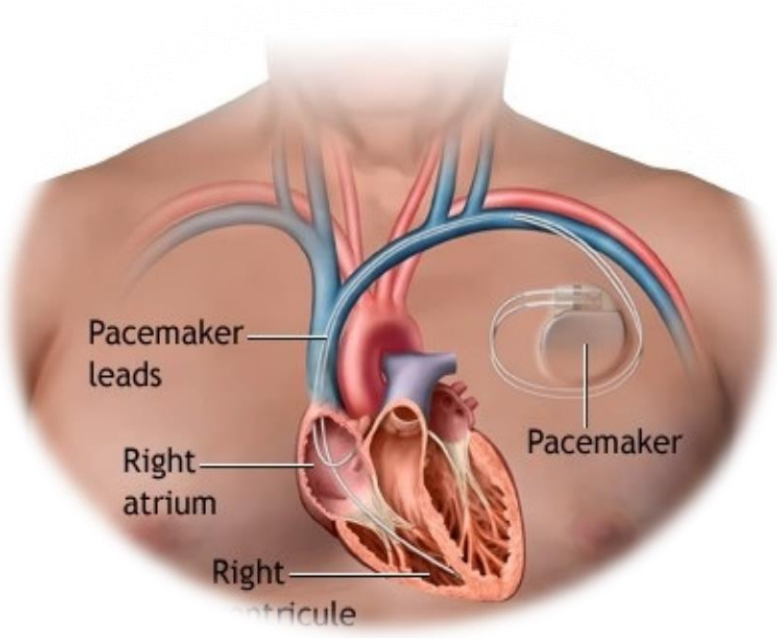

Figure 2.18: The WPT system for pacemakers

2.6. Literature review on wireless power transfer for implantable devices

WPT is an attractive technology that satisfies the power needs of implantable devices. Nevertheless, as implants decrease, so do their antennas/transducers, causing the efficiency of the power transfer link to decrease and forcing the use of high frequencies, which suffer more attenuation as they propagate through the tissue. In this section, we provide a literature review of WPT in biomedical devices such as that of *Shoulder et al*, who were among the first to propose WPT for biomedical applications. In 1961, they detailed the theoretical rationale for believing that inductive coupling between a simple pancake-shaped coil on the body's surface and a similar coil within the body was an efficient method of transporting power [54]. In the 1970s, IPT was used in other biomedical applications. As early as 1985, *Cochran et al*, accomplished prototype testing on an electromechanical internal fixation plate. This device combines a piezoelectric material with an internal fixation device as an integrated structure that provides mechanical stability and self-generated electrical stimulation for treating fractures and nonunion. Once that was done, it was later optimized in 1988. The intent was to deliver this current to electrodes at a fracture or osteotomy site to aid nonunion prevention or treatment. This study quantitatively examined the ability of external ultrasound to generate current from small piezoelectric ceramic elements placed in tissue [55]. Since then, many implantable devices have used similar power transfer methods. However, designing an implantable antenna poses several challenges that must meet specific requirements. Complex structures and large-area inductors often make them unsuitable for implant applications [32]. Several key factors need to be considered when developing a high-efficiency charging strategy for medical implants, including the transmission distance, coil structure, and resonance frequency [56]. Achieving a balance among these factors is crucial for optimizing the WPT system [51]. Alternative approaches, such as higher frequencies, have been proposed to reduce the coil size. However, it is imperative to note that higher frequencies can enhance energy coupling with biological tissues, which can cause harm. Therefore, a careful balance must be achieved between size reduction and the potential risks associated with higher-frequency operation [34]. To achieve this goal, several studies have examined the potential of WPT in implantable devices in light of the interests above. These papers are summarized in Table 2.2.

Table 2.2: Literature on wireless power transfer for implantable devices

Reference	Application	Year	Size (mm)		D12 (mm)	Frequency	PTE (%)	Objective
			Tx	RX				
[57]	Neuroprosthetic	2009	38	10	10	13.56 MHz	72.2	Modeling and optimization of printed spiral coils in air, saline, and muscle tissue environments
[58]	Subcutaneous Tissue	2009	44	4 x 8	40	13.56 MHz	-	A remotely powered implantable microsystem for continuous blood glucose monitoring is presented
[59]	–	2009	20	20	15	915 KHz	65	The application of simultaneous conjugate matching to WPT links to realize a maximum theoretical gain
[60]	Behavioral neuroscience	2009	168	30	70	13.56 MHz	80.2	A flexible clockless 32-ch simultaneous wireless neural recording system with an adjustable resolution provides a high level of flexibility.
[61]	Neuroprosthetic Implantable Devices	2010	79	10	10	13.56 MHz	95	Optimization of data coils in a multiband wireless link for neuroprosthetic implantable devices.
[1]	Biomedical implants	2010	60	22	10 to 20	700 kHz	80%	Optimization of resonance-based efficient wireless power
[62]	Biomedical implants	2011	62 x 25	25 x 10	10	13.56 MHz	69	The optimal power transfer guarantees a minimum transmitted power level and a maximum level to avoid brain tissue damage
[63]	Nerves	2011	28	10	10	13.56 MHz	71.1	Design and simulation of the printed spiral coil

[64]	Biomedical implants	2011	70 x 8	20 x 8	10	1-5 MHz	75	Maximum Achievable Efficiency in Near-Field
[65]	Stimulate and monitor nerves and muscles	2014	56	11.6	6	13.56 MHz	73	Development of the theoretical analysis and optimization of an inductive link based on coupling and spiral circular coil geometry
[66]	Implantable Mechanical Heart Support Systems	2015	83.2	24.2	20	800 KHz	95	Focuses on the design and realization of a highly efficient TET system and the minimization of the power losses in the implanted circuits in particular
[67]	The brain-implanted sensors	2015	45	9.5	10	13.56 MHz	55	Develop a comprehensive approach to optimizing a pair of coils for wireless powering of brain-implanted sensors.
[68]	Implantable DeepBrain Stimulation System	2015	19.86	15.94	5	403 KHz	10	Develop new deep-brain stimulation systems for long-term use in animals, to develop a variety of neural prostheses
[69]	Neuro Processing	2016	79	10	10	13.56 MHZ	52	Proposes a new and general method to optimize a working frequency and load resistance to realize highly efficient WPT
[70]	Biomedical implants	2016	80	20	30	13.56 MHz	77.9	Geometry optimization of inductively coupled printed spiral coils for powering a given implantable sensor system
[71]	Miniature pacemaker	2016	40	5	20	13.56 MHz	6	Designed a remote-controlled system and the cardiac component was miniaturized
[72]	Pacemaker	2017	70	46	8	20 KHz	77	WPT technology applied to recharge the battery of a pacemaker has been investigated using a considerably low optional frequency (20 kHz)
[73]	The brain and the eye	2018	28	24	50	13.56 MHz	1.22	Optimized the design of the f-DDM by a finite element analysis to prevent thermal damage during the laser transfer and the application of current density for reliable drug release through an electrochemical analysis.

[74]	biomedical devices.	2019	60	20	-	3.8 MHZ	74.8	Optimizing the quality factor and matched resonant frequency is required to achieve high efficiency
[75]	Biomedical implants	2019	60	18.8	-	13.56 MHZ	-	Investigate the impacts of perfect alignment, and lateral and/or angular misalignments on the overall PTE of the system
[76]	Biomedical implants	2019	45	9.5	10	13.56 MHZ	79	The description of the design of an inductive resonance coupling link used for powering small bio-implanted devices
[77]	Microstrip patch antenna and planner inverted-F antenna	2020	28 x 24 x 1.43	6.25 x 6 x 0.63	25	1.45 GHz	-	Investigate compact microstrip patch antennas in data telemetry link for retinal prosthesis
			26 x 24 x 1.4	7 x 6.93 x 0.63	-	2.48 GHz	-	
[78]	Implantable medical devices	2020	53.4	45.5	10	300 kHz	72	A WPT converter with LC/S compensation is presented for AIMDs, and has been transmitting and receiving coils that are magnetically modeled, and an electric-field common simulation is carried out to obtain a transient response of the converter.
[79]	_	2021	55	9.7	-	433 KHz	17	Optimize the Rx antenna with a high PTE
[80]	Pacemaker	2021	12.2	11.5	20	6.78 MHZ	93	Spider-web coil-MRC (SWC-MRC) design and practical implementation to overcome the battery life restricted in low-power BMIs
[81]	Miniature antenna	2021	-	44.63	-	2.47 GHz	-	A miniaturized and two-on-body antennas
[82]	Miniature antenna, Hilbert fractal shape	2021	11.1 x 11.1 x 1.27	10.25x10.25x1.27	-	2.48 GHz	-	A miniaturized and two-on-body antennas

[2]	Pacemaker	2022	55	35	-	13.56 MHz	92.24	The design and optimization of geometrical parameters for the MRC WPT-SP topology
[83]	Deep brain stimulation	2022	26	7	20	25 MHz	44.1	The optimization of the coupling coefficient (k) of the inductive link for the WPT system
[84]	Implantable neurostimulat	2023	55	-	8	6.78 MHz	52 to 68%	Propose a strategy for the design of a WPT system consisting of a class-E inverter for maximum power transfer efficiency. The design

2.7. Conclusion

This chapter provides an overview of WPT technology, including its historical evolution, diverse methods, and promising applications. We mentioned the advantages and disadvantages of various WPT techniques; this technique has the potential to revolutionize power delivery across various applications, from consumer electronics to electrical vehicles and biomedical devices. A literature review of various studies on WPT for IMDs was presented. In the next chapter, we will present the principle of resonant inductive coupling, providing a detailed modeling and analysis.

Modeling of a resonant inductive wireless power transfer

Chapter 3

3.1. Introduction

In recent years, bioimplantable devices have been predominantly powered by implanted batteries. However, this technique poses several significant risks to patients, such as susceptibility to infections and potential adverse health effects. Furthermore, these batteries can produce chemical by products and are limited by a finite lifespan, necessitating recurrent replacements. Researchers have investigated safer alternatives using magnetic inductive links for electrical energy transmission to address these issues. This cutting-edge approach mitigates the risks associated with implanted batteries and offers several advantages. By leveraging magnetic induction, implantable devices can continuously tap into a robust stream of high-energy resources conveniently controlled by an external apparatus through a magnetic link. Crucially, this decouples the battery's lifespan from that of the medical implant, ensuring sustained durability and functionality even in the face of the patient's daily routine.

In this chapter, the detailed modeling of the WPT using resonant inductive coupling is discussed. Initially, we described the operating principle of the inductive coupling WPT. Subsequently, we review WPT via a resonant inductive link and its topologies. An analytical model of the series-parallel (SP) resonant inductive link is then introduced to calculate the power transfer efficiency (PTE). Finally, a thorough analysis is conducted to identify the key geometrical coil parameters that impact the efficiency of the WPT system.

3.2. Inductive coupling architecture for bioimplanted devices

Typically, the structure of the inductive coupling link for bioimplanted devices depicted in Figure 3.1 consists of two coils: an extracorporeal coil (primary coil) placed outside the human body and an internal coil (secondary coil) implanted inside the human body at a short distance from the external coil [76].

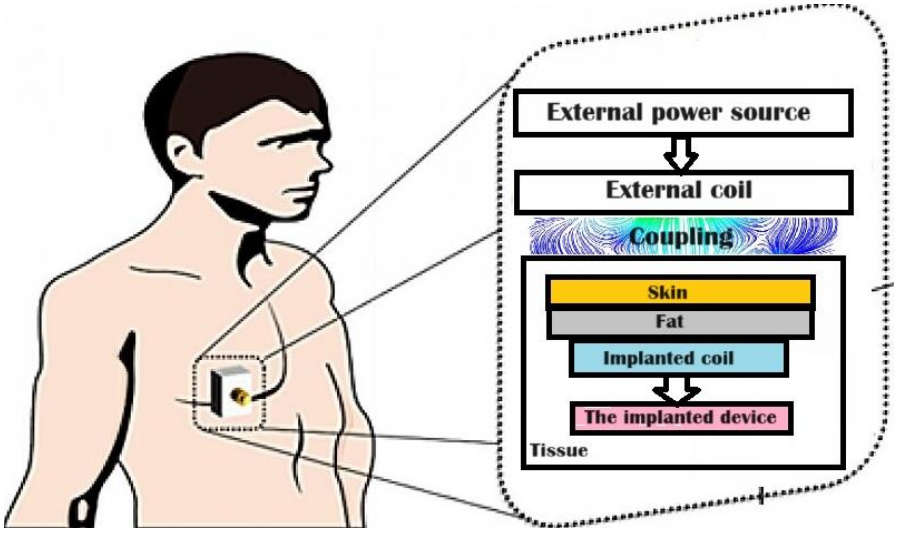

Figure 3.1: The illustration of an inductive link for bioimplanted devices

Bioimplantable devices optimized to the smallest feasible size should be implanted according to the functional depth in human biological tissues. This depth is generally less than 10 mm, for instance, microsystems implanted into the human body are inserted at depths ranging from 1 to 4 mm. Cochlear implants are usually situated at depths between 3 and 6 mm, while retinal implants require a depth of 5 mm[85]. Currently, the study of a wireless energy transfer system for bio-implantable devices primarily concentrates on the design and enhancement of transmitter and receiver coils (the implants) [86].

3.3. The operating principle of inductive coupling

The principle behind inductive coupling is that a source linked to a primary coil generates a magnetic field, which in turn induces a voltage across the secondary coil of the receiver, as illustrated in Figure 3.2.

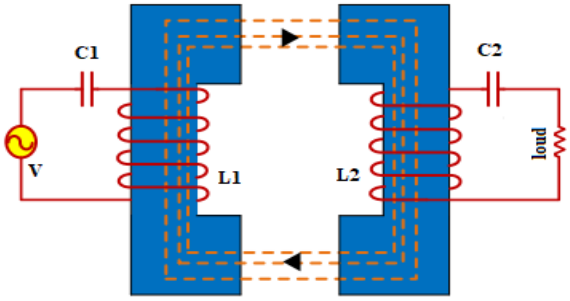

Figure 3.2: Inductive coupling WPT

The electrical equivalent circuit for inductive coupling is depicted in Figure 3.3, where R_1, R_2, and L_1, L_2 are the resistances and inductances of the transmitting and receiving coils, respectively. M_{12} represents the mutual inductance between the two coils, and R_L represents the equivalent AC load resistance [87].

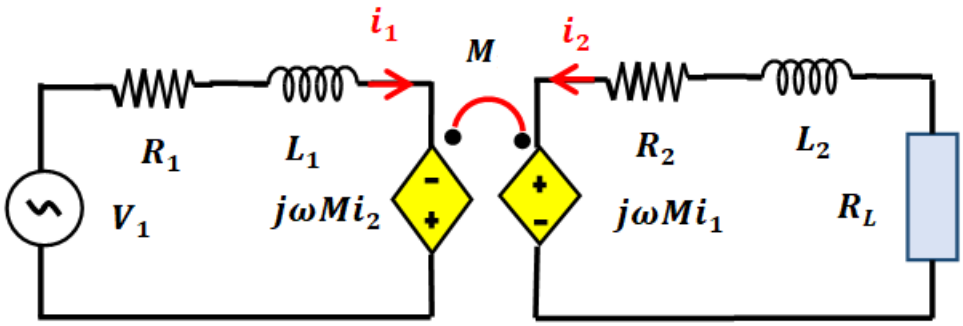

Figure 3.3: Equivalent circuit of inductive coupling

The transmission coil is excited with a sinusoidal voltage (V_1) of angular frequency ω. According to the electrical equivalent circuit model, the steady-state equations for the transmitter and receiver are as follows:

$$V_1 = R_1 I_1 + j\omega L_1 I_1 - j\omega M I_2 \tag{3.1}$$

$$j\omega M I_1 = R_2 I_2 + j\omega L_2 I_2 + R_L I_2 \tag{3.2}$$

$$j\omega M I_1 = I_2(R_2 + j\omega L_2 + R_L) \tag{3.3}$$

$$I_2 = \frac{j\omega M}{R_2 + j\omega L_2 + R_L} I_1 = \frac{j\omega M}{Z_2} I_1 \tag{3.4}$$

$$\frac{I_2}{I_1} = \frac{j\omega M}{Z_2} \tag{3.5}$$

with I_1 and I_2 are the currents flowing in the transmitting and receiving coils, respectively. Z_2 represents the equivalent impedance on the receiver side.

Substituting equation (3.4) into equation (3.1) gives:

$$V_1 = R_1 I_1 + j\omega L_1 I_1 + \frac{(\omega M)^2}{Z_2} I_1 \tag{3.6}$$

From the transmitter side, the total impedance Z_T can be expressed as follows:

$$Z_T = R_1 + j\omega L_1 + \frac{(\omega M)^2}{Z_2} \tag{3.7}$$

$$Z_T = Z_1 + Z_R \tag{3.8}$$

Z_1 represents the equivalent impedance on the transmitter side, and the reflected impedance Z_R at the transmitter side is given by[88]:

$$Z_R = \frac{(\omega M)^2}{Z_2} \tag{3.9}$$

From equations (3.4) and (3.7), the efficiency can be expressed as [87]:

$$\eta = \frac{{I_2}^2 R_L}{{I_1}^2 Re\{Z_T\}} = \frac{R_L}{R_1 + \frac{{L_2}^2}{M^2} + (R_2 + R_L)\left[1 + \frac{R_1(R_2 + R_L)}{(\omega M)^2}\right]} \tag{3.10}$$

3.4. Resonant inductive coupling

Magnetic resonance WPT operates on the same principle as inductive coupling, but it involves the addition of resonant circuits , as shown in Figure 3.4. This enhancement significantly increases the efficiency and the range of power transfer, allowing for greater distances between the transmitter and receiver coils. Unlike traditional inductive coupling, which requires precise coil alignment, magnetic resonance WPT offers more flexibility in positioning. Power transfer can occur then as long as the receiver coil is within the transmitter's magnetic field range [89].

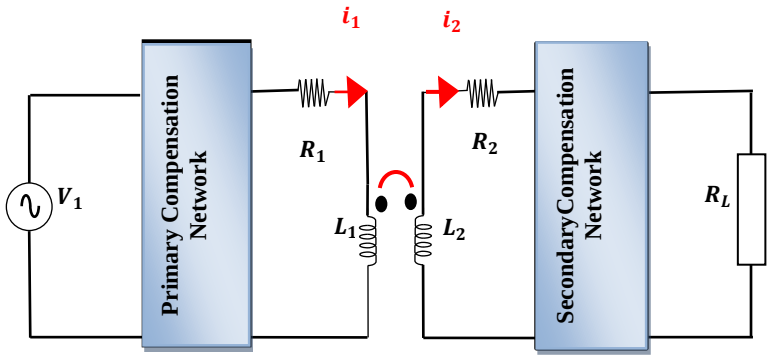

Figure 3.4: Circuit of magnetic resonance inductive coupling-WPT.

The operational frequency for these systems ranges from 5 to 15 MHz, and the spatial separation between the transmitter and receiver extends from a few to multiple tens of centimeters. Owing to the elevated operational frequency, the quality factor of the antenna in resonant magnetic coupling technology surpasses that of inductive magnetic coupling. High-quality factors indicate that energy efficiency is preserved even as the distance between antennas increases [90].

Increasing the air gap between two inductive coils increases the leakage inductance and magnetizing current, weakening the coupling between them. To compensate for the effects of leakage inductance and enhance the coupling, the circuit operates at a resonant frequency [91].

3.4.1. Different topologies for resonant inductive coupling

Resonant circuits are essential components of WPT systems [92]. A basic resonant circuit consists of a resistor, an inductor, and a capacitor, which can be arranged in either series or parallel configurations. These circuits operate at a resonant frequency to compensate for leakage inductance and enhance coupling between coils [93]. Compensating the secondary coil can also increase the pick-up coil's capability [94]. In magnetic resonance coupling for wireless power systems, electrical energy is transmitted by magnetic resonance on the transmitter (primary) and receiver (secondary) sides. When the primary inductance and capacitance are tuned to the resonant frequency, a strongly enhanced magnetic field develops in the transmitter coil due to resonance [95]. Multiple resonant circuit topologies can be used, including series-series (SS), series-parallel (SP), parallel-series (PS), and parallel-parallel (PP)topologies. Each topology affects parameters such as the coupling coefficient, load voltage, and load resistance, as shown in Figure 3.5.

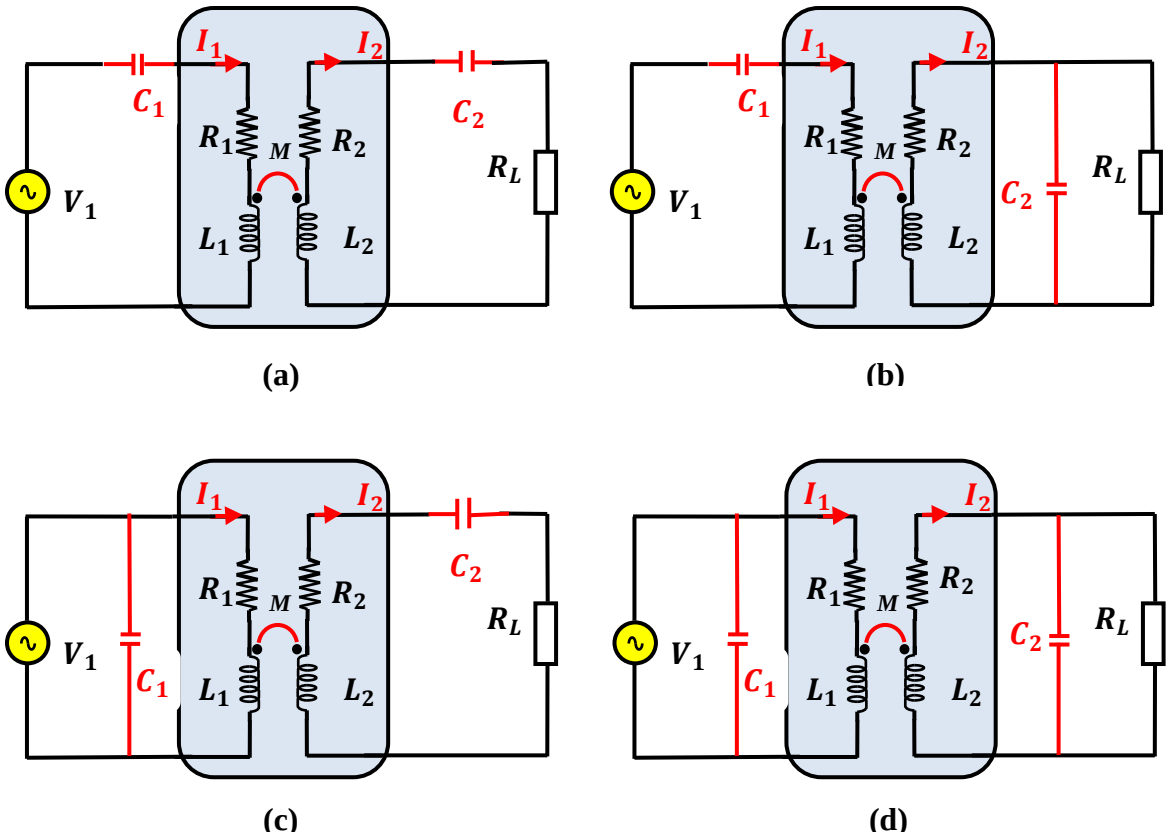

Figure 3.5: The basic topologies: (a) Series-Series (SS); (b) Series-Parallel (SP); (c) Parallel-Series (PS); (d) Parallel-Parallel (PP).

The values of the compensation capacitors are typically set at a predetermined fixed frequency f_0. This frequency is chosen to be equal to one of the primary or secondary resonant frequencies. The values of the compensation capacitors for each topology are shown in Table 3.1 [76, 97]

Table 3.1 The compensation capacitors for different topologies.

Topology	Primary capacitance ($C1$)	Secondary capacitance ($C2$)
SS	$\frac{1}{\omega_0^2 L_1}$	$\frac{1}{\omega_0^2 L_2}$
SP	$\frac{1}{\omega_0^2 (L_1 - \frac{M^2}{L_2})}$	$\frac{1}{\omega_0^2 L_2}$
PS	$\frac{L_1}{\left(\frac{\omega_0^2 M^2}{R_L}\right) + \omega_0^2 L_1^2}$	$\frac{1}{\omega_0^2 L_2}$
PP	$\frac{L_1 - \frac{M^2}{L_2}}{\left(\frac{\omega_0^2 R_L}{L_2}\right)^2 + \omega_0^2 (L_1 - \frac{M^2}{L_2})^2}$	$\frac{1}{\omega_0^2 L_2}$

It is important to note that SS and SP compensation are most commonly utilized in actual applications and implementation because they have the highest efficiency [43, 98, 99]. In SP, regardless of the load, some impedances are transferred to the primary, and at resonance, there is still a short circuit if the load is absent, which facilitates the need for a current limiting control [100, 101]

3.4.2. Circuit model and efficiency of a series-parallel (SP) resonant inductive link

In this section, we present the coupling of an inductive link with a series-to-parallel (SP) topology used to power implantable biomedical devices. Typically, the system consists of two resonant RLC circuits: the transmitter circuit, which represents the external circuit, and the receiver circuit, which represents the implanted circuit[101]. We use the primary circuit in series resonance to provide a low impedance load, and the secondary circuit is almost invariably parallel. Figure 3.6 illustrates the intricate nature of a general WPT system with series-parallel compensation.

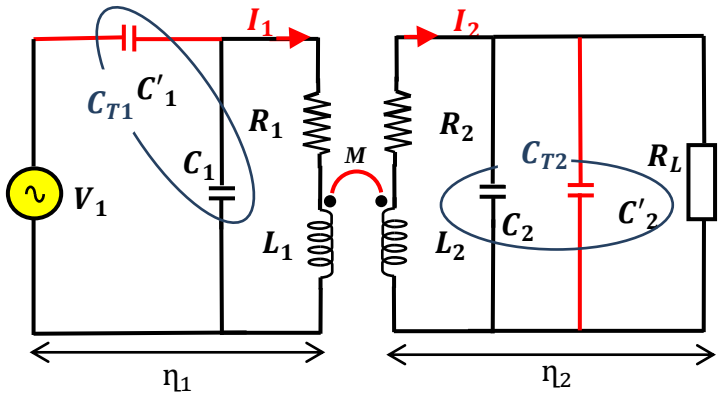

Figure 3.6: Series-parallel resonant inductive link.

The efficiency is maximized when the LC tanks are precisely tuned at the working frequency (ω).Assuming that ω equals both $\omega_1$and ω_2 [102], in an inductive power link, the L_1 and L_2 coils are meticulously tuned with C_{T1} and C_{T2}, respectively, and the efficiency of the transmitted power from source to load is dominated by the receiver side efficiency (η_1) and tag side efficiency (η_2) and can be demonstrated by:

$$V_1 = \frac{1}{j\omega C_{T_1}} I_1 + R_1 I_1 + j\omega L_1 I_1 - j\omega M I_2 \tag{3.11}$$

$$j\omega M I_1 = R_2 I_2 + j\omega L_2 I_2 + (R_L \,//\, Z_c) I_2 \tag{3.12}$$

$$j\omega M I_1 = R_2 I_2 + j\omega L_2 I_2 + (R_L + j\omega C_{T2}))I_2 \tag{3.13}$$

$$j\omega M I_1 = I_2(R_2 + R_L + j\omega L_2 + j\omega C_{T2}) \tag{3.14}$$

$$I_2 = \frac{j\omega M}{R_2 + R_L + j\omega(L_2 + C_{T2})} I_1 = \frac{j\omega M}{Z_2} I_1 \tag{3.15}$$

$$\frac{I_2}{I_1} = \frac{j\omega M}{Z_2} \tag{3.16}$$

Z_2 represents the equivalent impedance on the receiving side with SP compensation. Substituting equation (3.15) into equation (3.10) gives:

$$V_1 = \frac{1}{j\omega C_{T1}} + R_1 I_1 + j\omega L_1 I_1 + \frac{(\omega M)^2}{Z_2} I_1 \tag{3.17}$$

From the transmitter side, the total impedance Z_T can be expressed as follows:

$$Z_T = R_1 + j\omega L_1 + \frac{1}{j\omega C_{T1}} + \frac{(\omega M)^2}{Z_2} \tag{3.18}$$

$$Z_T = Z_1 + Z_R \tag{3.19}$$

Z_1represents the equivalent impedance on the transmitter side with SP compensation. The reflected impedance Z_R at the transmitter side is given by [88]:

$$Z_R = \frac{(\omega M)^2}{Z_2} \tag{3.20}$$

At resonance frequency, the coil-to-coil efficiency can be expressed by:

$$\eta = \frac{X\frac{R_2}{R_L}}{\left(1+\frac{R_2}{R_L}+X\frac{R_2}{R_L}\right)\left(1+\frac{R_2}{R_L}\right)} \tag{3.21}$$

Where: $X = \frac{M^2\omega^2}{R_1 R_2}$, or $X = K^2 Q_T Q_R$

Q_T, Q_R, and K represent the quality factors of the primary and secondary coils, and the coupling coefficient, respectively. By taking R_L as optimum, the maximum efficiency can be calculated as [5, 104]:

$$\eta_{\max} = \frac{K^2 Q_T Q_R}{\left(1+\sqrt{1+K^2 Q_T Q_R}\right)^2} \tag{3.22}$$

The coupling coefficient (K) measures the strength of the magnetic linkage between primary and secondary coils within a WPT system. A higher coupling coefficient corresponds to a more efficient power transfer process, minimizing magnetic flux loss and generating heat [104]. The coupling coefficient operates within the range of 0 to 1 (1 signifies a perfectly coupled system). The mathematical expression of K is given by:

$$K = \frac{M_{12}}{\sqrt{L_1 L_2}} \tag{3.23}$$

The most significant aspect of this process is the role of mutual inductance, which ensures WPT between the two coils. Various methods, including Maxwell's formula, Neumann's formula, and the Biot-Savart law, have been used to calculate the mutual [105]. The total mutual inductance between the external and implanted circuits is defined by [106]:

$$M_{12} = \theta \sum_{i}^{N_T} \sum_{j=1}^{N_R} M(x_i, y_i, d_{TR}) \tag{3.24}$$

Where θ is a constant that varies with the shape of the coil and is empirically, between 0.8 and 1.8 for a circular spiral coil. This depends on the number of turns, the pitch, and the diameter of the coil. The parameters N_T and N_R represent the number of turns in the primary and secondary coils, respectively. The variables x_i, and y_i denote the radius of the i^{th} turn in the primary coil and the radius of the j^{th} turn in the secondary coil, respectively, and d_{TR} is the relative distance between coils [76].The mutual inductance between the i^{th} turn of the primary coil and the j^{th} turn of the secondary coil is expressed by:

$$M(\mathrm{d}_{\mathrm{out}T}, \mathrm{d}_{\mathrm{out}R}, d_{TR}) = \frac{1}{2}\mu_0 \sqrt{\mathrm{d}_{\mathrm{out}T}.\,\mathrm{d}_{\mathrm{out}R}} \left[\left(\frac{2}{\gamma} - \gamma\right) k(\gamma) - \frac{2}{\gamma} E(\gamma)\right] \tag{3.25}$$

$$\text{Where: } \gamma = \sqrt{\frac{4\,\mathrm{d}_{\mathrm{out}T} \times \mathrm{d}_{\mathrm{out}R}}{(\,\mathrm{d}_{\mathrm{out}T} + \mathrm{d}_{\mathrm{out}R})^2 + {d_{TR}}^2}} \tag{3.26}$$

where, $k(\gamma)$ and $E(\gamma)$ are elliptic integrals of the first and second order; respectively and μ_0 is the permeability of the free space equal to $4\pi \times 10^{-9}$H/cm.

The geometrical approximation of the mutual inductance M between the external and implanted spiral circular coils is given by the expression[107]:

$$M_{12} = \frac{\mu_0 \pi N_T N_R {d_{outT}}^2 {d_{outR}}^2}{\sqrt{\left({d_{outR}}^2 + {d_{TR}}^2\right)^3}} \tag{3.27}$$

3.4.3. Modeling and design of circular spiral coils

3.4.3.1. Design using analytical expressions

In the field of WPT, the scientific literature has introduced different spiral coil shapes for optimal performance, such as circular, square, and octagonal coil shapes. The shape of the coil is an important factor to consider when designing WPT systems. These models are shown in Figure 3.7.

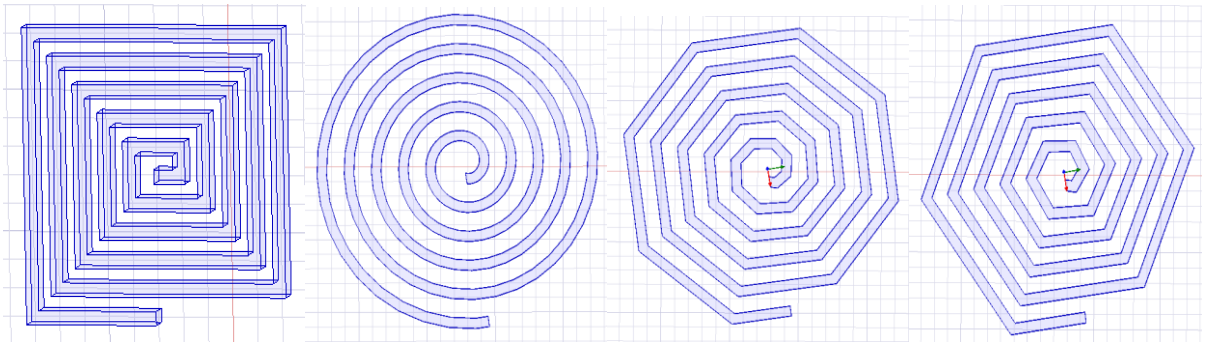

(a) (b) (c) (d)

Figure 3.7: Different coil shapes: (a) square, (b) circular, (c) octagonal, and (d) hexagonal.

In this work, we used circular spiral coils. Such coils are suitable for biomedical devices due to their uniformity, ease of fabrication, compactness, symmetry, and high Q factor. The choice of using a circular coil as opposed to other coil shapes in a specific biomedical application depends on various factors and design considerations, including the following:

- Circular coils can generate a more uniform magnetic field than other coil shapes.

- Circular coils are relatively easy to fabricate. Their shape is simple, and winding wire in a circular fashion is often straightforward.

- Circular coils can be designed to be compact and space-efficient. This can be crucial in biomedical applications where size constraints are a concern.

The geometric parameters of the flat circular coils are:

- The inner diameter d_{in}
- The outer diameter d_{out}
- The number of turns N
- The width of conductor W
- The spacing between the turns S

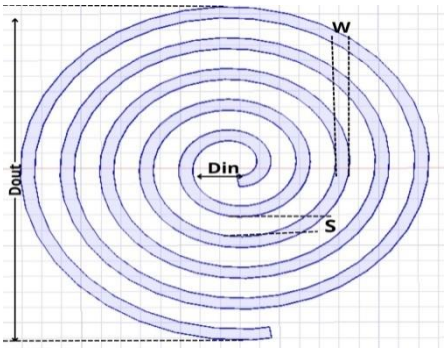

Figure 3.8: Geometry of a circular coil.

The equivalent circuit for this coil configuration is represented by a resistor (R) in series with an inductor (L), both of which are in parallel with a capacitor (C), as depicted in Figure 3.9.

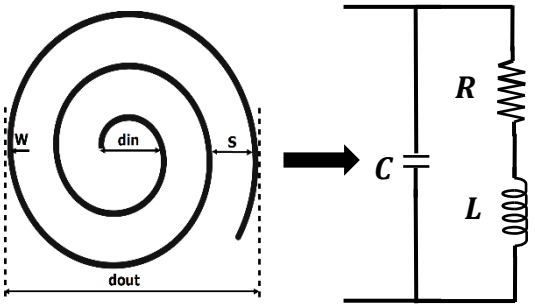

Figure 3.9: Circular coil and its equivalent electrical circuit.

Considering the illustrated coil in Figure 3.9, which encompasses all previously discussed parameters; it becomes evident that they are interrelated through the following formula:

$$d_{out} = d_{in} + 2 \times W + (N - 1) \times S \tag{3.28}$$

Correctly modeling coils requires understanding their lumped elements, such as capacitance, inductance, and resistance. These parameters are related to WPT efficiency.

- **The self-inductance L**

For circular coils, self-inductance mainly depends on their size and winding method and is generally unaffected by their relative positions to other coils [108]. Nonetheless, magnetizer and shielding layers can alter the natural magnetic field distribution, enhancing coupler performance and introducing self-inductance variability. the following formula is used to determine the self-inductance for circular spiral coils based on their geometric parameters [109]:

$$L = \frac{C_1 \mu_0 N^2 d_{avg}}{2}\left[\ln\frac{C_2}{\varphi} + C_3\varphi + C_4\varphi^2\right] \quad (3.29)$$

$$\text{Where: } d_{avg} = \frac{d_{in}+d_{out}}{2} \; ; \varphi = \frac{d_{in}-d_{out}}{d_{in}+d_{out}} \quad (3.30)$$

Inductance is determined by factors such as the number of coil turns (N), average coil diameter (d_{avg}), and permeability constant (μ), as shown in the equation above, φ is the fill factor, ranging from 0 (turns concentrated on the perimeter) to 1 (turns spiraling toward the center). Using the values from Table 3.2, we can determine the most appropriate coefficients for our specific geometric configuration.

Table 3.2: The coefficients for various coil shapes in a geometric arrangement.

Shape	C_1	C_2	C_3	C_4
Square	1.27	2.0	0.18	0.13
Hexagonal	1.09	2.23	0	0.17
Octagonal	1.07	2.29	0	0.2
Circular	1	2.46	0	0.2

- ***The quality factor Q***

In the context of magnetic resonance wireless power transfer (MR-WPT), the efficiency calculation relies not only on the coupling coefficient (K) but also on the quality factor (Q-factor) [110]. The quality factor is a critical parameter in the power transfer efficiency equation and is calculated using the following formula:

$$\mathrm{Q} = \frac{\omega L}{R} \quad (3.31)$$

Where ω represents the angular frequency, L is the self-inductance, and R is the total parasitic resistance of the coil.

Taking the skin effect into consideration, the total parasitic resistance R, is computed as follows [100]:

$$\mathrm{R} = \mathrm{R_{dc}}\frac{\mathrm{t_c}}{\delta\left(1-\mathrm{e}^{\frac{\mathrm{t_c}}{\delta}}\right)} \quad (3.32)$$

where R_{dc} represents the DC resistance: $\mathrm{R_{dc}} = \rho_c\frac{\mathrm{l_c}}{\mathrm{wt_c}}$; $\delta = \sqrt{\frac{\rho_c}{\pi\mu f}}$; $\mu = \mu_r\mu_0$, and

$l_c = 4N[d_{out} - (N-1)s - N \times W] - s$, t_c: Thickness of the conductor; f: operating frequency; ρ_c: resistivity of the conductor; μ: permeability constant; μ_r: relative permeability; l_c: length of the conductor; δ: depth of skin.

The angular frequency of resonance ω is calculated as follows:

$$\omega = \frac{1}{\sqrt{LC}} \tag{3.33}$$

To enhance a coil's efficiency in the megahertz (MHz) frequency range, it is imperative to design coils with increased self-inductance and lower losses. The quality factor is directly linked to the WPT efficiency. Achieving a high transfer quality factor in a constrained space involves optimizing the geometric parameters of the coil. While larger coils can facilitate higher power transfer efficiency by inducing more magnetic fields between transmitter and receiver coils, they tend to be bulky and unsuitable for smaller applications [111]. Tuning the Q-factor of a coil is a strategy for improving both distance and power transfer efficiency. A higher Q-factor allows the coils to reach maximum amplitude and resonance, minimizing energy loss and contributing to efficient power transfer. Thus, maintaining the same resonant frequency in the transmitter-receiver coil pair reduces energy loss, alongside considerations such as the number of coil turns and coil diameter. It is crucial to understand the influence of the coil's geometric parameters on the quality factors to improve the effectiveness of WPT. By recognizing how these factors impact the overall performance of the system, we can enhance efficiency and ensure optimal results [112].

3.4.3.2. Design in 3D Ansys Maxwell using FEM

The efficiency of WPT systems, as well as the performance of other electromagnetic devices, relies on accurate estimations of flux linkage and core loss [103]. However, these measures are highly nonlinear concerning input parameters, often due to saturation effects. This can make it difficult and inaccurate to predict the relationship between a WPT system's efficiency and geometric parameters using analytical expressions. Numerical methods such as the finite element method (FEMs) can create complex models that accurately determine the magnetic field distribution [5].

Various software tools are available for coil simulation based on the finite element method, and Ansys Maxwell 3D software is the most commonly used in electromagnetic field simulation. By using Maxwell's 3D design, we can simulate the behaviour of coils under various conditions

and analyze their performance. This section presents the step-by-step simulation coils for WPT using Maxwell 3D.

Step 1: Step 1: First, we begin preparing the workspace by selecting the menu item Project after that, we select the magnetic eddy currents as our solution type.

Step 2: We draw a parametric coil using the Draw tool, and we need to select User Defined Primitive, followed by SegmentedHelix, and then PolygonHelix. After this, we define all the coil parameters, such as the spacing between the turns (S), width of conductor (W), number of turns (N), inner diameter (d_{in}), frequency (f), and distance between the primary and the secondary coil (d_{TR}) , as shown in Figure 3.10. We declare these parameters as variables and the outer diameter as a function, which makes the coil parametric and variable. This means that we can easily vary its characteristics by adjusting a single parameter. This approach simplifies the process of modifying the coil's properties, making it easy to analyse and optimize.Additionally, we chose the coil material.

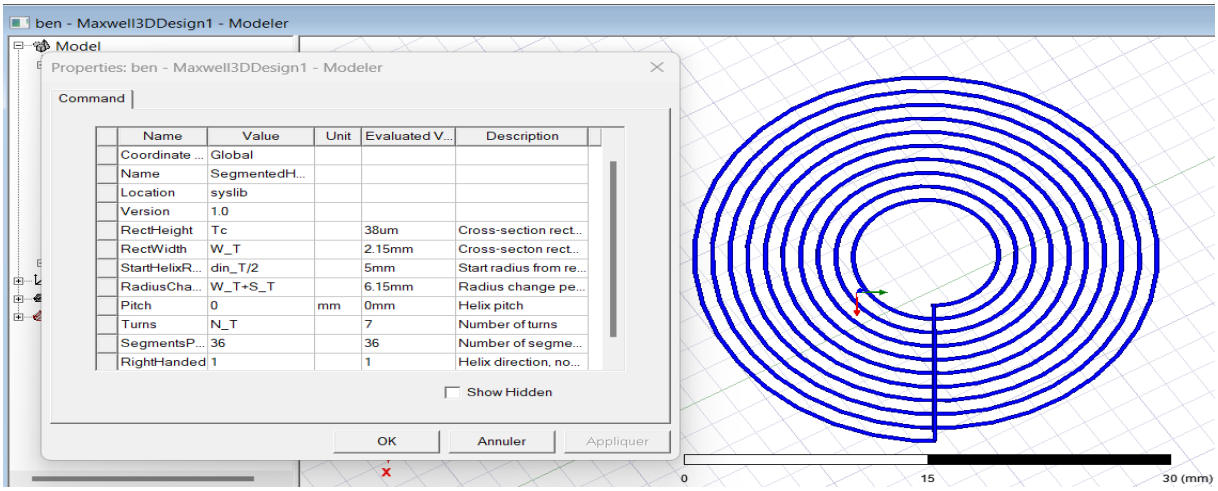

Figure 3.10: Modeling of the primary coil in 3DMaxwell.

Step 3: In this step, we create the secondary coil using the same process as the primary coil and move it to a distance of d_{TR} from the primary coil as shown in Figure 3.11. To simulate wireless power transfer (WPT), it is important to enclose the coils within a box. This box defines the simulation boundary, which helps to establish the appropriate boundary conditions for the propagation of electromagnetic fields. It also physically contains and isolates the coils, ensuring accurate modeling without external interference. Furthermore, the box helps in efficient meshing and analysis, simplifying the visualization and interpretation of the electromagnetic

field distribution and energy transfer characteristics within the simulation space. Using a box enhances the accuracy, efficiency, and ease of analysis in simulating WPT systems.

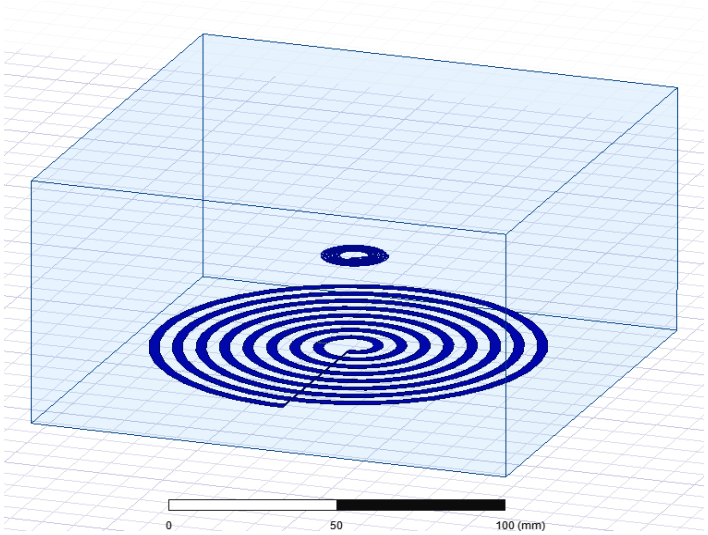

Figure 3.11: Final WPT coil design.

Step 4: We establish the boundary conditions by configuring the boundaries of each coil as insulating. Given that the coils overlap on both sides of the transmitter and receiver, practical scenarios necessitate the use of Litz wire, which inherently comes with insulation. Therefore, ensuring insulation at the coil boundaries replicates real-world conditions and facilitates accurate modeling of the electromagnetic behavior in our analysis , as shown in Figure 3.12.

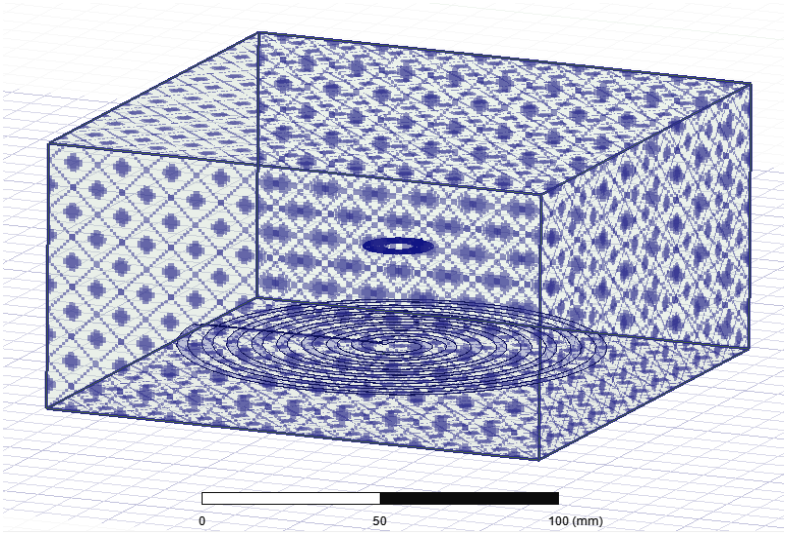

Figure 3.12: Coil boundaries.

Step 5: We model the coils using windings and coil terminals to analyse the eddy current phenomena in this system. The number of turns is represented by the number of conductors,

which we treat as a variable for each coil. In our setup, we have a total of 'N' windings, each connected to a corresponding coil on both the transmitter and receiver sides. Each winding is then individually linked to its respective coil terminal excitation.

3.5. Impact of coil parameters on WPT performance

In this section, we evaluate the characteristics of coils and analyze the impact of various parameter sets on the WPT efficiency. By systematically varying a particular parameter while keeping others fixed, we can investigate the influence of geometric parameters on electrical parameters and efficiency. Table 3.3 shows the specific parameters that remained constant during the analysis.

Table 3.3: Constant parameters of coil design.

The coils parameters	Values
Distance between coils $(\boldsymbol{d_{TR}})$	30 mm
The inner diameter of the secondary coil $(\boldsymbol{din_R})$	8 mm
The inner diameter of a primary coil $(\boldsymbol{din_T})$	10 mm
Operating frequency **(*f*)**	13.56 Mhz
Substrate thickness $(\boldsymbol{t_s})$	1.5 mm
Conductor thickness $(\boldsymbol{t_c})$	38 µm

When two coils are positioned close to each other on a surface with no air gap separating them, the degree of coupling between them is likely to increase. This means that the magnetic field produced by one coil will have a greater effect on the other, resulting in a stronger electrical connection. As illustrated in Figure 3.13, this phenomenon and shows the impact of coil positioning on the coupling strength and efficiency. It is important to consider the effects of coupling when designing coils to optimize their performance and minimize interference.

Several constraints, such as application and manufacturing constraints exist in biomedical applications when implementing inductive power transfer. To optimize the power transfer efficiency while minimizing the risk to human skin, we specifically chose a transfer distance of 30 mm and a frequency of 13.56 MHz. This specific frequency is ideal for biomedical applications because it is compatible with most existing medical devices and can penetrate human tissue without causing any harm. By selecting these parameters, we can ensure that the IPT system operates safely and effectively in a healthcare environment.

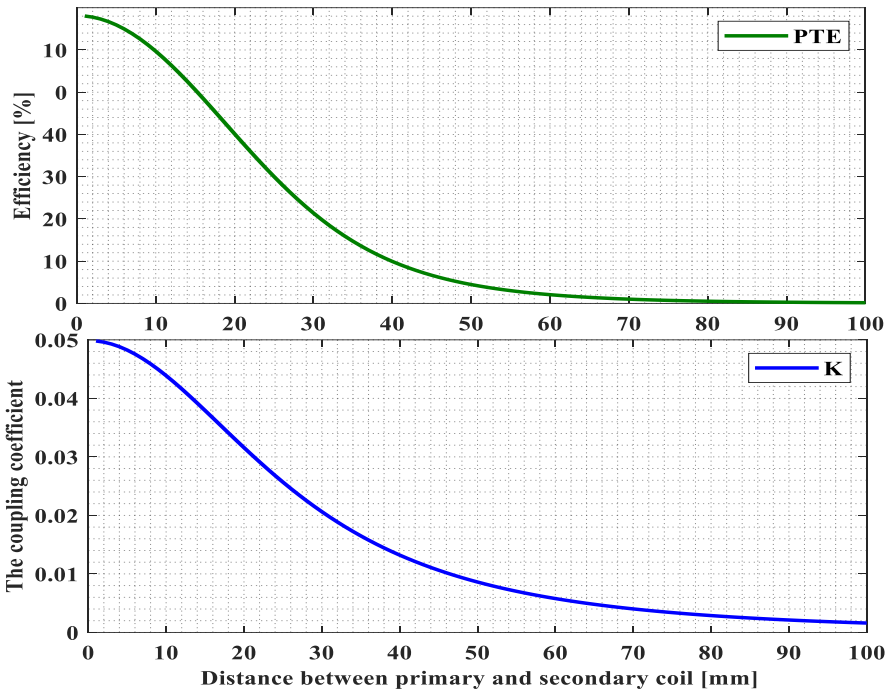

Figure 3.13: The Effect of the distance between coils on the efficiency and coupling coefficient.

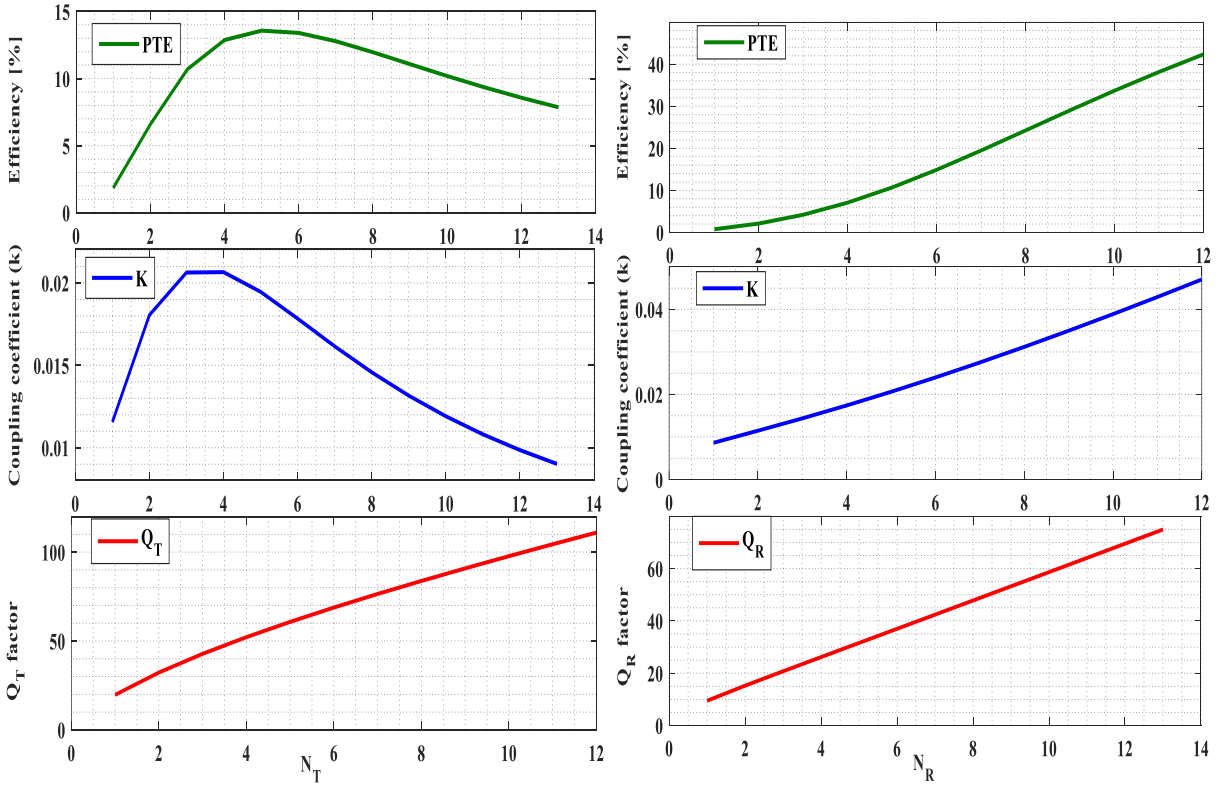

(a) (b)

Figure 3.14: WPT performances versus the number of turns in (a) primary coil and (b) secondary coil.

Figure 3.14, shows the relationships between the power transfer efficiency, coupling coefficient, and quality factor and the variations in the number of turns in the primary and secondary coils. The graph indicates an increasing relation between these factors and N_R. For the number of turns in the primary coil, we noted that with a single turn (N_T=1), the efficiency is smallest 2%. After that, as the number of turns increases, the efficiency improves, reaching a peak of 14.8% with five turns (N_T=5). Beyond this value, further increasing the number of turns results in a decrease in efficiency.

Conductors are critical to an inductive power transfer (IPT) system. They carry the current between the transmitter and receiver coils. A conductor with a larger width can significantly reduce the resistance, skin effect, and proximity effect. Figure 3.15 shows how the efficiency varies withthe conductor width of the primary and secondary coils (W_T, W_R) and reveals that increasing the conductor width (W_T, W_R) directly enhances the power transfer efficiency.

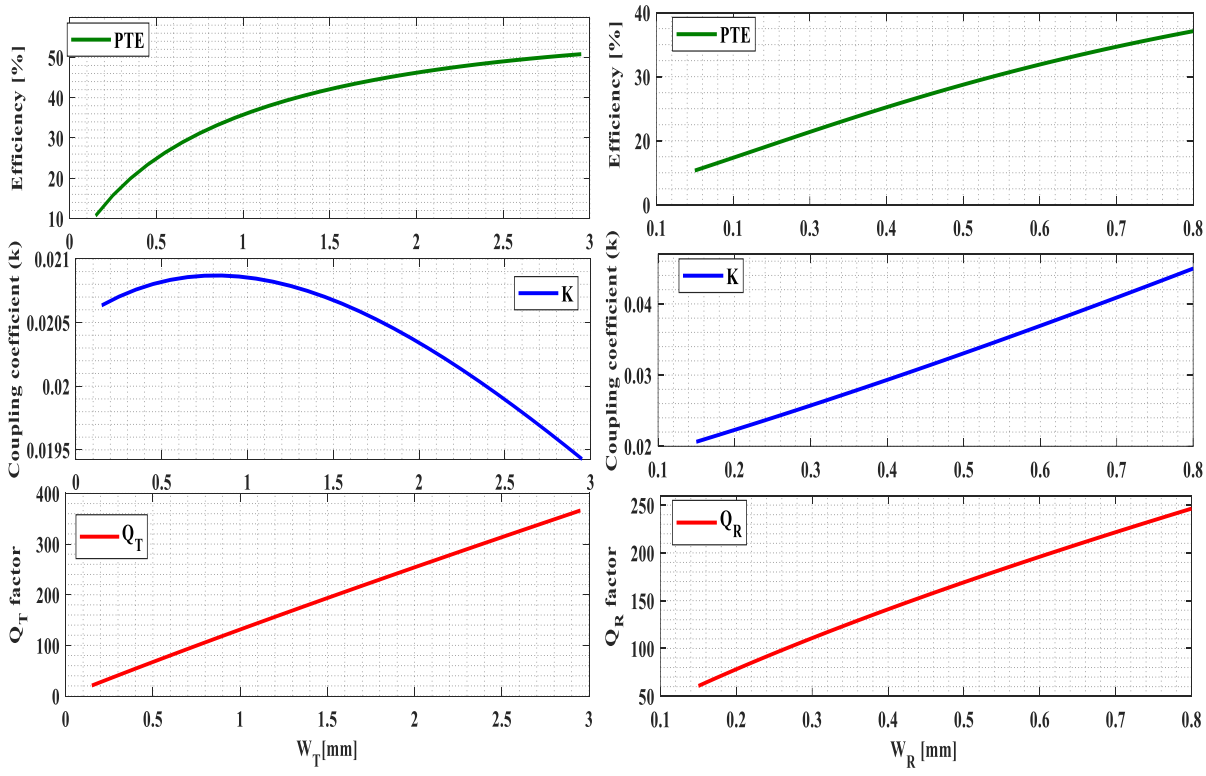

(a) (b)

Figure 3.15: WPT performance versus conductor width: (a) primary coil and (b) secondary coil.

The spacing between conductors within each coil is a significant factor in determining the strength and coupling of the magnetic field. Therefore, determining its optimal value is

important for achieving higher efficiency. Figure 3.16 shows the effect of the spacing between the turns (S_T, S_R) of the primary and secondary coils on the efficiency. The maximum efficiency is obtained for small values of S_T and decreases with increasing S_T for the primary coil. For the secondary coil, it is the opposite of S_T. We note that the efficiency is higher for large values of S_R.

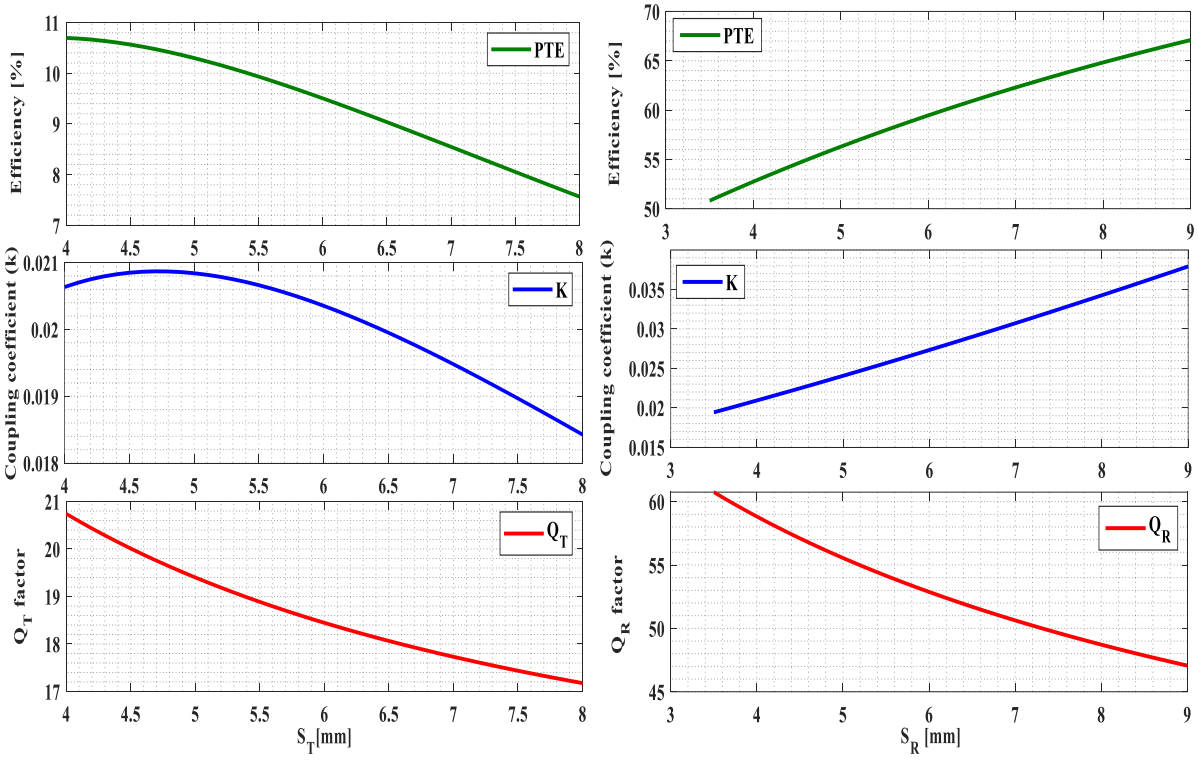

(a) (b)

Figure 3.16: WPT performances versus the spacing between turns for the (a) primary coil and (b) secondary coil

The coupling coefficient (K) and quality factors (Q_T, Q_R) are fundamental to efficiency. Higher K and Q generally translate to greater efficiency. However, their impact is not always straightforward, as Figure 3.15a demonstrates. Q_T can effectively compensate for decreased K, highlighting its crucial role in maintaining efficiency. Furthermore, a reduction in Q_R with decreasing S_R can still lead to increased efficiency as depicted in Figure 3.16b, emphasizing the complex relationships between efficiency and the quality factor and coefficient coupling. Maximizing IPT efficiency is not about maximizing one factor but about finding a balance between them. This can be achieved through a joint optimization strategy targeting $Q_T \times Q_R \times K^2$or by directly optimizing the efficiency itself.

Figure 3.17 shows the variation in efficiency according to two geometric parameters, including the number of turns between the coils (N_T, N_R), the width of the conductor (W_T, W_R), and the spacing between the turns (S_T, S_R). The aim is to show how the efficiency can be improved by combining two geometric parameters.

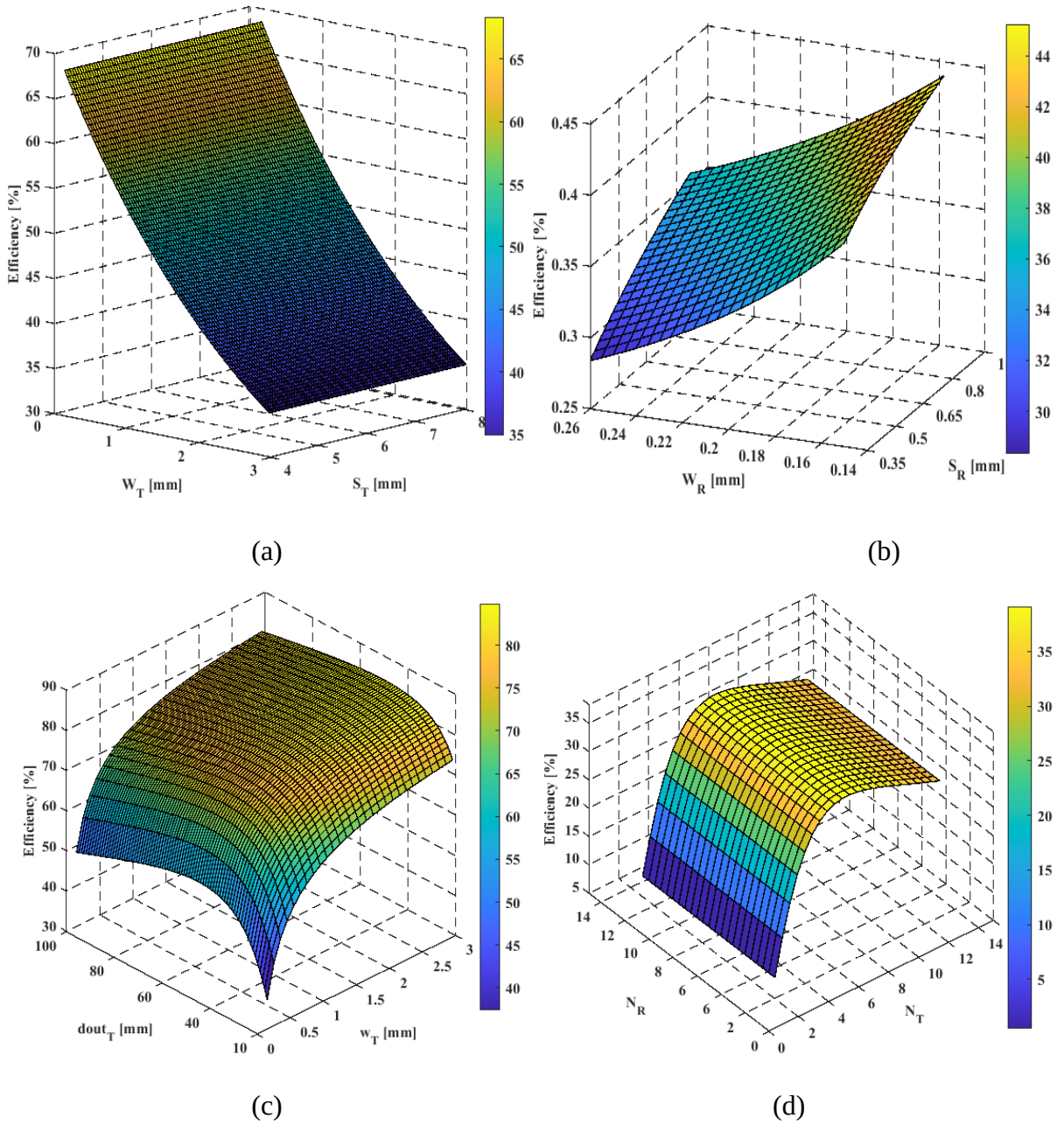

Figure 3.17: Efficiency versus coil parameters (a): Efficiency versus W_T and S_T, (b): Efficiency versus W_R and S_R, (c): Efficiency versus $dout_T$ and W_T, (d): Efficiency versus N_R and N_T.

As seen in the afreomentionned study, it is revealed that changes in geometric coil parameters significantly impact efficiency. While enhancing certain parameters results in higher efficiency, others may lead to a decrease. Therefore, achieving peak efficiency requires careful optimization of these parameters.

3.6. Conclusion

This chapter explored the modeling of resonant inductive WPT systems, particularly for bioimplantable devices. First, we presented the fundamental principles of inductive coupling, examined various topologies, and delved into the series-parallel (SP) resonant inductive link, providing a detailed analytical model to calculate the power transfer efficiency. Then, we presented both analytical and numerical models of coil structures. Finally, we studied the impact of geometric coil parameters on the coupling coefficient, quality factor, and power transfer efficiency, demonstrating the need to optimize the coil parameters of the WPT for maximum efficiency.

In next chapter, we will present optimization methods based on analytical and numerical models to determine the optimal geometric parameters for maximizing transfer efficiency.

Coil design for high efficiency wireless power transfer

Chapter 4

4.1. Introduction

when designing a WPT system via inductive coupling, the power transfer efficiency (PTE) emerges as the most important critical factor to consider. The design of a highly efficient WPT system is notably challenging due to the specific design constraints required for its application. For instance, the WPT systems applied in biomedical implants, sensor applications, or IoT devices necessitate compact receiver coils while also maintaining a high PTE. The optimal PTE is achieved when both coupling and quality factors of the coils are maximized. This chapter addresses the geometric design and optimization of resonant inductively coupled spiral coils to power a biomedical implant. Coil optimization is a potent means to significantly boost WPT efficiency. Therefore, achieving maximum efficiency requires optimizing the coils' geometric parameters. For this purpose, within this chapter, the detail procedure of the coil design and optimization of the WPT system is discussed. The focal point is the optimization of the geometric parameters of the circular spiral coil with a planar shape, which is designed for a series-parallel (SP) inductive coupling WPT system intended for biomedical use. Initially, an analytical approach implementing either iterative or metaheuristic optimization methods was proposed. This approach utilizes simple mathematical models to approximate the coil parameters and link efficiency values. Subsequently, a numerical simulation based optimization approach (GA-FEM) is presented; the GA-FEM integrates the finite element method (FEM) with a genetic algorithm (GA) as a search strategy.

4.2. Geometric coil design of a WPT system based on an analytical approach

The performance of a WPT depends on various design aspects, including the WPT coil size, transfer distance, frequency, and coil characteristics. The coils notably impact the WPT efficiency. To enhance this, the primary optimization targets are the quality factor of the coils and the coupling coefficient between them, assuming an optimum load state. High-quality factor coils benefit from a low AC resistance while maintaining a high inductance. In certain WPT applications, such as for biomedical implants, the receiving coil needs to be compact. This necessitates a coil design methodology that accommodates constraints on coil size. This thesis aims to develop a method for identifying the optimal coil parameters for WPT applications to maximize efficiency while considering the constraints on the receiving coil size. To this end, we have employed various optimization methods: iterative and metaheuristic methods.

The optimization problem can be formulated as follows:

$$\begin{cases} \eta = \max(f(\mathrm{N_T}, \mathrm{N_R}, \mathrm{S_T}, \mathrm{S_R}, \mathrm{W_T}, \mathrm{W_R})) \\ \text{Subject to: } d_{outR} = f(N_R, S_R, \mathrm{W}_R) \leq 20mm \end{cases} \quad (4.1)$$

Within such design approaches, specific parameters are governed by the application's constraints, while others must be meticulously selected to guarantee optimal values of inductive link efficiency. The design constraints and initial values are given in Table 4.1.

Table 4.1: Design constraints and initial values

Parameters		***Symbol***	***Design value***
Design constraints	Operating frequency	f	13.56 MHz
	Implanted coil outer diameter	d_{outR}	≤ 20mm
	The relative distance between coils	d_{TR}	30 mm
	Secondary loading resistance	R_L	300 Ω
	Conductor thickness	t_c	38 µm
	Substrate thickness	t_s	1.5 mm
Initial values	Receiver inner diameter	d_{inR}	8 mm
	Transmitter inner diameter	d_{inT}	10 mm
	Transmitter conductor spacing	S_T	[4mm to 8 mm]
	Receiver conductor spacing	S_R	[0.35mm to 0.9 mm]
	Transmitter conductor width	W_T	[0.15mm to 3 mm]
	Receiver conductor width	W_R	[0.15mm to 0.35 mm]

4.2.1. Optimization by the iterative method (IP)

The iterative method refers to a broad spectrum of techniques that use successive approximations to obtain more accurate solutions to a linear system at each iteration. An optimization algorithm repeatedly evaluates and enhances the solutions as part of these iterative processes, progressively converging closer to an optimal or significantly improved result. This iterative characteristic permits incremental improvements and adjustments, catering to the fulfillment of the set optimization objectives. The iterations persist until a predefined condition is met [113].

This section presents a novel strategy for the iterative optimization process, aimed at determining the optimal parametric geometries for a pair of circular spiral coils. In this optimization strategy, some parameters are limited by application constraints, whereas others require deliberate selection to ensure the most favorable coil parameters and attain maximum efficiency. The figure 4.1 summarizes the steps and procedures of the proposed iterative method.

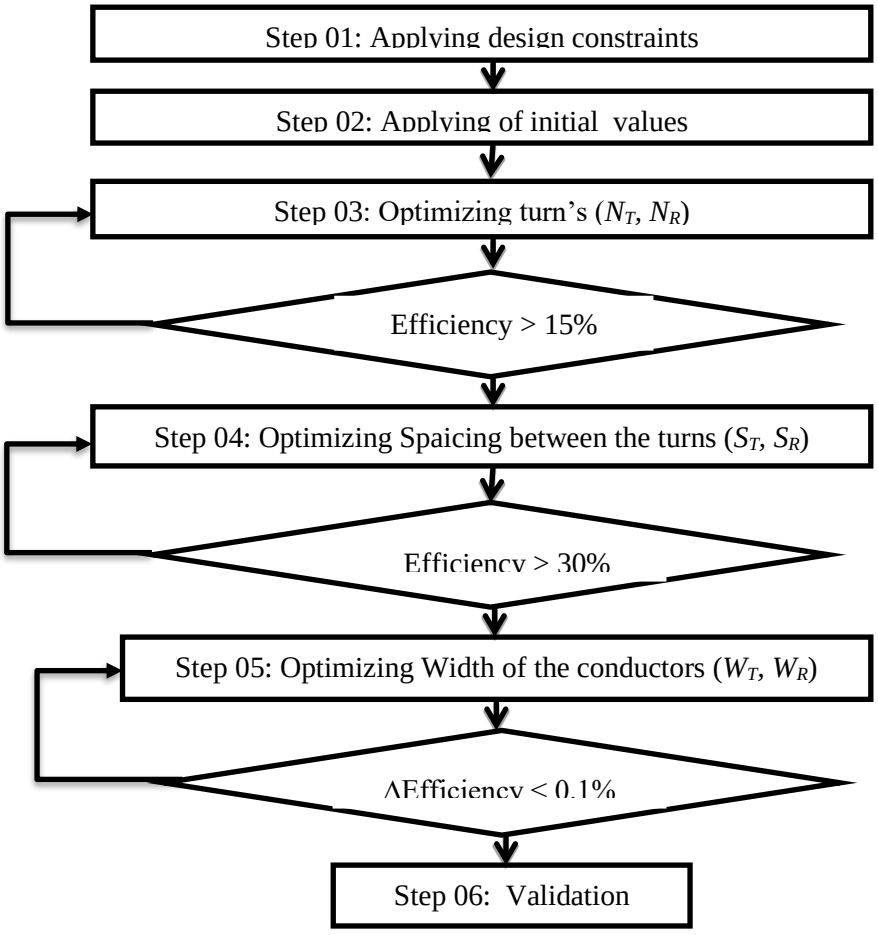

Figure 4.1: Flowchart of the iterative procedure (IP) for WPT design

Step 01: Applying design constraints

The factors associated with the chosen application impose a set of parameters affecting the power transfer efficiency. This step entails defining the design constraints of the primary and secondary coils. In our study, we focus on biomedical applications with constraints on the size of the secondary coil (the external diameter does not exceed d_{outR}=20 mm) and other factors are related to the manufacturing technology. These are the minimum sizes yielding acceptable for manufacture (such as minimum internal diameters d_{inT}=10 mm and d_{inR}=8 mm.

Step 02: Applying the initial values

In this step, we initialize the design parameters, as given in Table 4.1. For this study, the number of turns (N_T, N_R), the spacing between the turns (S_T, S_R), and the width of the conductors (W_T, W_R) for the primary and secondary coils are the selected variables to be optimized. These parameters are directly related to the outer diameter, defined according to equation (3.28). It is worth noticing that we have meticulously chosen the minimum width and spacing to be the minimum achievable values based on the fabrication resolution, ensuring the utmost precision in our study. These values are set as follows: N_T= 2, N_R= 2, S_T = 4 mm, S_R = 0.35 mm, and W_T, = W_R = 0.15 mm.

Step 03: Optimize the number of turns of the primary and secondary coils.

In this step, we will optimize the number of turns of the primary and secondary coils with a fixed width of the conductor and the spacing between the turns of the transmitter and receiver coil. equations (3.22) to (3.32) are applied using initial values from the previous two steps to determine the efficiency when N_T and $N_R$are in the ranges [2 to 13] and [2 to12], respectively. We observe a substantial increase in the optimum efficiency by 44% , as shown in Figure 4 .2, corresponding to primary and secondary coil turns number of 6 and 9, respectively. Following this, optimization turns numbers yielding an efficiency exceeding 15% are retained for the subsequent optimization step.

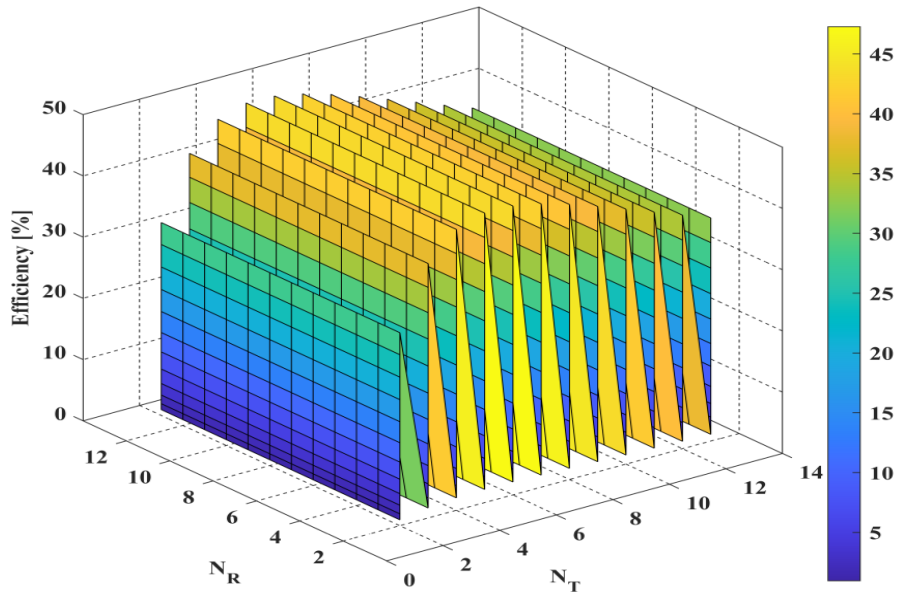

Figure 4.2: Optimization of the number of turns of primary and secondary coil.

Step 04: Optimize the spacing between the turns of the primary and secondary coil. After determining the number of turns in step 3, we focus on the spacing between the turns of the primary and secondary coils (S_T and S_R). We optimize it within the intervals [4mm, 8mm] and [0.35mm, 0.9mm], respectively.

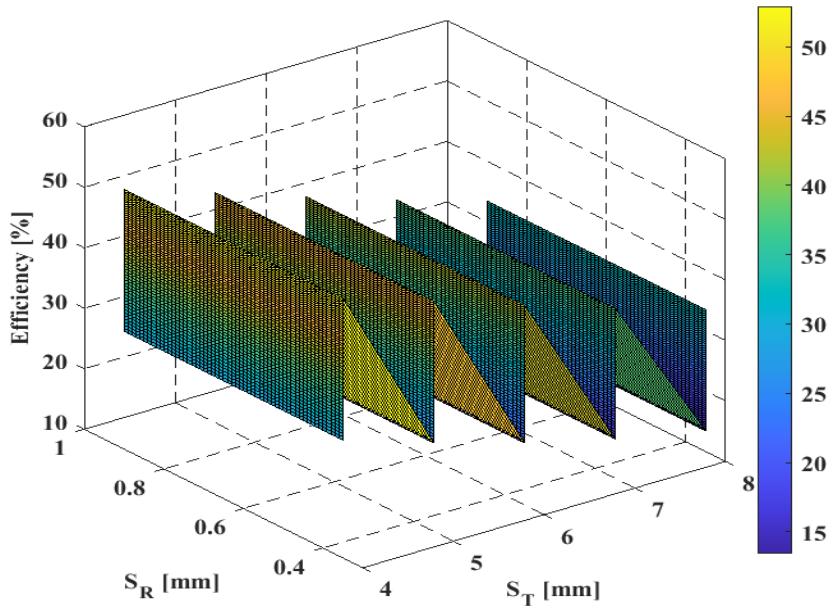

Figure 4.3: Results after optimization of spacing between the turns of primary and secondary coil.

Figure 4.3 shows that the maximum efficiency is achieved at the minimum value of the spacing between the turns, defined by S_T = 4 mm and S_R= 0.35 mm, with an efficiency of 48%. The results show an improvement of 4% compared to the previous step because the values optimal of S_T and $S_R$takes their initial values. After that, as the spacing between the turns increases, the value of efficiency decreases. We passe to the next step, if the efficiency was greater than 30%.

Step 05: Optimize the width of the conductor of the primary and secondary coils.

In this step, we optimize the width of the conductor W_T and W_R in the intervals [0.15 mm, 3mm] and [0.15 mm, 0.35 mm], respectively. For this step, we applied the optimal values resulting from steps 3 and 4 (N_T = 6, N_R= 9, S_T = 4mm, S_R = 0.35mm). The obtained values are W_T = 3 mm and W_R= 0.25 mm, with an efficiency of 78% , as shown in Figure 4.4. The results show an improvement of 177% compared to step 3.

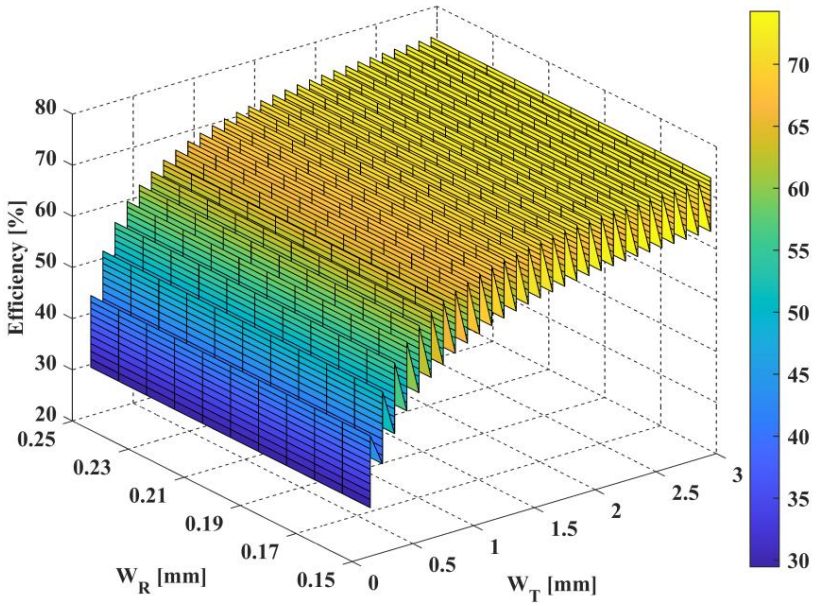

Figure 4.4: Results after optimization of the width of the conductor of the primary and secondary coils

Step 06: Improvement of the efficiency

The efficiency values from step 5 have been significantly improved compared to those from step 3. However, we can achieve further improvement by iterating through steps (3 and 5). Iterations continue until the objective of less than 0.1% improvement per iteration is reached. Finally, the optimal parameters obtained using the IP method is summarized in Table 4.2.

Table 4.2: Optimal inductive link coil designs using an iterative procedure.

Parameters	Initial value	Optimal value
N_T	2	6
N_R	2	9
W_T [mm]	0.15	3
W_R [mm]	0.15	0.25
S_T [mm]	4	4
S_R [mm]	0.35	0. 35
d_{outR} [mm]	10	20
d_{outT} [mm]	32	90
Efficiency (η)	3%	78%
Validation by FEM	0.8%	70%

4.2.2. Optimization by metaheuristic methods

Metaheuristics, such as genetic algorithms (GAs) and coyote optimization algorithms (COA), have proven highly effective in optimizing WPT systems, addressing the significant challenge of achieving efficient designs and higher levels of efficiency in this field.

These algorithms involve three fundamental processes. First, we define the problem we aim to solve by establishing the fitness function, calculating the efficiency of the inductive link from equations 3.22 to 3.33, and identifying the number of variables. Second, setting the algorithm parameters is highly important. This includes determining the number of iterations, a critical factor in configuring the optimization algorithm. Third, a new population is generated by changing the existing solutions, which helps explore potential solutions. In this optimization process, the number of turns (N_T, N_R), the spacing between the turns (S_T, S_R), and the conductor width (W_T, W_R) are the variables. The algorithms that are used in this process as follows:

4.2.2.1. Genetic Algorithm (GA)

The genetic algorithm (GA) is a powerful metaheuristic search method that utilizes the principles of natural evolution to generate optimized solutions for a wide range of complex problems. The algorithm involves creating a diverse population of individuals, each with its own unique set of chromosomes representing optimized parameters[114]. These chromosomes are subject to three primary genetic operators: selection, crossover, and mutation. Individuals with higher fitness scores are more likely to survive and reproduce in the selection process. The crossover operator then combines the genetic material of two individuals to create offspring that inherit traits from both parents[115]. Finally, the mutation operator randomly alters some of an individual's genetic material to introduce new variations into the population. Repeating

these steps gradually makes the population more refined and eventually converges to an optimal solution. This is achieved by gradually weeding out individuals with lower fitness scores and retaining those who perform better. As the population evolves, it becomes increasingly specialized and better suited to the problem[116]. The flowchart in Figure 4.5 describes the optimization process based on genetic algorithms (GAs). As the design criterion is to maximize the transfer efficiency constrained by the limited size of the secondary coil, the fitness function is defined as equation (4.1).

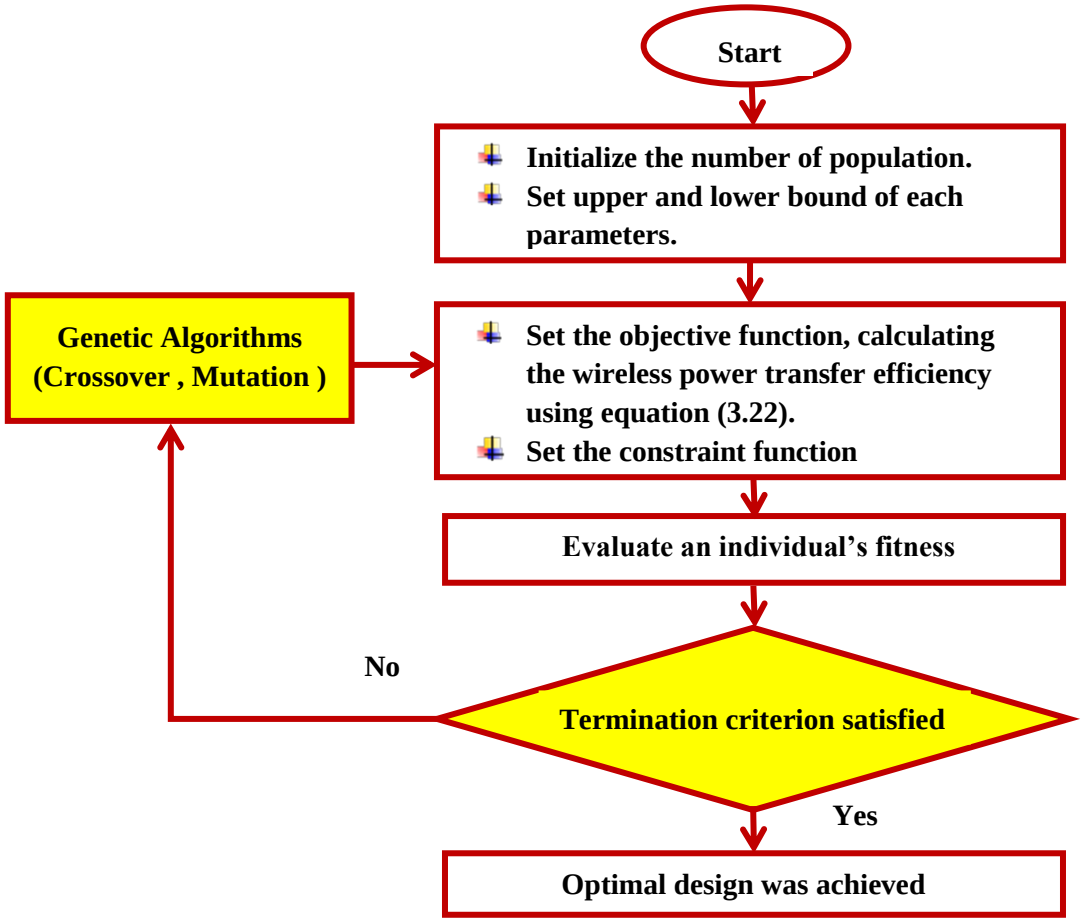

Figure 4.5: Flowchart of genetic algorithms for WPT design.

Step 01: In this step, we configure the optimization process by defining the population size(N_{pop}), the number of iterations ((N_{it}), and the number of variables (N_{var}), which in this case are six: the number of turns (N_T, N_R), the spacing between turns (S_T, S_R), and the conductor width (W_T, W_R) for both the primary and secondary coils. Furthermore, we establish minimum and maximum values for each variable, as detailed in Table 4.1.

Step 02: When using a genetic algorithm, the first and foremost step is understanding and clearly defining the problem we aim to optimize. We must precisely define the objective function to be optimized. In fact, this objective function is based on the calculating of the WPT efficiency using equations 3.22 to 3.33.

Step 03: To ensure the proper functioning of an implantable medical device, several factors related to the size of the device's secondary coil must be considered. The secondary coil must be as small as possible to minimize the device's overall size. Additionally, we must respect a fabrication constraint requiring the spacing between turns to be greater than the conductor width. These constraints are all outlined in detail in Table 4.1.

Step 04: In this step, we evaluate the fitness of each chromosome within the population using the objective function, which serves as its efficiency.

Step 05: Select the fittest chromosomes in a population to parent the next generation through a fitness-proportionate or rank-based selection method. The selected parents are combined using a crossover operator that swaps genes between parent chromosomes to create new solutions. To add diversity to the population, a mutation operator is applied to some offspring by randomly changing some genes on the chromosome. The offspring's fitness is evaluated using the objective function, and the fittest offspring are selected to form the next generation.

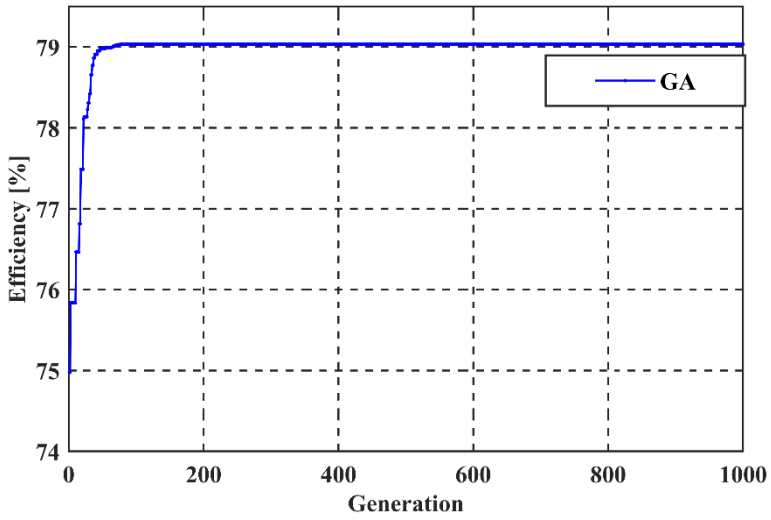

Figure 4.6: Efficiency optimization by GA.

This process is repeated until a specified stopping criterons is met, such as a maximum number of generations or a fitness level. In this optimization, the process is terminated after 1000 generations, and the final optimal values of the geometric characteristics and maximum

efficiency are provided in Figure 4.6 and Table 4.3. Figure 4.6 demonstrates the effectiveness of genetic algorithms in optimizing coil parameters, achieving 79% efficiency in a WPT system.

Table 4.3: Optimal inductive link coil designs using GA

Parameters	Analytical-GA
N_T	6
N_R	10
W_T [mm]	3
W_R [mm]	0.25
S_T [mm]	4
S_R [mm]	0.35
d_{outR} [mm]	20
d_{outT} [mm]	90
Efficiency (η)	79%
Validation by FEM	70%
Computational time	95 s

The evolution of the geometric coil parameters over generations is illustrated in Figure 4.7. Clearly, it shows the rapid convergence of the GA algorithm, finding optimal coil parameters within approximately 40 generations.

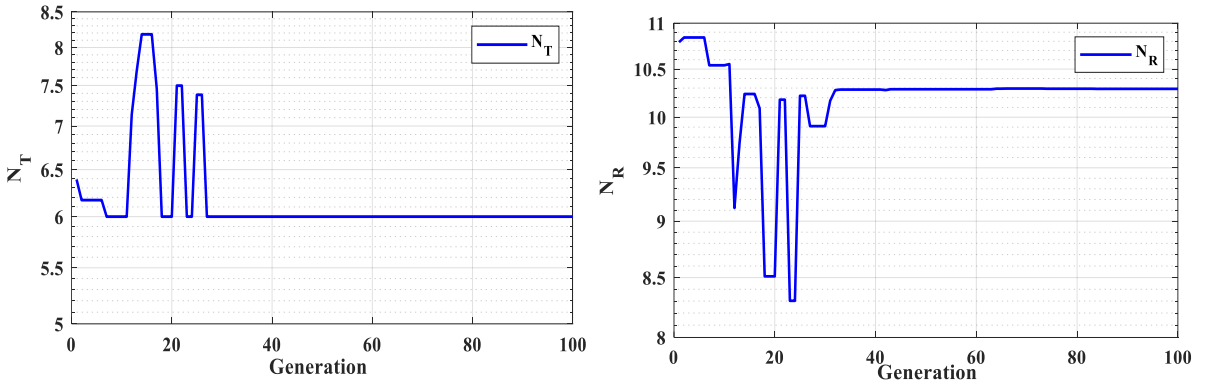

(a)

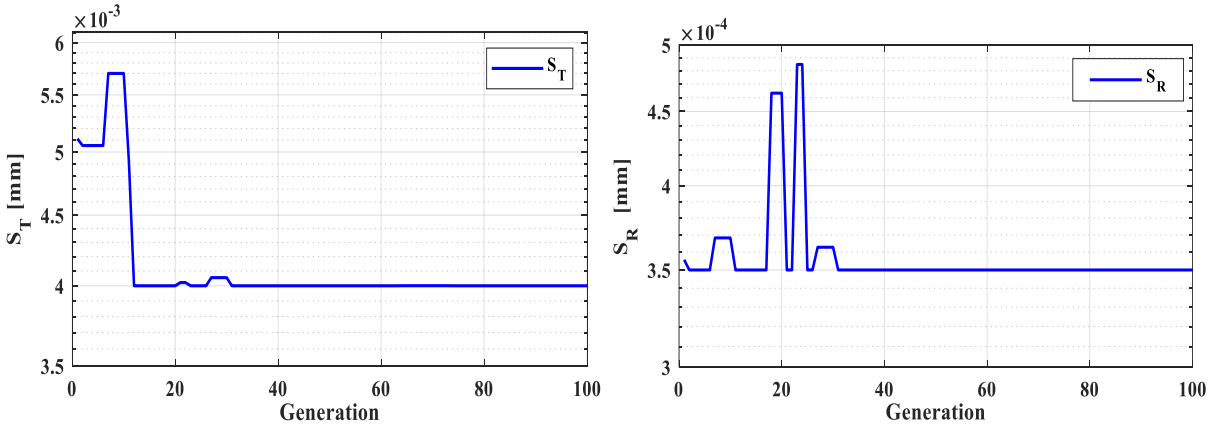

(b)

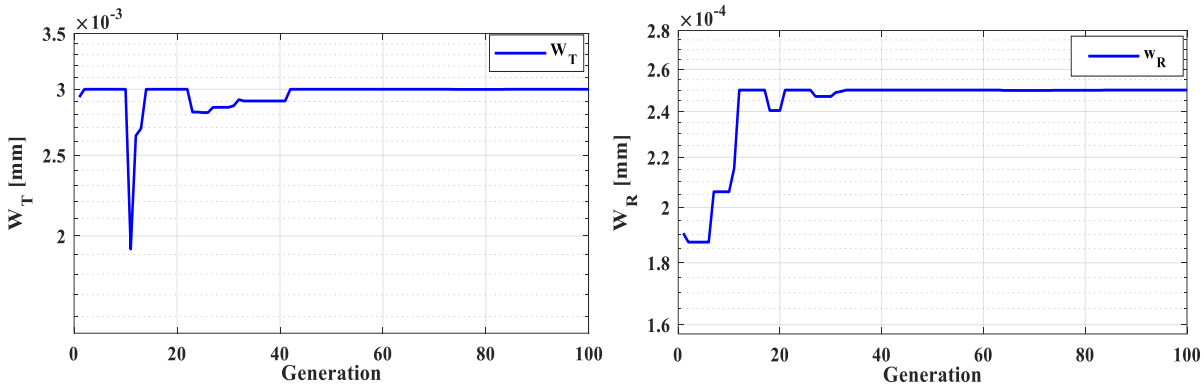

(c)

Figure 4.7: Geometric parameters versus the number of generation: (a) number of turns, (b) spacing between conductors, and (c) width of conductors.

4.2.2.2.The Coyote Optimization Algorithm (COA)

The coyote optimization algorithm (COA) is a nature-inspired optimization algorithm inspired by the hunting behavior of a coyote. Researchers in the optimization field first introduced the COA in their study published in 2018 [117]. The COA algorithm begins by initializing a population of coyote agents randomly generated at the start. Once the fitness function has been defined, each coyote's fitness is evaluated based on the given parameter. The coyote with the highest fitness value is then updated, and based on its position and each coyote's position; the position of each coyote is calculated. The algorithm continues to iterate through this process until a stopping criterion is met; at this point, the algorithm terminates. The stopping criterion can be any predefined condition, such as reaching a certain number of iterations or achieving a satisfactory fitness level [118].

This process starts by assigning the birth rate of coyotes (x), The social state (SOC) of the c^{th} coyote in the p^{th}pack of the j^{th} dimension, can be initialized in the following ways [7]:

$$x = (x_1, x_2, x_3, \dots \dots . x_j) = SOC_C^{p,t} \tag{4.2}$$

$$SOC_{C,j}^{p,t} = lb_j + r_j\left(ub_j - lb_j\right) \tag{4.3}$$

where r_j is a random variable such as $r_j \in [0,1]$, lb_j and ub_j represent lower and upper limits respectively. The fitness function that describes the coyotes' adaptability to the social environment can be calculated as follows:

$$f_C^{p,t} = f_C^{p,t}\left(SOC_C^{p,t}\right) \tag{4.4}$$

Coyotes are known to form packs (N_C) during the beginning of their reproductive process, with a certain probability (P_e) of leaving their existing groupings.

$$P_e = 0.005 * N_C^2 \tag{4.5}$$

The act of transferring coyotes between packs helps to enhance relationships and promote diversity within populations. One of the three alphas in COA ($alp^{p,t}$) is selected and presented in the following manner:

$$alp^{p,t} = \left\{ SOC_C^{p,t} \middle| arg_{C=(1,2,\ldots..,N)} \ min f\left(SOC_C^{p,t}\right) \right\} \tag{4.6}$$

In the field of COA, it is assumed that every coyote has a similar level of social organization and culture. Therefore, the information gathered from coyotes is analyzed and interpreted as a collective cultural tendency, as described below [119]:

$$Culture_j^{p,t} = \begin{cases} O^{p,t}_{\frac{(N_C+1)}{2},j} & N_C \ is \ old \\ \frac{O^{p,t}_{\frac{N_C}{2},j} + O^{p,t}_{\frac{(N_C+1)}{2},j}}{2} & otherwise \end{cases} \tag{4.7}$$

The coyote population's organized social structure at a specific moment in park *P* is represented as $O^{p,t}$. The creation of a young coyote will be portrayed by taking into account the social circumstances of two randomly selected parents and the influence of the environment.

The social conditions of r_1 and r_2 at time t are denoted by $SOC_{r1,f}^{p,j}$ and in the p^{th} *pack*. The two ends of the problem are identified as $j_1$and j_2, where R_j is the random number within the set limits. COA calculates the ages of coyotes, known as $C^{p,t}$ using the following method:

$$pup_j^{p,t} = \begin{cases} SOC_{r1,f}^{p,j} rnd_j < p_{sc} & or \ \ j = j_1 \\ SOC_{r2,f}^{p,j} \quad rnd_j < p_{sc} + p_{ac} & or \ \ j = j_2 \\ R_j & Otherwise \end{cases} \tag{4.8}$$

Finally, p_{sc} and p_{ac} represent the probabilities of scattering and association, respectively, which are computed as follows:

$$p_{sc} = \frac{1}{D} \tag{4.9}$$

$$p_{ac} = \frac{(1 - p_{sc})}{D} \tag{4.10}$$

with *D* is the task dimension. The different rules are enforced to govern the birth and death of coyotes. Algorithm 1 shows the synchronism of the birth and death of coyote (where ω is the group that adjusts least to the environment than young ones, and φ is the group of coyote that adjusts less to the group size) [120].

Algorithm1. Synchronism of the birth and death of the coyotes.

Calculate ω and φ
If $\varphi = 1$ *then*
    Retain the young coyote and eliminate the only coyote in φ
else if $\varphi > 1$ *then*
    Retain the young coyote and eliminate the oldest coyote in ω
Else
Eliminate the young coyote
End if

Assuming that the coyotes are subject to the alpha impact (*δ1*) and group effect (*δ2*), the calculation can be recalculated as:

$$\delta_1 = alp^{p,t} - SOC_{C_{r1}}^{p,t} \tag{4.11}$$

$$\delta_2 = Cult^{p,t} - SOC_{C_{r2}}^{p,t} \tag{4.12}$$

The equilibrium point of a coyote is altered based on the alpha and pack influences, where C_{r1} and C_{r2} are representative of random coyotes.

$$SOC_C^{p,t,new} = SOC_C^{p,t,old} + r_1 \times \delta_1 + r_2 \times \delta_2 \tag{4.13}$$

Random numbers within the range of [0,1] are generated by a uniform probability distribution to represent the alpha and pack influence weights, denoted by r_1 and r_2, respectively. The next step involves assessing the feasibility of the new positions, followed by evaluating the fitness function under the latest social conditions.

$$fit_C^{p,t,new} = f(SOC_C^{p,t,new}) \tag{4.14}$$

To update the social situation, the conditions mentioned below must be fulfilled:

$$SOC_C^{p,t+1} = \begin{cases} SOC_C^{p,t,new} & fit_C^{p,t,new} < fit_C^{p,t} \\ SOC_C^{p,t} & Otherwise \end{cases} \tag{4.15}$$

Accordingly, algorithm 2 outlines the steps of the coyote optimization algorithm (COA). This algorithm repeatedly simulates a pack of "coyotes" (representing potential solutions) until a stopping condition is met.

Algorithm 2. Pseudo code of coyote

Create ***Np*** packs with ***Nc*** coyotes in each pack using ***equation (4.3)***
Assess the adaptation of each coyote ***equation (4.4)***
while stopping criteria satisfied **do**
for each **P** pach **do**
find the pack's alpha coyote ***equation (4.6)***
for each *cth coyote* of *pth pack***do**
Generate new social conditions ***equation (4.13)***
Check the boundary condictions ***equation (4.16)***
Estimate the new social conditions ***equation (4.14)***
Decide whether to move or not ***equation (4.15)***
end for
Simulate the brith and death of the coyotes using ***equation (4.8)*** and ***algorithm 1***
end for
Transition between packs ***equation (4.5)***
Update the coyotes' ages
end while
Select the coyote with most potential to adapt to the environment

The flowchart shown in Figure 4.8 summarizes the steps involved in the COA process for WPT optimization.

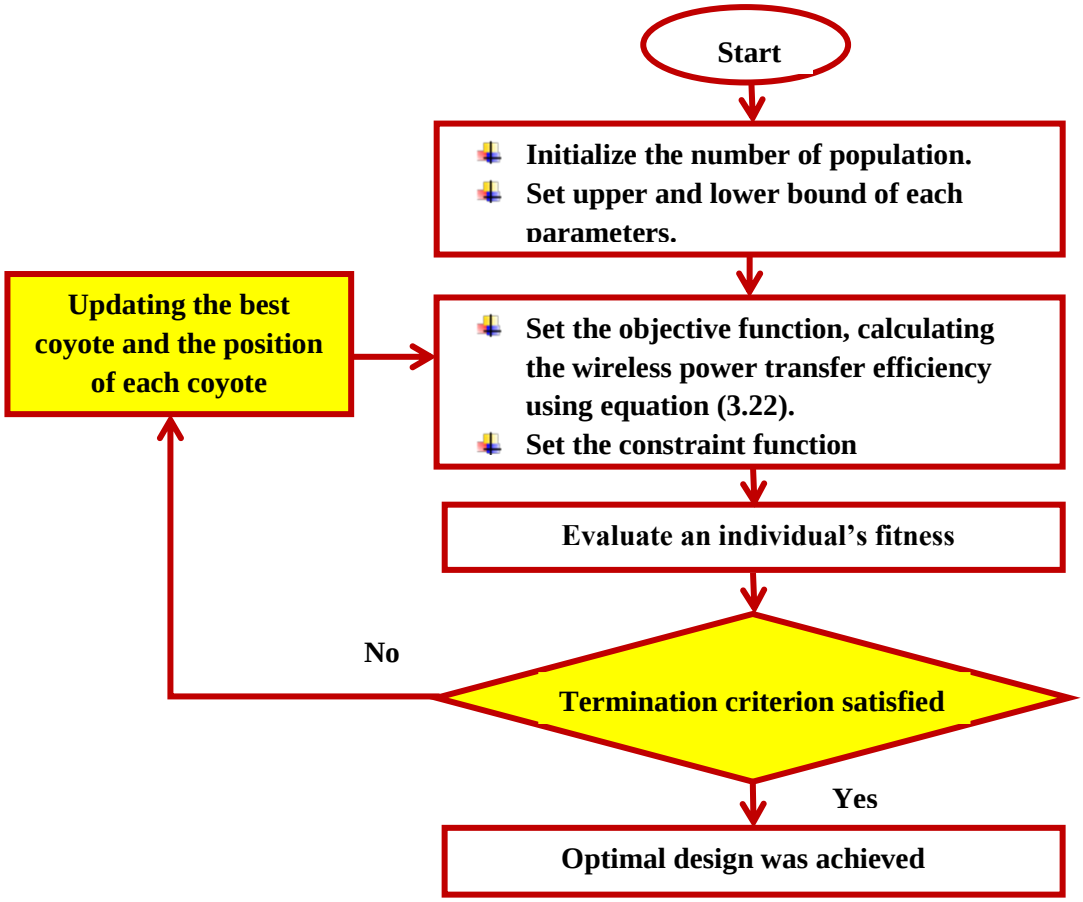

Figure 4.8: Flowchart of coyote algorithm for WPT design.

Figure 4.9 represents the optimization process results for the WPT efficiency using the coyote optimization algorithm (COA). The algorithm achieved the highest efficiency of 79.2% after 100 iterations. This presents a significant improvement over previous optimization attempts, demonstrating the effectiveness of the COA algorithm in enhancing WPT efficiency. Figure 4.10 shows the convergence curves of the individual parameters, demonstrating the exploration of the solution space by the coyote. We noted that the coyote remains active in its search for the first 200 iterations, after which it gradually stabilizes around the optimal solution. However, the stabilities of the parameters are different. For instance, the number of turns of the primary coil stabilizes approximately 800 iterations, while the other parameters reach stability before 400 iterations.

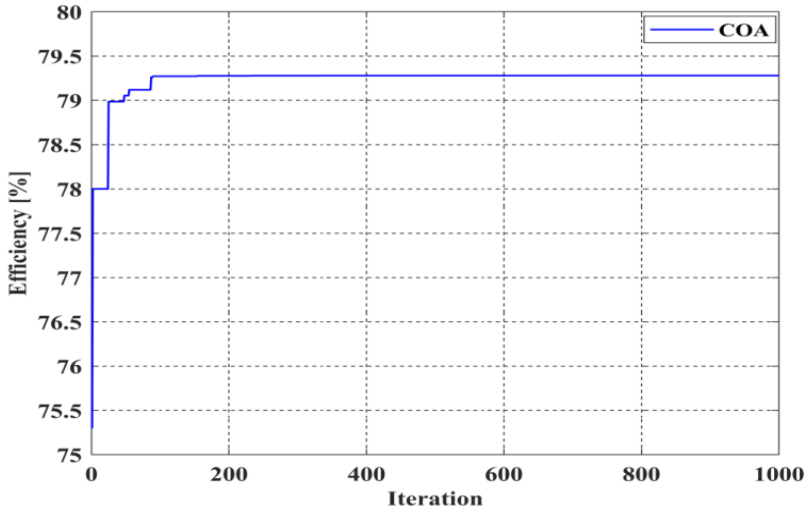

Figure 4.9: Optimization of WPT efficiency by COA algorithm

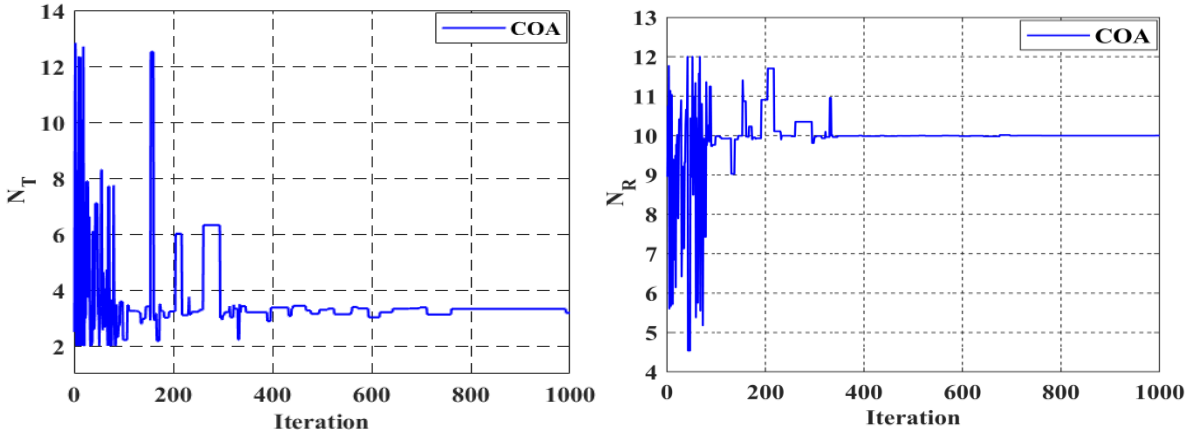

(a)

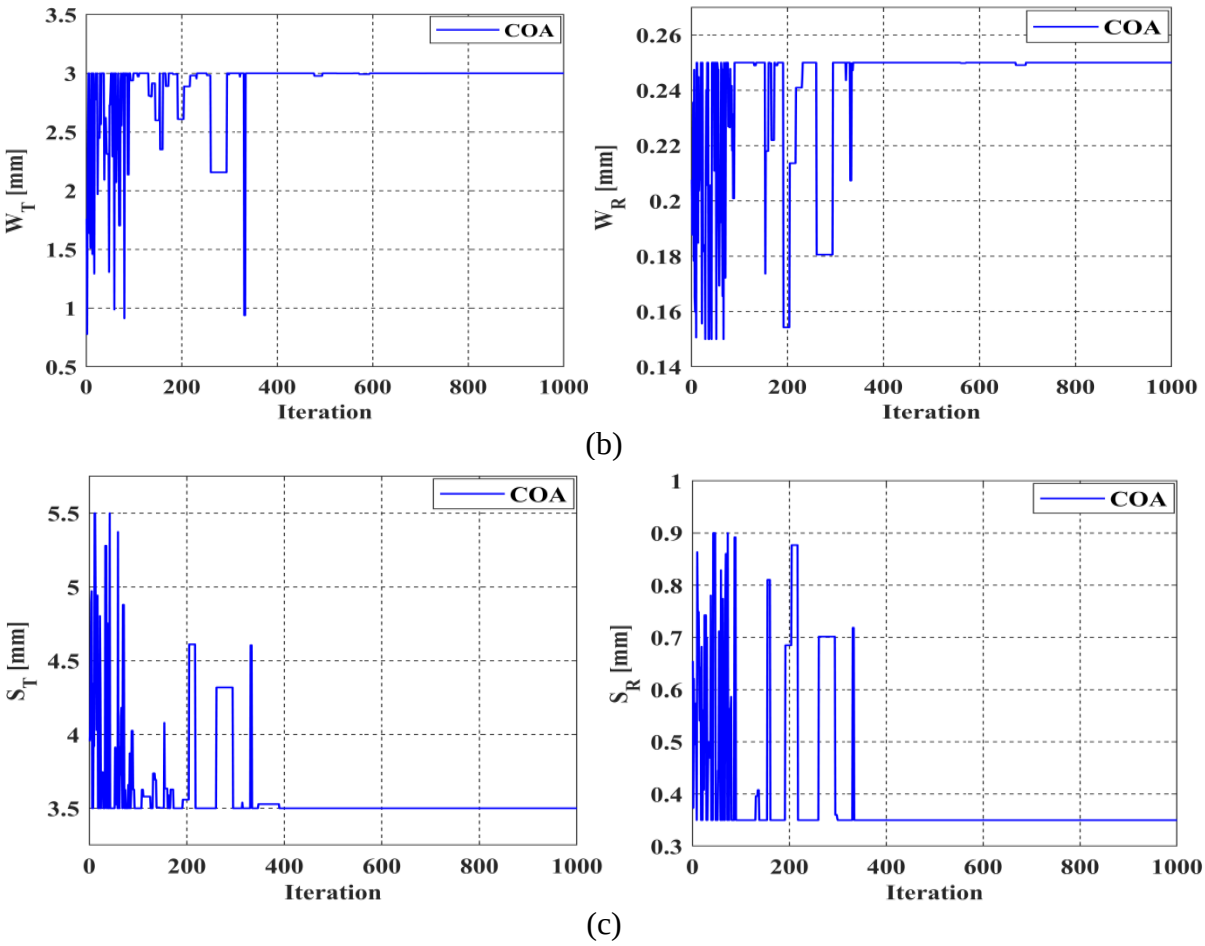

Figure 4.10: Geometric parameters versus the number of iterations: (a) number of turns, (b) width of conductors, and (c) spacing between conductors

By comparing the results from Tables 4.2, 4.3, and Table 4.4, it is evident that metaheuristic methods such as the GA and COA offer the potential for greater efficiency and faster convergence than iterative method. However, all three methods may need more accuracy. This problem can be addressed by applying metaheuristic algorithms within a numerical model.

Table 4.4: Optimal inductive link coil designs using COA algorithms.

Parameters	Analytical-COA
N_T	3
N_R	10
W_T [mm]	3
W_R [mm]	0.25
S_T [mm]	3.5
S_R [mm]	0.35
d_{outR} [mm]	19.8
d_{outT} [mm]	115
Efficiency (η)	79.3 %
Validation by FEM	71.77%
Computational time	2 min

4.3.Geometric coil design of the WPT system based on FEM

Optimization results based on analytical models often need more accuracy because they are based on mathematical expression. Calculating the objective function (efficiency) based on these models typically involves a series of complex equations, which can introduce errors and limit the precision of the optimization, such as mutual inductance. This section discusses step by step numerical GA-FEM optimization approach implemented using the Ansys Maxwell FEM simulator. It combines the finite element numerical simulation method with a GA-based search strategy, which calculates the efficiency directly from the coil geometry.

Based on Figure 4.11 and Table 4.5, we can summarize that numerical methods such as the finite element method (FEM) accurately determine the PTE and directly relate efficiency to coil geometry, offering highly precise results.

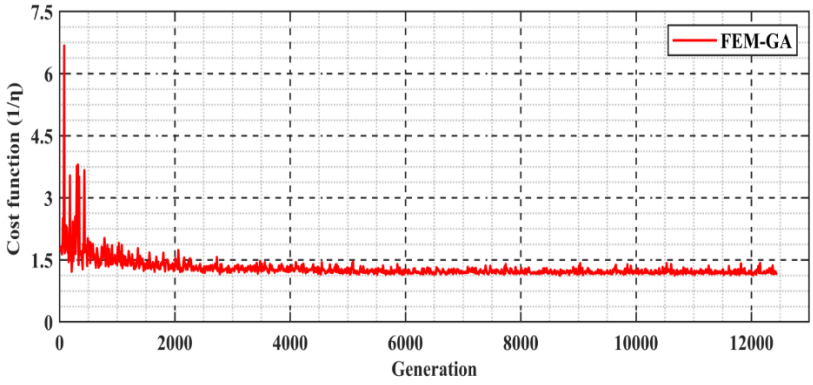

Figure 4.11: Wireless power transfer optimization using FEM-GA

However, as noted the FEM is time-consuming, which poses a significant problem in the fabrication field, where both time and accuracy are critical.

Table 4.5: Optimal inductive link coil designs using FEM-GA

Parameters	FEM-GA
N_T	8
N_R	10
W_T [mm]	2.956
W_R [mm]	0.2313
S_T [mm]	4.083
S_R [mm]	0.3792
d_{outR} [mm]	20
d_{outT} [mm]	120.5
Efficiency (η)	74%
Validation by FEM	74%
Computational time	4 months

4.4. Conclusion

This chapter demonstrates the effectiveness of metaheuristic algorithms such as GA and COA in achieving high WPT efficiency (around 79%), comparable to iterative methods (around 78%). However, the validation through FEM simulation gives an efficiency of 70%, indicating a discrepancy of approximately 9% between analytical results and simulation results. This discrepancy highlights the need of applying metaheuristic algorithms to numerical model.

FEM-based optimization using GA provides high accuracy; it has slightly lower efficiency (74%) and takes a long time compared to previous methods. This discrepancy emphasizes the need for a novel approach that integrates the strengths of both analytical and numerical methods (rapidity and accuracy). In the next chapter, we propose a novel optimization approach that fuses metaheuristic algorithms with a machine-learning model trained based on FEM data. This hybrid approach aims to overcome the problem of analytical and numerical methods.

Optimization of wireless power transfer using artificial intelligence

Chapter 5

5.1. Introduction

Traditional design methods for WPT systems suffer from numerous drawbacks, such as time-consuming computations and high error due to inaccurate model parameters. As artificial intelligence (AI) continues to gain traction across industries, its ability to provide quick decisions and solutions makes it highly attractive for system optimizations. In this thesis, a new approach for optimizing WPT parameters based on machine learning (ML) combined with metaheuristic methods is proposed. The artificial neural network is adapted for training and predicting the performance of coupled coils under a set of input parameters. The proposed approach directly predicts the efficiency of the WPT system without the need to calculate the coupling coefficient and quality factor, which can reduce the time for the optimization process.
In this chapter, the basic idea of the proposed method will be described in detail. First, we give an overview of machine learning. Second, we describe the proposed machine learning approach for predicting the WPT efficiency directly from the geometric parameters of the coils. Next, a proposed optimization procedure is constructed, combining the machine learning model and meta-heuristic methods. The procedure finds optimal geometric coil parameters. Finally, we compare our approach with the existing methods.

5.2. Artificial intelligence (AI)

Artificial Intelligence (AI) is a broad field encompassing technologies and methodologies that empower machines to mimic human intelligence by learning, reasoning, and problem-solving. AI systems utilize advanced algorithms, machine learning techniques, and data analytics to analyze vast datasets, identify patterns, and optimize various processes[121].

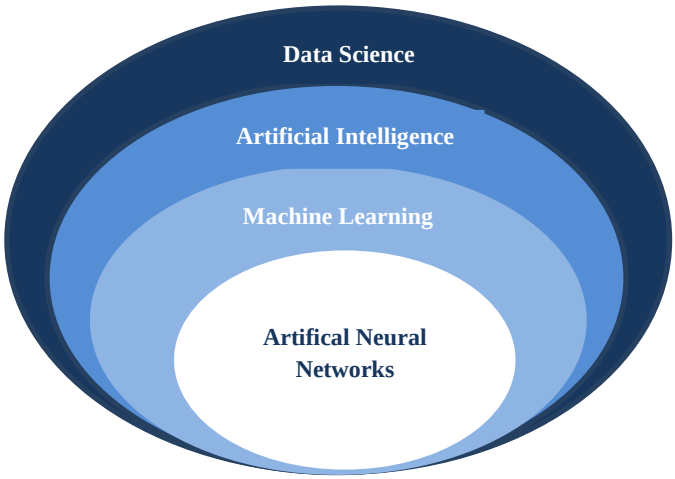

Figure 5.1: The close connection and overlap between the Artificial Intelligence fields.

Several techniques are used in artificial intelligence (AI), and the choice of technique often depends on the problem being addressed. Some of the most often used techniques in AI include [122]:

5.2.1. Machine learning

Machine learning is a subset of artificial intelligence that teaches machines to learn from data without explicit programming. It uses computational techniques to learn directly from data and improve performance over time. Machine learning approaches include supervised, unsupervised, and reinforcement learning [125, 126].

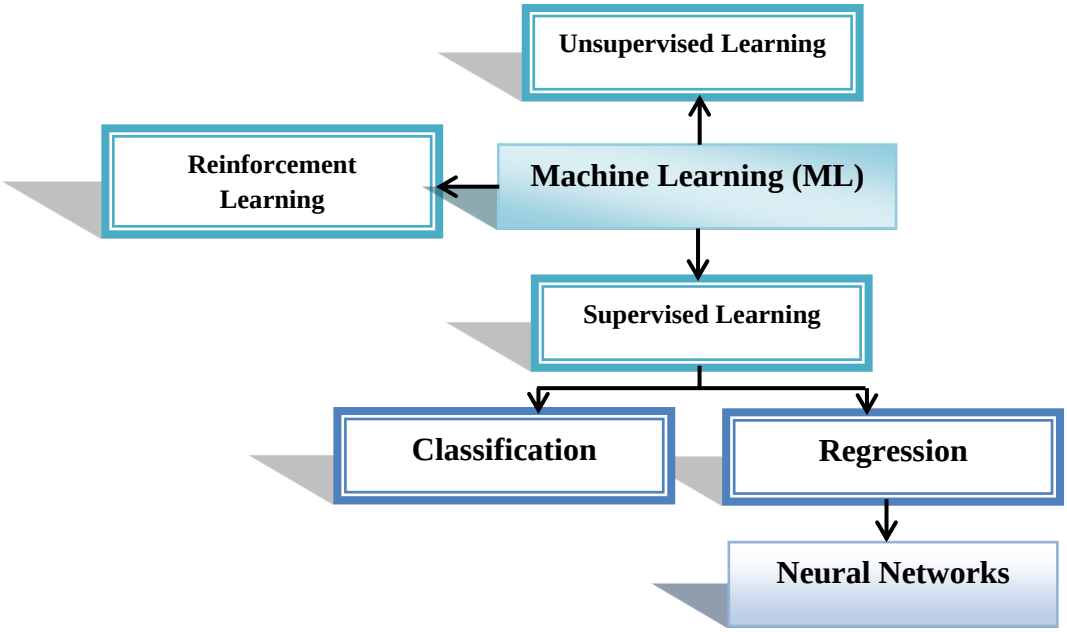

Figure 5.2: Flowchart of machine learning methods.

5.2.1.1. Supervised machine learning(SML)

Supervised learning is a machine learning method. The idea is to train the algorithm to learn based on pre-labeled examples of expected outcomes. Artificial intelligence then learns from each example by adjusting parameters to reduce the gap between the achieved and expected results. As a result, the error rate decreases throughout training so that new cases can be predicted and learning can be generalized [125].

5.2.1.2. Unsupervised machine learning (USML)

Unsupervised Learning (USML) is a type of machine learning that involves the creation of models from unlabeled datasets. This technique identifies similarities among data points and groups them into categories without any prior knowledge of the categories. There are two primary USML techniques: clustering and association rule mining. Clustering involves grouping similar items, and the features of the data determine the number of clusters. If the data items have varied features, there will be more clusters, and vice versa. Association rule mining involves finding patterns in a sequence of activities that may occur one after another [126].

5.2.1.3. Reinforcement learning

Reinforcement Learning is a powerful machine-learning technique that allows algorithms to learn from their mistakes. It can learn how to make the best decisions by directly presenting the AI program with choices. It is penalized if it makes an incorrect choice, while correct choices are rewarded. The AI strives to optimize its decision-making abilities to achieve more rewards continually[127].

5.2.1.4. Artificial neural network

The basis of artificial neural networks (ANNs) is the artificial neuron, also known as a node. The operation performed by each neuron is relatively simple: it sums its weighted inputs, applies a non-linear activation function, and then outputs the result. These processes are illustrated in Figure 5.3. Although each unit executes a straightforward operation, they can represent highly complex functions when densely arranged. The weights of each neuron, determined during training, define these functions [128].

The multilayer perceptron (MLP) constitutes the basic structure of ANNs, as depicted in Figure 5.4. It comprises three nodes and one or more hidden layers [129]. The input layer distributes

the inputs to the next layer without performing any operation. The number of neurons in the input layer corresponds to the number of inputs in the model. The hidden layers accept the output of the previous layer's neurons and pass it on to the next layer [130]. These layers can have any number of neurons. Finally, the output layer receives the output of the last hidden layer, which corresponds to the model's output. Designing just an input and output layer without hidden layers is also possible.

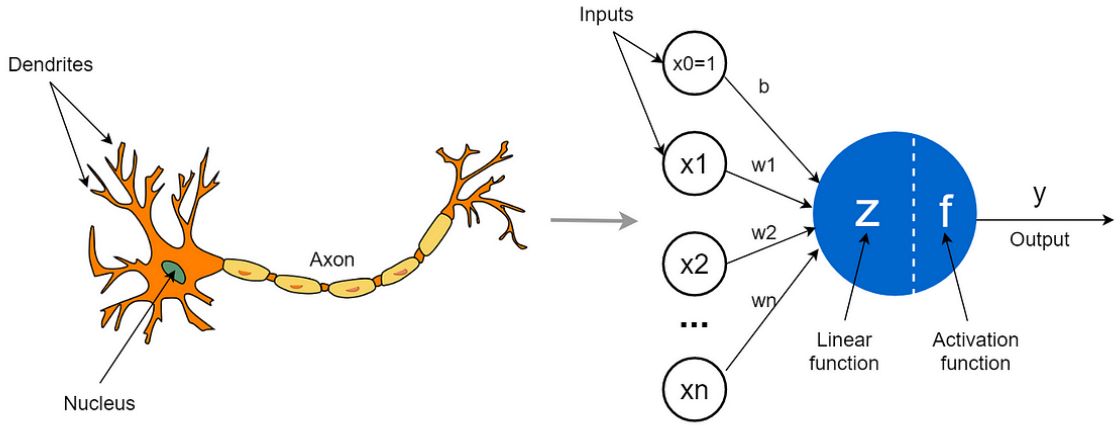

Figure 5.3: Representation of an artificial neuron

As depicted in Figure 5.4, fully connected layers are the most common layer structure in earlier models, where each neuron's output is an input to every neuron in the next layer. Other configurations are possible, such as convolutional layers where the nodes' output is connected only to some nodes in the next layer or residual layers where the outputs of some layer are passed over the next layer and added before the activation function of the following layer. The MLP is not the only type of ANN, and different neural networks, such as convolutional and recurrent, have been shown to perform well for specific types of problems [131]. For instance, CNNs are particularly well-suited for classification problems.

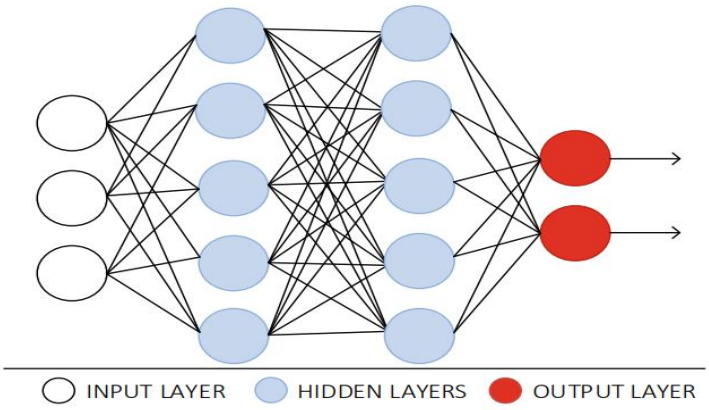

Figure 5.4: Fully connected ANN with hidden layers.

Artificial neural networks have four fundamental characteristics[132]:

- **Nonlinear**

Nonlinear relationships are universal. The human brain is intelligent due to its nonlinear processing capabilities. ANNs simulate this behavior using artificial neurons that can be activated or inhibited, resulting in a nonlinear relationship. ANNs that consist of neurons with thresholds perform better and are more fault-tolerant with increased storage capacity.

- **Non-limited**

ANNs consist of multiple interconnected neurons. The overall behavior of the network depends not only on the individual neuron's characteristics but also on the interaction and connection of all neurons. This modeling approach simulates the non-limited nature of the human brain. ANNs can exhibit non-limited associative memory.

- **Non-qualitative**

ANNs have self-adaptive, self-organizing, and self-learning abilities. They process information and can undergo various changes. The dynamic nature of ANNs means that they constantly change when processing information, and the iterative process is often used to describe this evolution.

- **Non-convexity**

The evolution of an ANN depends on a particular state function under certain conditions. For example, the energy function corresponds to the system's most stable state. Non-convexity

means that this function has multiple extrema, leading to the diversity of system evolution. As a result, ANNs have multiple stable equilibrium states.

5.2.1.5. Deep learning

In the past, neural network algorithms were limited by computing power and data volume, resulting in shallow networks with only one to four layers, which restricted their expression ability. However, with the advancement of computing power and data volumes, highly parallelized graphics processing units (GPUs) and massive data made it possible to train large-scale neural networks.

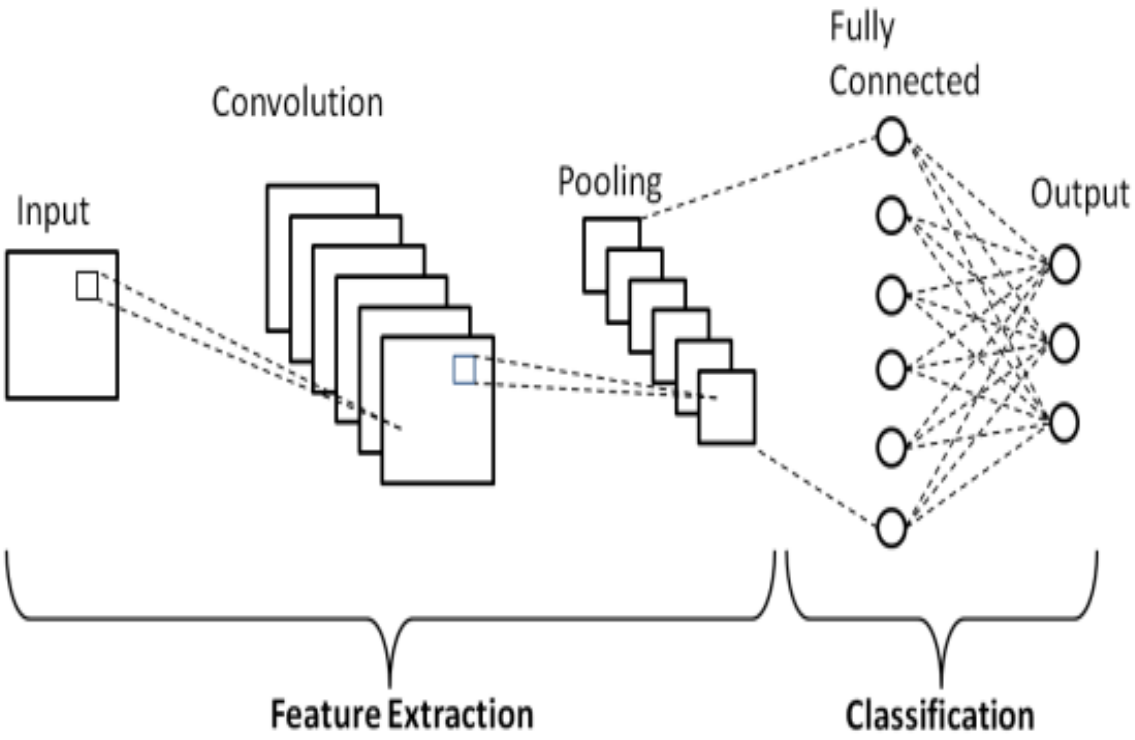

Figure 5.5: Deep Learning.

Geoffrey Hinton proposed the concept of deep learning in 2006, and in 2012, the eight-layer deep neural network called AlexNet achieved significant performance improvements, specifically in classification. Since then, neural network models with dozens, hundreds, and even thousands of layers have been developed, demonstrating strong learning ability. Deep learning models refer to algorithms implemented using deep neural networks. Unlike other algorithms, rule-based systems generally use explicit logic specific to certain tasks and

unsuitable for others. Deep learning algorithms allow neural networks to learn and improve over time by adjusting the weights and biases of the neurons [134-137].

5.2.2. The fundamental concepts of machine learning

Building a machine learning model requires selecting training sets, target functions, function approximation algorithms, and minimization of error by optimization of the model. In this section, we will describe the fundamental concepts of machine learning[136].

5.2.2.1. Dataset

The dataset is the key to ML procedures. Generating a high-quality dataset is crucial for developing and executing accurate machine-learning models [137], so datasets are usually large and obtained differently [138]. Also, the data can be collected, organized, and stored for easy access and analysis. In supervised learning, the dataset contains two types of variables: the target variable (y) and the features (x).

- ✓ **The target variable (y)** is the ultimate goal of any machine learning model. The model's accuracy depends on how well it can predict this objective.
- ✓ **The features (x)** are the factors that influence the value of y.

In machine learning, the number of examples in the data set is denoted by m, and the number of features is denoted by n.

5.2.2.2. Models

Models in machine learning are functions that can predict outputs based on inputs. Various functions exist, each suited to different tasks and datasets. Examples of such models include neural networks, support vector machines (SVM), regression functions, Gaussian functions, and more. Each type of model has its strengths and weaknesses, and the choice of the model depends on the specific characteristics of the data and the nature of the prediction task at hand [139].

- **Linear Regression**

A linear regression model is an easy-to-interpret model used when there is a linear relationship between input features and output labels. It works well for continuous variables, but there may

be better options if the relationship between features and output is nonlinear. In such cases, the model may need to be improved [140].

- **Logistic Regression**

This algorithm classifies categorical output labels. It is a good choice when dealing with binary classification problems. Implementation and interpretation are relatively straightforward but must improve when the relationship between the features and the output is nonlinear[141].

- **Decision tree**

A decision tree is an algorithm that can be used for regression and classification. They are instrumental as they are easy to interpret and can handle nonlinear relationships between the features and the output. However, one should be careful of overfitting, especially when the tree is deep[142].

- **Random Forests**

A random forest combines multiple decision trees to improve the model's performance. They are less prone to overfitting and can handle nonlinear features-output relationships[143]. However, they may be more difficult to interpret than a single decision tree.

- **Support Vector Machines (SVMs)**

SVM is an algorithm that can be used for regression and classification tasks. They are instrumental when dealing with high-dimensional data and can handle nonlinear relationships between the features and the output. However, they may be computationally expensive and challenging to interpret [144].

- **Neural Networks**

An algorithm that performs regression or classification can be called a neural network. They are instrumental when dealing with complex features and output relationships. However, they may be computationally expensive and challenging to interpret[145].

5.2.2.3. Cost function

Each machine learning model results in a biased solution to the learning problem, so evaluating how well the algorithm is learned is important. Cost function in machine learning refers to the

mathematical function used to measure the performance of a machine learning model. It quantifies the difference between the predicted and actual output, allowing the model to adjust its parameters and improve its accuracy. Different methods are used to calculate the cost function, such as gradient-based methods and penalty parameters tuning [148, 149]. In quantum computation, embedding the cost function into a quantum circuit is necessary to manipulate it directly by a quantum computer [148]. Cost-sensitive learning methods, like the modified Stein loss function, have been proposed to address class imbalance learning and improve the performance of machine learning models [149]. Additionally, adjusting the cost function coefficients is crucial for training machine learning interatomic potentials, as it affects the reproducibility of physical properties [150].

5.3. Proposed machine learning approach for optimal wireless power transfer

In this section, we will outline our proposed approach for utilizing machine learning to predict the efficiency based solely on the geometric parameters of the coils. Figure 5.6 provides an overview of the entire process for optimizing and designing a spiral coil using machine learning, including data collection, ML model training, and optimization using meta-heuristic algorithms. To determine the most efficient design using meta-heuristic algorithms, the fitness of each potential solution must be evaluated, which entails solving the 3D Maxwell problem for many designs.

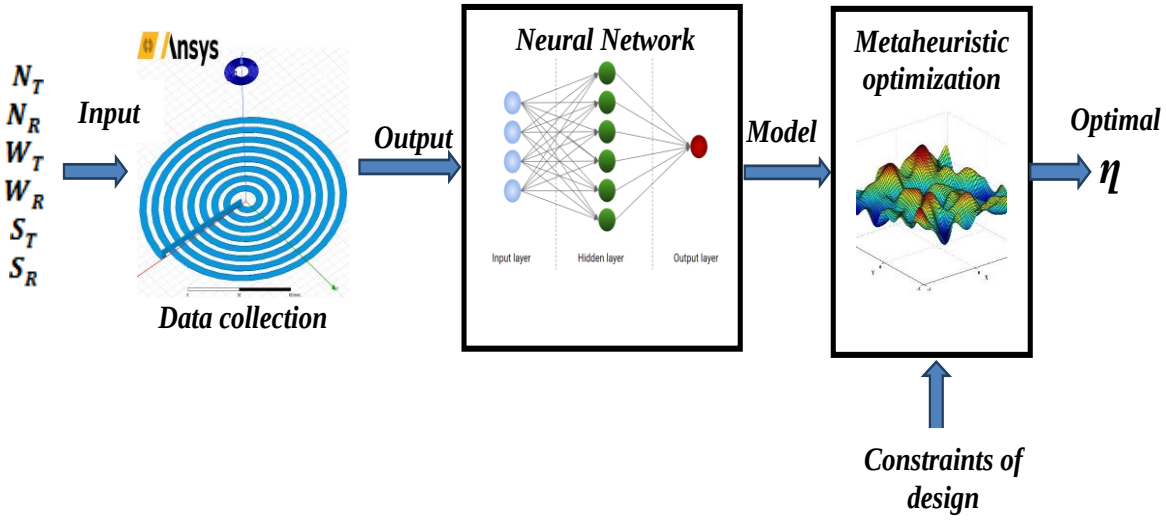

Figure 5.6: The system architecture used for the spiral coil design using ML optimization

This process is time-consuming and computationally intensive. As a solution, an ML-based model is created to predict efficiency based on the geometric parameters of the coil. In

conjunction with a meta-heuristic algorithm, this model is used to identify the optimal coil design for maximum efficiency. Using this approach has resulted in a significant reduction in the overall optimization time. In this work, a neural network model is used to predict the efficiency, as this approach is well-suited for solving nonlinear problems.

5.3.1. Neural network model for efficiency prediction

The proposed neural network model is used to predict the transfer efficiency. The neural network is chosen due to its potential to mimic the nonlinear relationship between the input and the output [151]. The input to the NN is the geometric parameters of the primary and secondary coils. The proposed NN have six inputs (N_T, N_R, W_T, W_R, S_T, S_R) and one output (η) to be generated. The ranges of the design parameters are defined in Table 4.1. The used NN is based on feed-forward architecture. A specific structure is employed to enhance the predictive accuracy of the neural network. Each neural network comprises an input layer with six neurons, a hidden layer with 60 neurons, and an output layer, as illustrated in Figure 5.7.

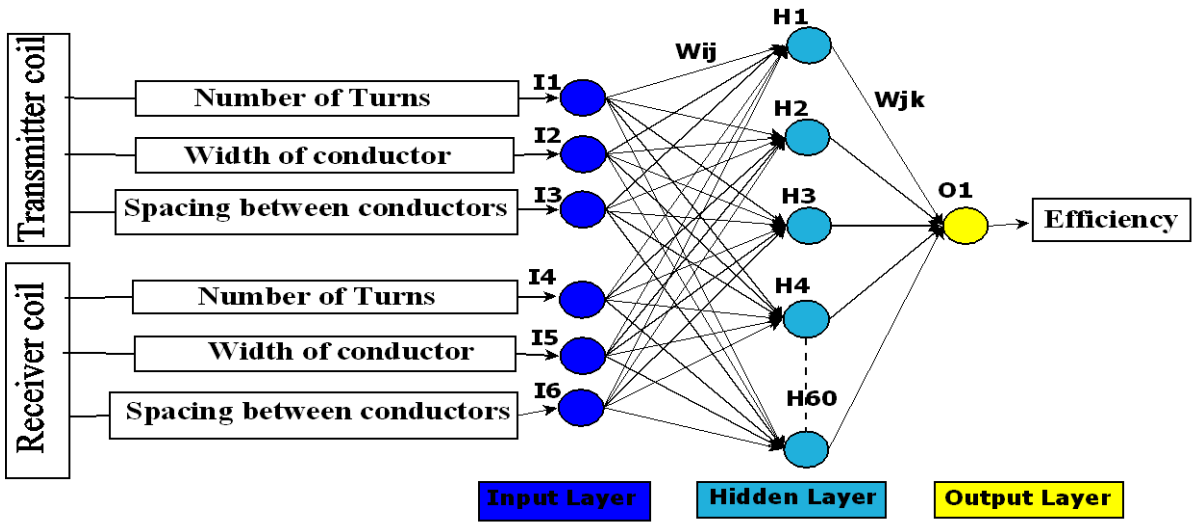

Figure 5.7: Architecture of neural network model.

To clarify the employed methodology, we provide a concise overview of the sequential steps:

Step 1: Begin by creating a parametric FEM model of the WPT system using Maxwell 3D. This model is defined by six key geometric parameters: N_T, N_R, W_T, W_R, S_T, $and\ S_R$

Step 2: Run the FEM model with a sweep of the six geometric parameters, extracting the lumped parameters R, L, C and M. These parameters are used to assess the quality factors for primary and secondary coils using equation (3.31).

Step 3: Evaluate the transfer efficiency using the analytical expression given by equation (3.22).

Step 4: Collect the simulation data generated by FEM model, including the geometric parameters and power transfer efficiency.

Step 5: Employ the collected data to train a neural network model for predicting the power transfer efficiency.

Step 6: Employ the trained model as a fitness function for the meta-heuristic algorithms (GA and COA) to optimize the power transfer efficiency.

Step 7: To validate the results, use the optimized geometric parameters to re-simulate the WPT system with Maxwell 3D.

5.3.2. Neural network model training

The Ansys-Maxwell 3D simulator and neural network Matlab toolbox were used to prepare the training and evaluation data [152]. First, we created a spiral coil model dictated by eight geometric parameters, including the outer diameters ($dout_T$, $dout_R$), the number of turns (N_T, N_R), the spacing between conductors (S_T, S_R), and the width of the conductors (W_T, W_R) of primary and secondary coils, respectively as shown in Figure 5.8.

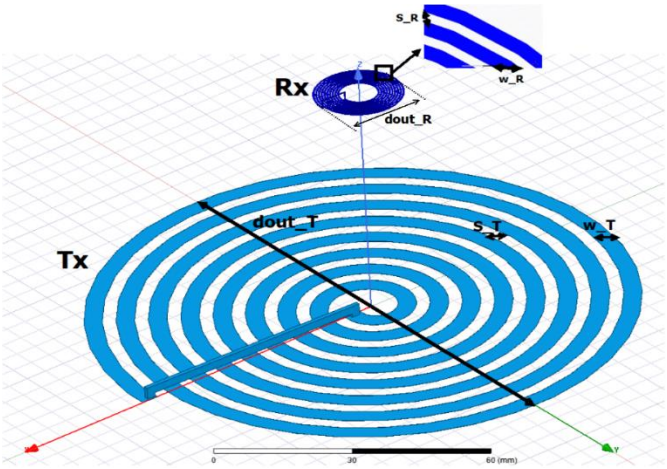

Figure 5.8: Parametric circular spiral coil designed by Ansys-3D Maxwell.

The numerical model was analyzed by the 3D eddy current solver at selected operating frequency (13.56 MHz) to extract the lumped parameters (the inductance L, the parasitic resistance R, and the capacitance C) of the designed spiral coils. Then, the efficiency is calculated by using analytical equation (3.22). Simulations were performed on a desktop

computer with an Intel Core I7 10700K processor, 16 GB of RAM, and a 64-bit operating system, specified by Windows 10 professional version 21H2, each design required approximately (3~ 10 minutes) and (7 ~ 17 hour) for 100 designs.

The dataset involved in this work was prepared by evaluating 35211 different designs over a period of 210 days and 10 hours by using Ansys-Maxwell 3D as shown in Figure 5.8. The datasets consist of six inputs which are the design parameters (N_T, N_R, W_T, W_R, S_T, S_R), and a single output which is the transfer efficiency (η). Building a predictive model requires appropriate evaluation techniques to ensure accuracy and robustness.

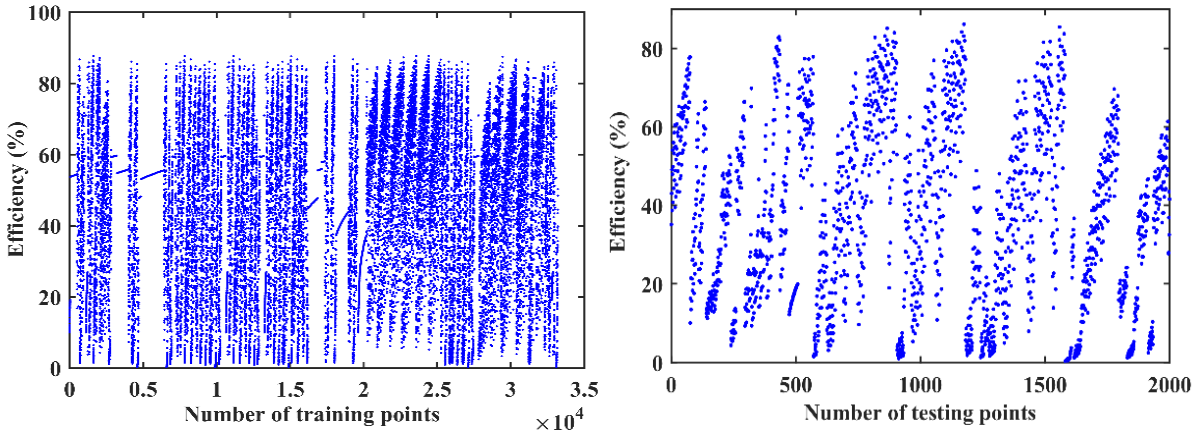

(a) (b)

Figure 5.9: The dataset used for the NN model: (a) training points (b) testing points

In this case, we performed two evaluations: For the first evaluation, we divided the dataset comprising 33,211 designs into three subsets: training, validation, and test. We randomly mixed the samples and used 80% for training, 10% for validation, and 10% for testing. This division ensures that the model is not biased towards one subset. The training set is the data used to train our predictive model. The validation set optimizes model parameters and prevents over fitting. Finally, the test set evaluates the model's performance after training and validation. Once a predictive model is developed, it is essential to ensure its reliability and accuracy by testing its ability to make precise predictions with updated data. To evaluate our model's robustness, we subjected it to a second round of testing using a fresh dataset of 2,000 designs, as depicted in Figures 5.9.

5.3.3. Performance evaluation of the neural network model

To assess the prediction accuracy of the NN model, we used two performance evaluation indices, mean squared error (MSE), and R-squared (R^2) defined as [35, 36]:

$$MSE = \frac{1}{m}\sum_{i=1}^{m}(y_i - \hat{y}_i)^2 \tag{5.1}$$

$$R^2 = 1 - \frac{\sum_{i=1}^{m}(y_i - \hat{y}_i)^2}{\sum_{i=1}^{m}(y_i - \bar{y}_i)^2} \tag{5.2}$$

m is the number of data samples, $\widehat{y}$ is the predicted output value, y is the actual output value, and $\overline{y}$ is the mean value.

The graph in Figure 5.10 displays the mean square error (MSE) for the training, validation, and test sets as a function of the number of training epochs. The graph illustrates that the neural network model is learning as the MSE starts from a high value and decreases gradually over time. As depicted in the figure, the training process was terminated at epoch 335 when the validation error increased. The final MSE is small, and the test and validation errors exhibit similar trends. No noticeable over-fitting was observed at epoch 335, which had the highest validation performance. The training data were learned with a very good accuracy, with an MSE value of 0.000096. A low MSE implies that the model is making accurate predictions.

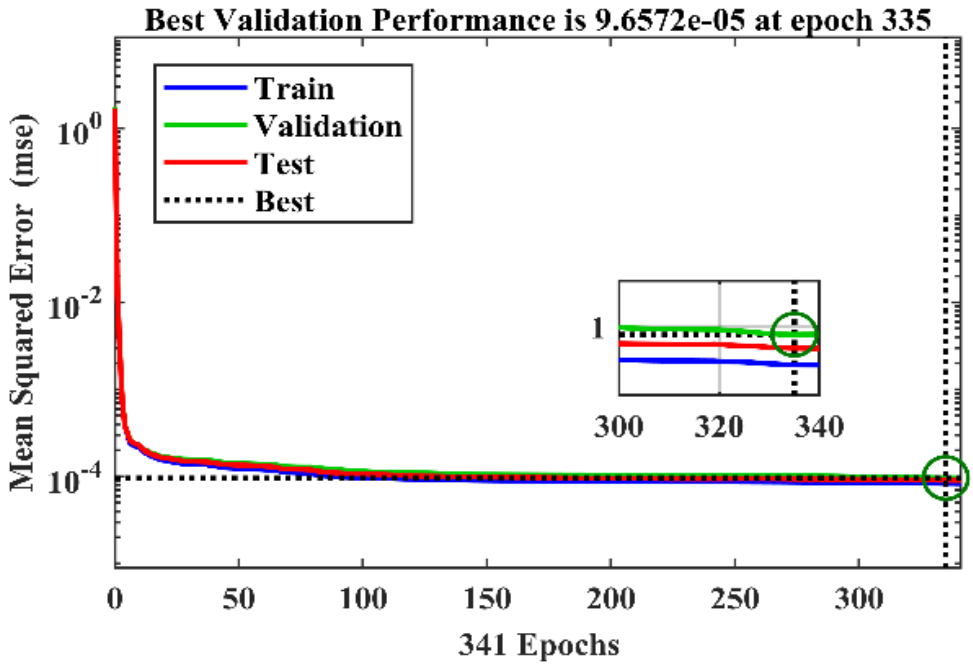

Figure 5.10: Training performance analysis of the NN model

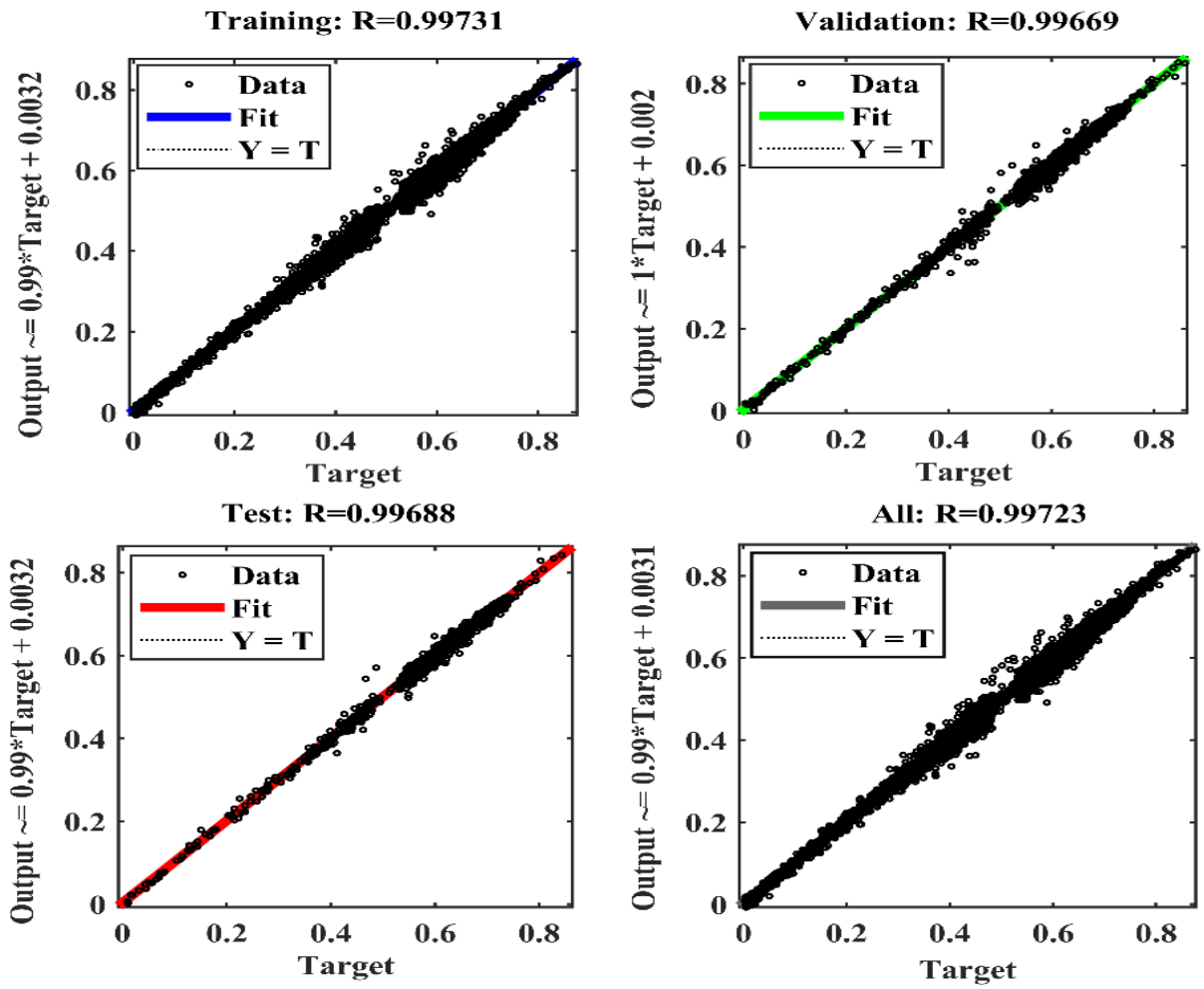

Figure 5.11: Regression performance analysis of the NN model

A regression analysis with training, validation, test, and all data is shown in Figure 5.11. The theoretical and predicted values at epoch 335 almost coincide, and all data points are scattered on the prediction line. *R* is close to 1, indicating the model achieves high prediction accuracy. The designed ANN model is stable and reliable, making it a suitable tool for efficient power transfer prediction.

To verify the accuracy of our model, we assessed its performance using a new dataset that was not utilized during the training and validation phases. The dataset is presented in Figure 5.9.c. Our analysis revealed a robust correlation between the predicted and actual values, as evidenced by a high correlation coefficient (*R)* value of 0.996, as shown in Figure 5.12.a Additionally, we plotted the error distribution using the new dataset, as depicted in Figure 5.12.b. Remarkably, the majority of the error values fell within the narrow range of [-0.03 and 0.03], indicating a

low error rate of only 3% and an impressive accuracy of over 97%. These results underscore our model's high accuracy and generalization ability.

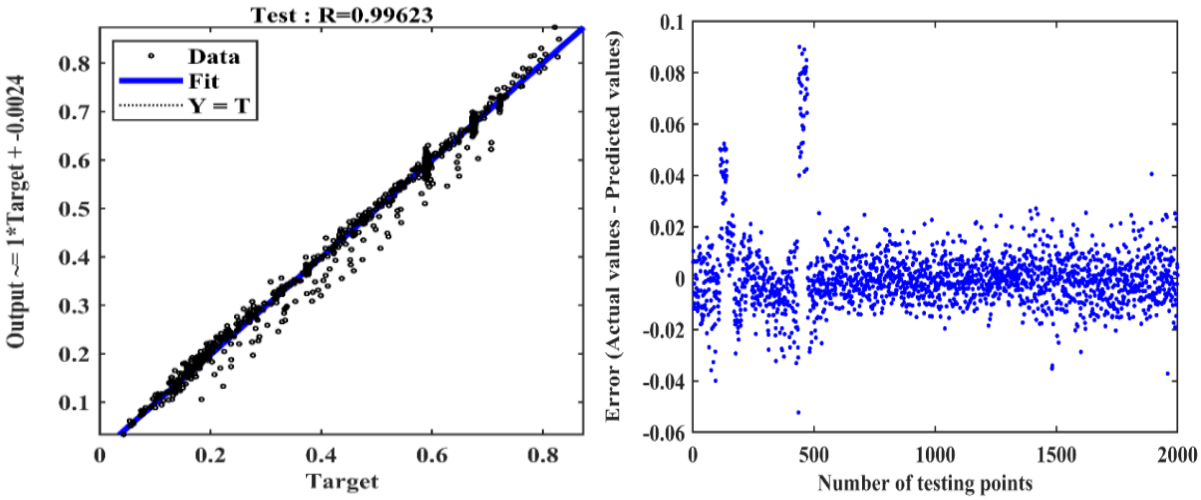

(a) (b)

Figure 5.12: NN model performance analysis for 2000 designs: (a) Correlation coefficient, (b) Error rate

Figure 5.13 (a)-(f) compare actual and predicted efficiency versus geometric parameters, demonstrating that the predicted efficiency closely matches the actual efficiency. This analysis selected random efficiency values for testing using the NN model. This approach enhances the generalizability of our findings and underscores the model's versatility across diverse real-world situations.

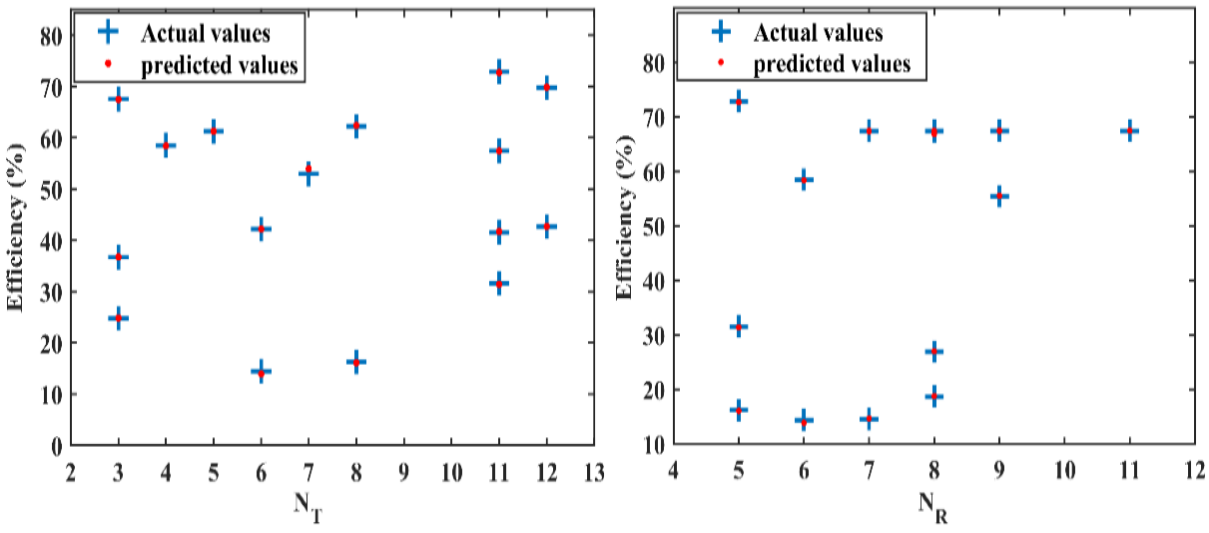

(a) (b)

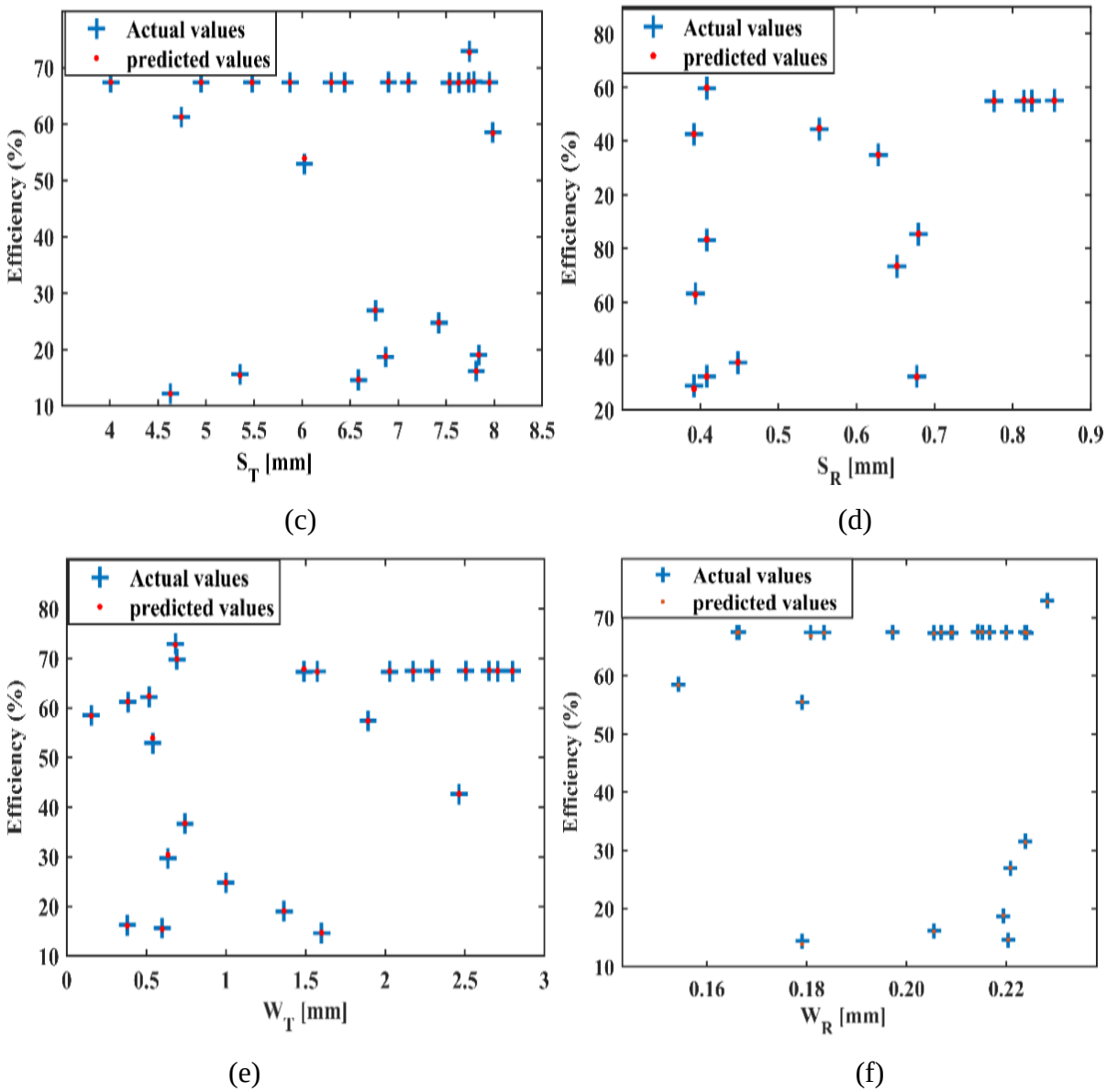

Figure 5.13: True and predicted efficiency versus geometric parameters for randomly selected test dataset

5.3.4. Neural network and meta-heuristic optimization

Many WPT applications must be realized with a space restriction for receiving coil. For example, WPT for biomedical implants must be realized with a miniaturized receiving coil because the available space for the implantable Rx is minimal. On the other hand, a Tx coil can be substantially larger for such an application. Therefore, there is a requirement for the derivation of a coil design approach when coil size constraints are imposed. This section utilizes the methodology described to investigate coil geometric parameter optimization for WPT with miniaturized Rx coil. Specifically, we employ two meta-heuristic algorithms: the genetic algorithm (GA) and the coyote algorithm (COA) to extract the optimal design point. Before

optimizing, a preliminary study must identify the critical geometric parameters influencing efficiency. This objective will be the focus of the upcoming section.

5.3.5. Exploring the impact of geometric parameters on efficiency

Figure 5.14 illustrates the correlation between the efficiency of the coil and its geometric parameters. The analysis indicates that the efficiency of the coil is positively correlated with the parameters of the secondary coil (N_R, W_R, *and* S_R) and the width of the conductors in the primary coil (W_T). Conversely, an increase in the number of turns of the primary coil (N_T) and the spacing between the conductors of the primary coil (S_T) results in a decrease in efficiency. Therefore, a balance between the geometric parameters of the coils must be determined to achieve maximum efficiency while considering the constraints of biomedical applications at a specific coupling distance. This is the aim of the next section.

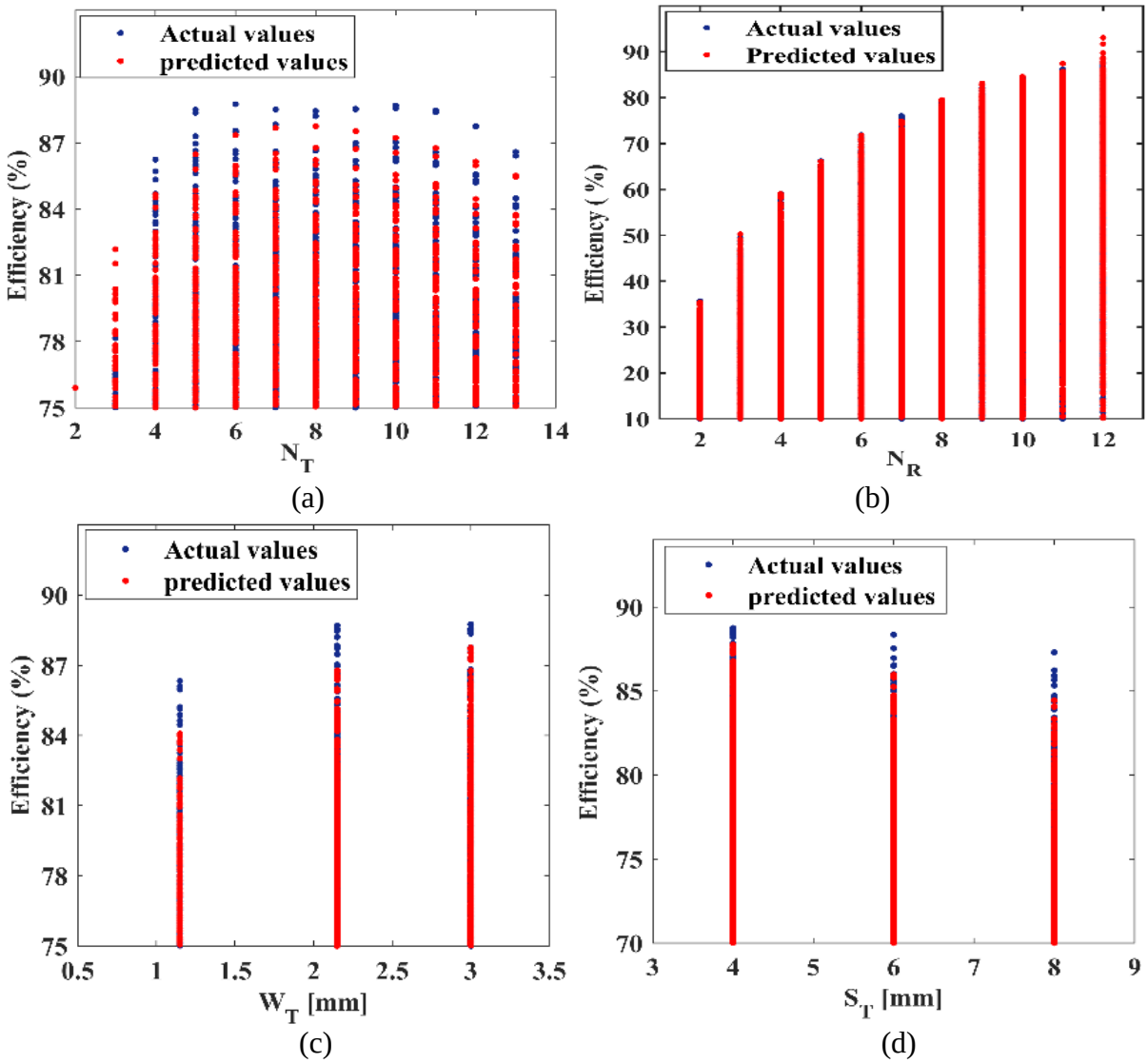

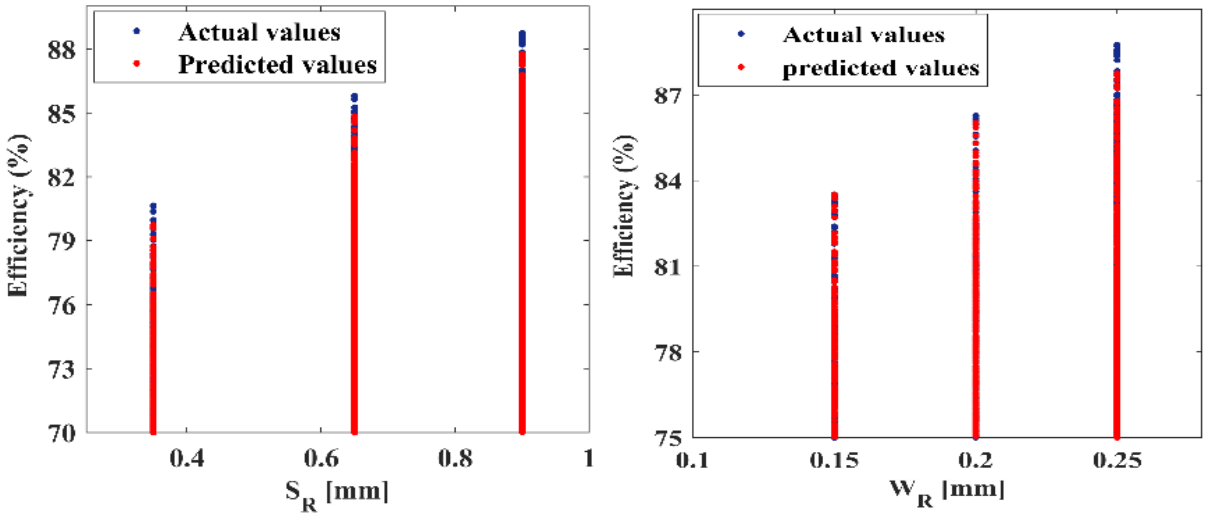

(e) (f)

Figure 5.14: The efficiency versus the geometric parameters of the coils

5.3.6. Optimization algorithms

The aim of this optimization is to find the optimal geometric parameters of the coils that maximize transfer efficiency.

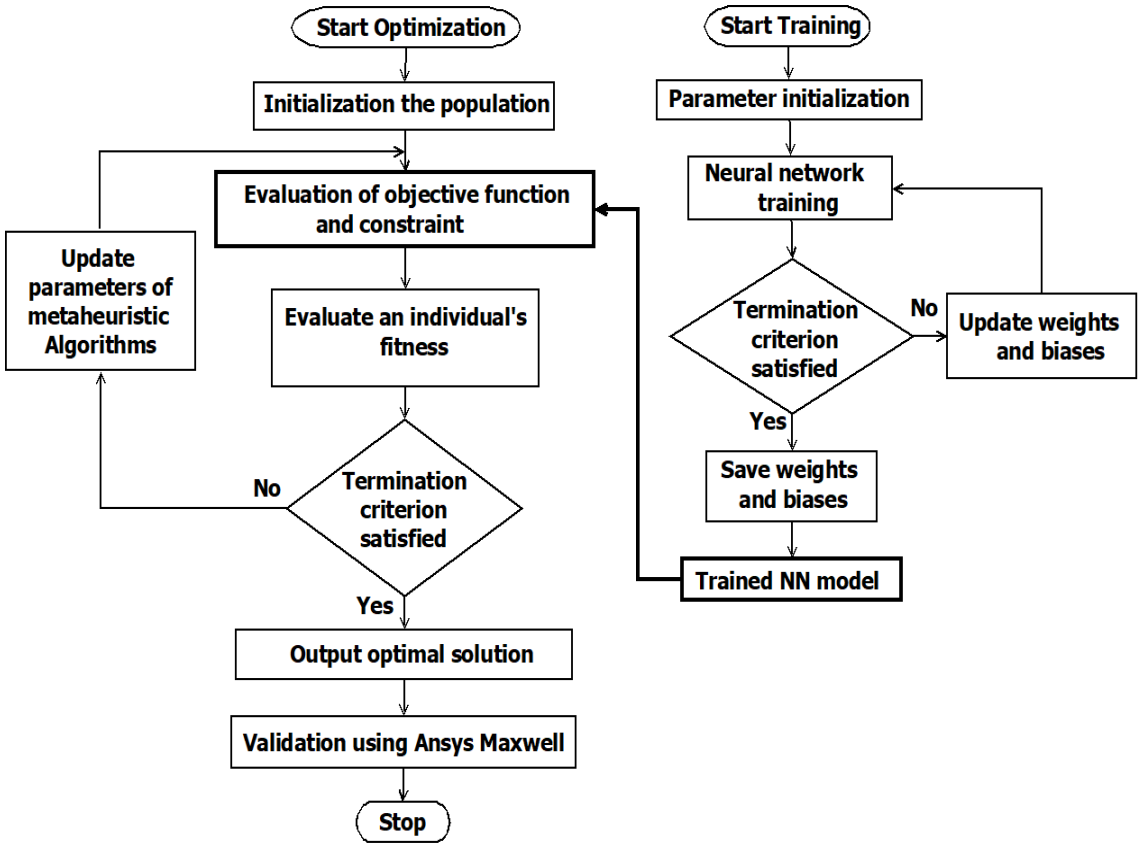

Figure 5.15: Flowchart of ML-metaheuristic based coil optimization.

The flowchart in Figure 5.15 describes the optimization process based on meta-heuristic algorithms (GA, COA). For a biomedical application, the limited size of the secondary coil (external diameter $dout_R$ which does not exceed 20mm) is defined as a constraint for the optimization problem formulated by equation (4.1). Different methods can be used to solve the optimization problem. In this study, we have chosen two meta-heuristic algorithms, the genetic algorithm (GA) and coyote algorithm (COA), to find the optimal solutions for this problem. The neural network model is called by the meta-heuristic algorithms in each iteration to evaluate the objective function.

5.3.7. Optimization results and discussion

In this section, we study the proposed GA and COA algorithms' performance in solving the optimization problem to achieve high efficiency. The optimization process is stopped when the average change in the fitness value and constraint violation drops below a set tolerance value. The objective function's variation against the number of iterations for GA and COA algorithms is depicted in Figure 5.16 The corresponding geometric parameters versus the iterations are shown in Figure 5.17 and summarized in Table 5.2. As depicted in Figure 5.17, the NN-GA algorithm requires only a few cycles to reach optimal values, making it significantly faster than the NN-COA algorithm. As reported in Table 5.2, both algorithms (GA and COA) yield almost identical optimal parameters, resulting in a high efficiency of 76%, which validates our proposed approach.

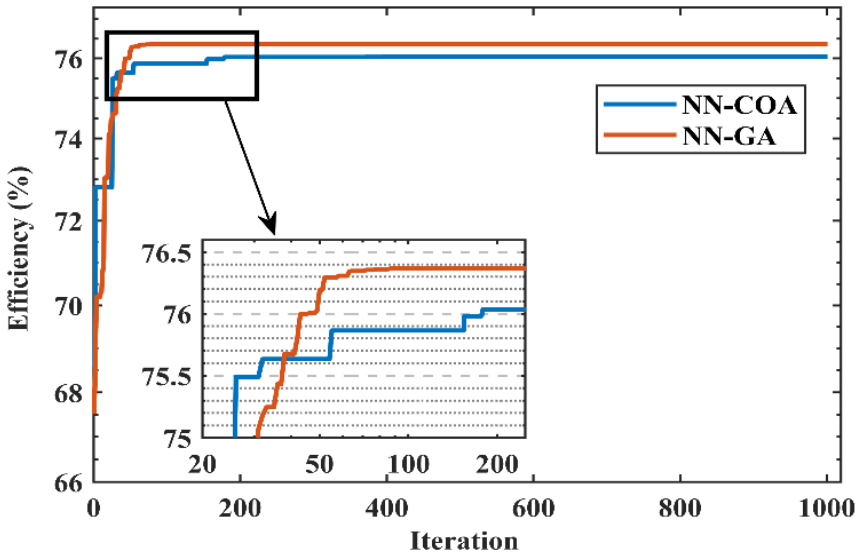

Figure 5.16: Efficiency versus number of iterations

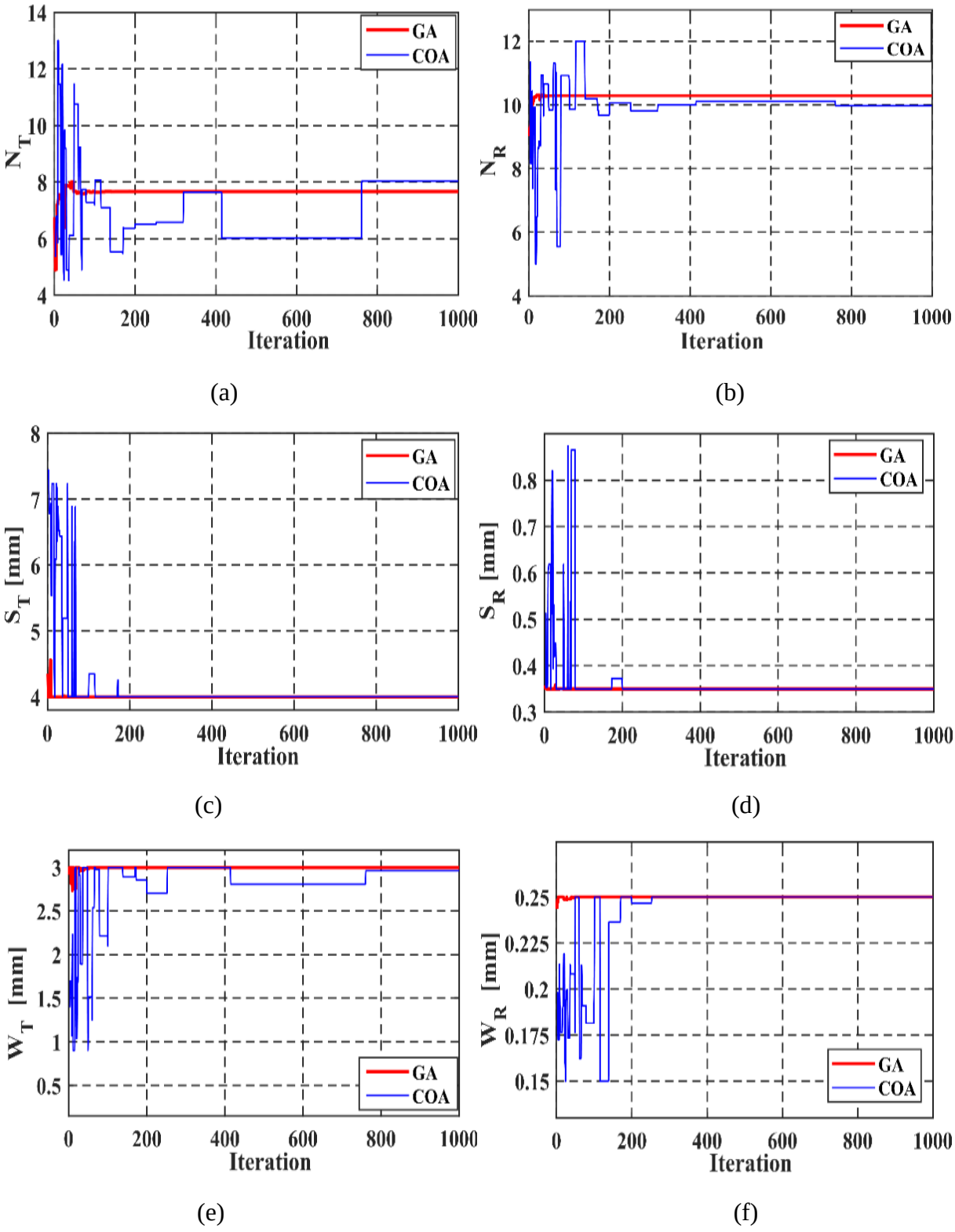

Figure 5.17: Geometric parameters versus the number of iterations

By comparing the efficiency achieved using the initial values listed in Table 4.1 to the efficiency attained with the optimal values listed in Table 5.1, it becomes evident that there has been a remarkable increase in efficiency from $\eta = 0.2\%$ to $\eta = 76\%$. This represents an improvement

in efficiency of 76%. Moreover, while both algorithms exhibit similar efficiency levels, noteworthy differences are observed in their convergence behavior. The genetic algorithm reaches convergence within 80 iterations, whereas the coyote algorithm requires approximately 200 iterations to achieve a stable efficiency state.

Table 5.1: Optimization results of NN-metaheuristic approach

Geometric parameters	**NN-COA**		**NN-GA**	
	Primary coil	Secondary coil	Primary coil	Secondary coil
Number of turns ***(N)***	7.9660	10.14	7.6568	10.291
Width of a conductor ***(W)*** [mm]	3	0.25	3	0.25
Spacing between conductors ***(S)*** [mm]	4	0.35	4	0.35
Outer diameter coil (d_{out}) [mm]	120	19.8	115	19.8
Efficiency *(η)*	76.01%		76.36%	
Iteration	200		80	
Validation (FEM model)	76.22%		76%	

Table 5.2 highlights the effectiveness of utilizing the ML-based approach in the design optimization process compared to traditional methods (analytical and numerical). This table clearly shows that the validation results are in close agreement with those of analytical and numerical methods. When comparing the different approaches, it becomes evident that NN-GA and FEM-GA exhibit high accuracy. This accuracy can be attributed to numerical-based optimization considering real resistances, parasitic capacitances, and all types of coil losses. In contrast, the analytical-GA approach demonstrates higher efficiency than NN-GA and FEM-GA but lower accuracy than validation results; it exhibits a 9% error. This reasonable error originates from our use of simplified mathematical models to approximate coil electrical parameters, disregarding various losses such as capacitive, proximity and eddy current losses.
Additionally, the results indicate that the ML-based approach significantly reduces the computational time needed for the optimization process, with a 99% decrease compared to traditional FEM-based optimization methods. While FEM-based optimization takes four months, the ML-based approach takes only few seconds. Although the initial computational cost for acquiring and training the algorithm was seven months, the prediction and optimization are very fast and accurate once completed. As demonstrated in this study, the incorporation of machine learning techniques in the design optimization process can lead to faster and more efficient design iterations.

Table 5.2. Comparison of characteristics

Parameters	Analytical-GA	NN-GA	FEM-GA
N_T	6	7.6568	8
N_R	10.2	10.291	10
W_T [mm]	3	3	2.956
W_R [mm]	0.25	0.25	0.2313
S_T [mm]	4	4	4.083
S_R [mm]	0.35	0.35	0.3792
d_{outR} [mm]	20	19.8	20
d_{outT} [mm]	90	115	120.5
Efficiency (η)	79%	76.36 %	74%
Validation by FEM	70%	76%	74%
Computational time	95 s	23 s	4 months

5.4. Comparative analysis of the NN technique with respect to other methods

One of the appealing features of our proposed ML-based coil design method is its notable reduction in computation time for coil design. As depicted in Figure 5.18.a, the proposed method requires only 0.005 seconds to predict 1000 sample designs. In contrast, simulation tools like Ansys-3D Maxwell demand 3~10 minutes for each sample design on a standard desktop computer. This means that it takes 50~170 hours to explore 1000 sample designs. Furthermore, the proposed method reach optimal efficiency within 3 seconds for 100 iterations, while Ansys-3D Maxwell takes 14 hours for the same iterations, as depicted in Figure 5.18.b. Consequently, our proposed approach to coil design not only enhances efficiency but also results in significant time savings during the design and optimization process.

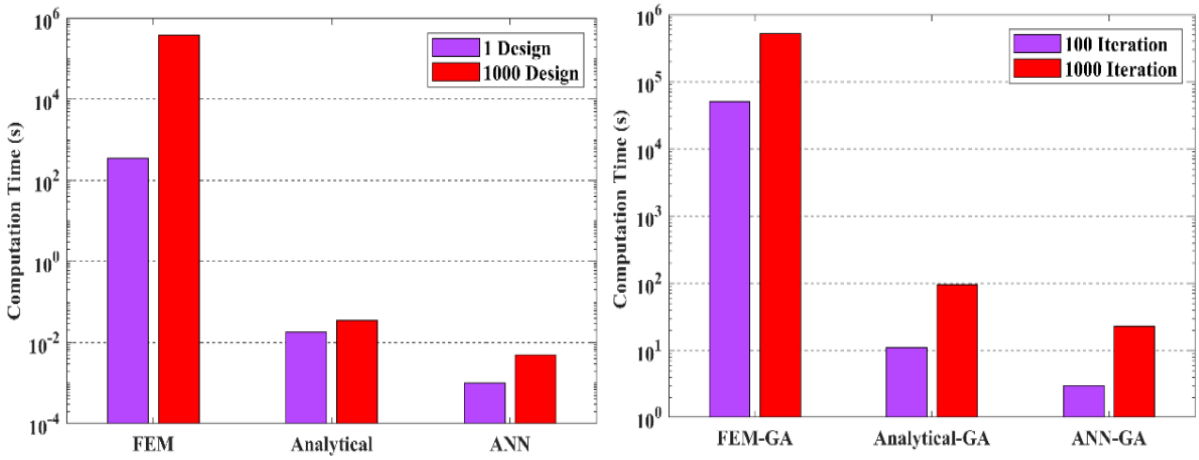

(a) (b)

Figure 5.18: Comparison of the computation time for the coil design: (a) Prediction, (b) Optimization.

Remarkably, our ML-based coil design approach offers several advantages over traditional approaches, as outlined in Table 5.3. The proposed approach enables the efficient design of coils of varying sizes with high efficiency, eliminating the need for complex analyses or lengthy simulations. Notably, our design approach not only ensures exceptional prediction accuracy but also achieves this with minimal computational intensity and reduced resource requirements. While analytical approaches can optimize a design quickly, they often rely on simplified equations that may be inaccurate. In contrast, our ML-based approach utilizes a data-trained model for optimization instead of analytical equations. Particularly, our optimization method employs metaheuristic algorithms to efficiently yield optimal designs without the need for calculating lumped elements. Consequently, our proposed method is adaptable to design changes, fast, and provides high accuracy. Additionally, finite elements methods (FEM) simulators produce accurate results and explore various configurations. However, the accuracy of FEM simulations comes at the expense of increased computational time, as demonstrated in Figure 5.18. This trade-off could result in reduced productivity in industrial applications.

Table 5.3: Performance comparison of design methods of WPT coils

Methods	**Preparation**	**Accuracy**	**Latency**	**Design flexibility**	**Industrial applications**
Analytical method **[2], [70], [111]**	Lumped elements (R, L and C), equations	Low	Fast	Poor	Bad
FEM method **[2], [103]**	Simulators (3D Maxwell, HFSS.)	Very high	Slow	Moderate	Moderate
ML method **[7], [9], [14]**,**[153]**	Data set and trained models	High	Fast	Good	Good
Proposed method [154]	**Data set and trained models**	**Very High**	**Faster**	**Good**	**Very Good**

- **Validation**

As shown in figure 5.19, we can see the optimal geometric shape of both primary and secondary coils, as determined by using Ansys Maxwell. These designs, derived from an extensive design and optimization process, yield a remarkable efficiency of 76.22%.

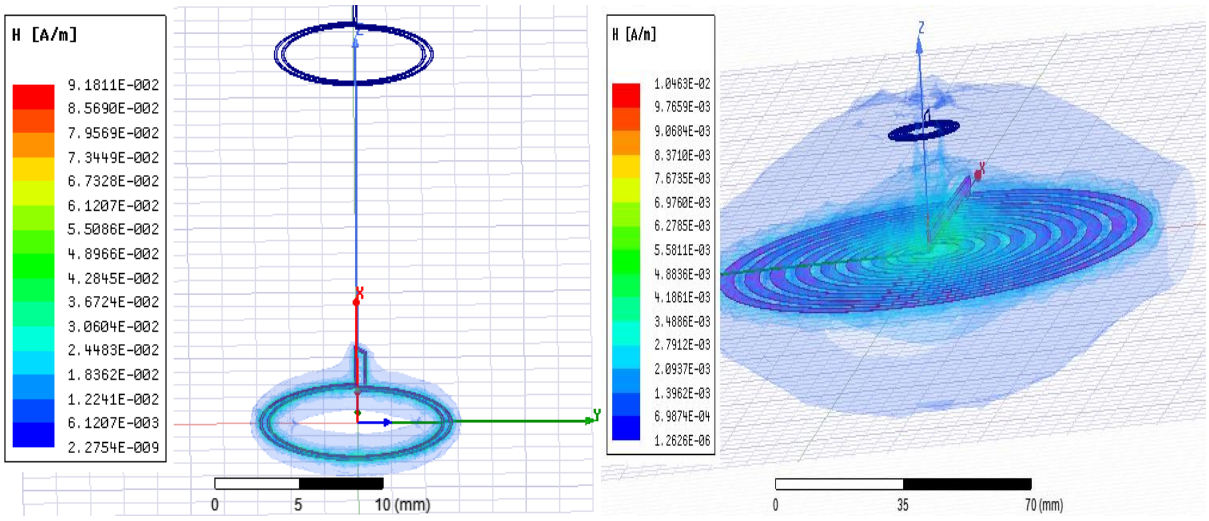

(a) (b)

Figure 5.19: 3D model of coils designed with optimal parameters: (a) Initial coil geometry (before optimization), (b) Optimal coil geometry (after optimization)

Additionally, the observed variations in magnetic field distribution provide valuable insights into the characteristics that differentiate these two designs. Notably, in the case of the initial coil shape, the flux lines originating from the first coil fail to reach the second coil due to their nearly identical sizes, leading to a weak coupling coefficient. Conversely, in the case of the optimal coil shape, the flux lines successfully reach the second coil, resulting in a strengthened coupling coefficient and enhanced efficiency.

5.5. Conclusion

In this chapter, we introduced a novel approach to optimize the design of miniaturized, high-efficiency WPT coils for biomedical implants. Our approach combines machine learning and meta-heuristic algorithms to optimize the geometric coil parameters to maximize transfer efficiency. We meticulously trained a neural network model, leveraging an extensive dataset of over 35,000 samples of geometric parameters. This rigorous training resulted in a remarkable model accuracy rate exceeding 97%. Furthermore, we employed meta-heuristic methods to expedite searching for optimal coil parameters that maximize transfer efficiency. Our approach has demonstrated impressive effectiveness in WPT coil design optimization, leading to notable enhancements in transfer efficiency and significantly reducing the required processing time compared to traditional optimization methods. The satisfactory obtained results were validated using finite element simulation based on Ansys Maxwell 3D.

Conclusion and Future Works

Chapter 6

6.1. Conclusion

This thesis investigated the optimization of wireless power transfer (WPT) systems for biomedical implants, focusing on maximizing efficiency while minimizing the size of the receiving coil. The transfer distance was also increased to 30 mm. This research presented a comprehensive approach that combines metaheuristic algorithms with machine learning to achieve maximum WPT efficiency.

First, we thoroughly analyzed and identified the geometric coil parameters that impact the efficiency of the WPT system. Then, we proposed an analytical approach incorporating iterative or metaheuristic optimization methods. However, the optimization results derived from analytical models may lack accuracy, as they are based on calculating the objective function (efficiency) using a series of simplified equations. This can introduce errors and limit the precision of the optimization.

To overcome the limitations of analytical models, this work incorporated numerical simulations using the finite element method (FEM) based on Ansys Maxwell 3D. This approach allowed more precise efficiency calculations, leading to highly accurate results. However, the time-consuming nature of FEM simulations presents a significant challenge for fabrication design iterations.

Recognizing the need for a tradeoff between accuracy and speed, this thesis introduced a novel machine learning-based approach. This approach employed an artificial neural network (ANN) model trained on a large dataset of FEM simulation results. The trained model

achieved remarkable accuracy, exceeding 97%, in predicting efficiency based on geometric coil parameters.

To further enhance the optimization process, this thesis integrated the trained ANN model with metaheuristic algorithms, namely the genetic algorithm (GA) and the coyote optimization algorithm (COA). These algorithms efficiently identified optimal coil designs that maximized efficiency while adhering to size constraints.

This research demonstrated the significant advantages of machine learning-based approaches compared to traditional methods. It achieved high accuracy, comparable to FEM-based optimization, but with a remarkable reduction in computational time, exceeding 99% faster compared with GA-FEM optimization. Additionally, we have established the feasibility of using machine learning for rapid and accurate WPT coil design optimization. The proposed approach offers a powerful tool for accelerating the development of high-performance WPT systems for various applications, particularly in biomedical implants.

6.2.Future Works

Our future research will aim to significantly advance WPT technology, particularly for biomedical applications.

- We will be actively engaged in developing and implementing a WPT circuit.
- We will address coil misalignment, and an AI-driven system will be developed to precisely determine the primary coil's position and enable real-time adjustments.
- We will further enhance the machine learning model by incorporating additional factors such as tissue properties and electromagnetic interference. This will further improve the model's accuracy and robustness in the biomedical field.
- We propose to study the possibility of sticking the coil on a plate to increase the magnetic field. The plate material will be selected after a study about its effect on human skin to ensure that there aren’t adverse effects.

6.3.The following publications resulted from this research

Journal Publications

Bennia, F.,Boudouda, A. &Nafa, F. "Optimal design of wireless power transfer coils for biomedical implants using machine learning and meta-heuristic algorithms", *Electr. Eng.*, pp. 1–16, 2024. https://doi.org/10.1007/s00202-024-02345-4

Conference Publications

Fatima Bennia, Aimad Boudouda, Fares Nafa, "Iterative methods based optimization of wireless power transfer for biomedical implants," in1st International Conference on Advances in Electronics, Control and Communication Systems (ICAECCS 2023), Blida. Algeria, 6-7 March 2023.https://doi.org/10.1109/ICAECCS56710.2023.10104669

Fatima Bennia, Aimad Boudouda, Fares Nafa, "Wireless power transfer optimization using meta-heuristic algorithms," in 2nd IEEE International Conference on Electrical Engineering and Automatic Control (ICEEAC 2024), Setif, Algeria, 12-14 Mai 2024

List of references

[1] A. K. RamRakhyani, S. Mirabbasi, and M. Chiao, 'Design and optimization of resonance-based efficient wireless power delivery systems for biomedical implants', *IEEE Trans. Biomed. Circuits Syst.*, vol. 5, no. 1, pp. 48–63, 2010.

[2] D. Ahire, V. J. Gond, and J. J. Chopade, 'Geometrical parameter optimization of planner square-shaped printed spiral coil for efficient wireless power transfer system to biomedical implant application', *E-Prime-Adv. Electr. Eng. Electron. Energy*, vol. 2, p. 100045, 2022.

[3] C.-L. Yang, S. P. Cheng, and C.-E. Yu, 'Fused Helico-Spiral Coil Design Using Both Neural Network and Generic Algorithms', in *2018 IEEE International Symposium on Antennas and Propagation & USNC/URSI National Radio Science Meeting*, IEEE, 2018, pp. 2537–2538.

[4] M. Kim, M. Jeong, M. Cardone, and J. Choi, 'Characterization of the quality factor in spiral coil designs for high-frequency wireless power transfer systems using machine learning', in *2022 IEEE 23rd Workshop on Control and Modeling for Power Electronics (COMPEL)*, IEEE, 2022, pp. 1–8.

[5] T. Guillod, P. Papamanolis, and J. W. Kolar, 'Artificial neural network (ANN) based fast and accurate inductor modeling and design', *IEEE Open J. Power Electron.*, vol. 1, pp. 284–299, 2020.

[6] Y. Li, G. Lei, G. Bramerdorfer, S. Peng, X. Sun, and J. Zhu, 'Machine learning for design optimization of electromagnetic devices: Recent developments and future directions', *Appl. Sci.*, vol. 11, no. 4, p. 1627, 2021.

[7] A. Ali, M. N. Mohd Yasin, M. Jusoh, N. A. M. Ahmad Hambali, and S. R. Abdul Rahim, 'Optimization of wireless power transfer using artificial neural network: A review', *Microw. Opt. Technol. Lett.*, vol. 62, no. 2, pp. 651–659, 2020.

[8] M. Kim, M. Jeong, M. Cardone, and J. Choi, 'Design of a Spiral Coil for High-Frequency Wireless Power Transfer Systems Using Machine Learning', *IEEE J. Emerg. Sel. Top. Ind. Electron.*, 2023.

[9] M. Kim, M. Jeong, M. Cardone, and J. Choi, 'Optimization of spiral coil design for WPT systems using machine learning', in *2023 IEEE Applied Power Electronics Conference and Exposition (APEC)*, IEEE, 2023, pp. 822–828.

[10] F. Wen *et al.*, 'Research on optimal receiver radius of wireless power transfer system based on BP neural network', *Energy Rep.*, vol. 6, pp. 1450–1455, 2020.

[11] H. Zhang, P. Tan, X. Shangguan, X. Zhang, and H. Liu, 'Machine learning-based parameter identification method for wireless power transfer systems', *J. Power Electron.*, vol. 22, no. 9, pp. 1606–1616, 2022.

[12] A. O. Hariri, T. Youssef, A. Elsayed, and O. Mohammed, 'A computational approach for a wireless power transfer link design optimization considering electromagnetic compatibility', *IEEE Trans. Magn.*, vol. 52, no. 3, pp. 1–4, 2015.

[13] S. Inoue *et al.*, 'Fast design optimization method utilizing a combination of artificial neural networks and genetic algorithms for dynamic inductive power transfer systems', *IEEE Open J. Power Electron.*, vol. 3, pp. 915–929, 2022.

[14] E. Noh, J. So, and S.-H. Lee, 'Machine-Learning Based Optimal Design of a Wireless Power Transfer Coil for Battery-Powered Tram', in *2023 11th International Conference on Power Electronics and ECCE Asia (ICPE 2023-ECCE Asia)*, IEEE, 2023, pp. 1867–1872.

[15] I. P. Pohan, 'A Compact S-Band Front-End Rectenna for Wireless Power Transfer Application', PhD Thesis, Universiti Teknologi Malaysia, 2006.

[16] J. C. Maxwell, *A treatise on electricity and magnetism*, vol. 1. Oxford: Clarendon Press, 1873.

[17] N. Tesla, 'Apparatus for transmitting electrical energy.' Google Patents, Dec. 01, 1914.

[18] N. Shinohara, 'History, present and future of wpt', *Wirel. Power Transf. Radiowaves*, pp. 1–20, 2013.

[19] M. Zellagui, 'Introductory Chapter: Overview of Wireless Power Transfer Technologies', *Wirel. Power Transfer–Recent Dev. Appl. New Perspect.*, 2021.

[20] S. Hui, 'Planar wireless charging technology for portable electronic products and Qi', *Proc. IEEE*, vol. 101, no. 6, pp. 1290–1301, 2013.

[21] M. Qiu, 'Research and classification of wireless power transfer with relative application', in *Journal of Physics: Conference Series*, IOP Publishing, 2021, p. 012036.

[22] W. C. Brown, 'The history of wireless power transmission', *Sol. Energy*, vol. 56, no. 1, pp. 3–21, 1996.

[23] A. Kurs, A. Karalis, R. Moffatt, J. D. Joannopoulos, P. Fisher, and M. Soljacic, 'Wireless power transfer via strongly coupled magnetic resonances', *science*, vol. 317, no. 5834, pp. 83–86, 2007.

[24] K. Detka and K. Górecki, 'Wireless power transfer—A review', *Energies*, vol. 15, no. 19, p. 7236, 2022.

[25] D. Van Wageningen and T. Staring, 'The Qi wireless power standard', in *Proceedings of 14th International Power Electronics and Motion Control Conference EPE-PEMC 2010*, IEEE, 2010, pp. S15-25.

[26] M. M. El Rayes, G. Nagib, and W. A. Abdelaal, 'A review on wireless power transfer', *Int. J. Eng. Trends Technol. IJETT*, vol. 40, no. 5, pp. 272–280, 2016.

[27] A. Triviño, J. M. González-González, and J. A. Aguado, 'Wireless power transfer technologies applied to electric vehicles: A review', *Energies*, vol. 14, no. 6, p. 1547, 2021.

[28] A. MAHESH, B. CHOKKALINGAM, and L. MIHET-POPA, 'Review on Inductive Wireless Power Transfer Charging for Electric vehicles–A Review'.

[29] N. Sharma, T. Bheda, R. Chaudhary, Mohit, and S. Urooj, 'Wireless Power Transfer Using Microwaves', in *Next-Generation Networks: Proceedings of CSI-2015*, Springer, 2018, pp. 307–311.

[30] X. Zhu, K. Jin, Q. Hui, W. Gong, and D. Mao, 'Long-range wireless microwave power transmission: A review of recent progress', *IEEE J. Emerg. Sel. Top. Power Electron.*, vol. 9, no. 4, pp. 4932–4946, 2020.

[31] K.-R. Li, K.-Y. See, W.-J. Koh, and J.-W. Zhang, 'Design of 2.45 GHz microwave wireless power transfer system for battery charging applications', in *2017 Progress in Electromagnetics Research Symposium-Fall (PIERS-FALL)*, IEEE, 2017, pp. 2417–2423.

[32] K. Jin and W. Zhou, 'Wireless laser power transmission: A review of recent progress', *IEEE Trans. Power Electron.*, vol. 34, no. 4, pp. 3842–3859, 2018.

[33] A. Baraskar, H. Chen, Y. Yoshimura, S. Nagasaki, and T. Hanada, 'Verify the wireless power transmission in space using satellite to satellite system', *Int. J. Emerg. Technol.*, vol. 12, no. 2, pp. 110–118, 2021.

[34] F. Lu, H. Zhang, and C. Mi, 'A review on the recent development of capacitive wireless power transfer technology', *Energies*, vol. 10, no. 11, p. 1752, 2017.

[35] S. Wang, J. Liang, and M. Fu, 'Analysis and design of capacitive power transfer systems based on induced voltage source model', *IEEE Trans. Power Electron.*, vol. 35, no. 10, pp. 10532–10541, 2020.

[36] M. T. Nguyen *et al.*, 'Electromagnetic field based wpt technologies for uavs: A comprehensive survey', *Electronics*, vol. 9, no. 3, p. 461, 2020.

[37] N. Korakianitis, G. A. Vokas, and G. Ioannides, 'Review of wireless power transfer (WPT) on electric vehicles (EVs) charging', in *AIP conference proceedings*, AIP Publishing, 2019.

[38] A. Mehdipour, B. Moarref, A. S. Kia, and M. Yazdanipour, 'Evaluation of inductive coupling and RF-DC for Wireless Power Transmission', in *2012 Ninth International Conference on Wireless and Optical Communications Networks (WOCN)*, IEEE, 2012, pp. 1–5.

[39] I. Alhamrouni, M. Iskandar, M. Salem, L. J. Awalin, A. Jusoh, and T. Sutikno, 'Application of inductive coupling for wireless power transfer', *Int. J. Power Electron. Drive Syst.*, vol. 11, no. 3, p. 1109, 2020.

[40] A. Mahesh, B. Chokkalingam, and L. Mihet-Popa, 'Inductive wireless power transfer charging for electric vehicles–a review', *IEEE Access*, vol. 9, pp. 137667–137713, 2021.

[41] N. D. Madzharov and V. S. Nemkov, 'Technological inductive power transfer systems', *J. Electr. Eng.*, vol. 68, no. 3, pp. 235–244, 2017.

[42] Y. Zhou, C. Liu, and Y. Huang, 'Wireless power transfer for implanted medical application: A review', *Energies*, vol. 13, no. 11, p. 2837, 2020.

[43] C.-L. Lin, Z.-Q. Wong, and J. Yang, 'A secured wireless charging scheme with data transmission', *Electr. Eng.*, vol. 105, no. 5, pp. 2795–2804, 2023.

[44] Y. Liu, B. Li, M. Huang, Z. Chen, and X. Zhang, 'An overview of regulation topologies in resonant wireless power transfer systems for consumer electronics or bio-implants', *Energies*, vol. 11, no. 7, p. 1737, 2018.

[45] H. Hoang, S. Lee, Y. Kim, Y. Choi, and F. Bien, 'An adaptive technique to improve wireless power transfer for consumer electronics', *IEEE Trans. Consum. Electron.*, vol. 58, no. 2, pp. 327–332, 2012.

[46] W. C. Cheah, S. A. Watson, and B. Lennox, 'Limitations of wireless power transfer technologies for mobile robots', *Wirel. Power Transf.*, vol. 6, no. 2, pp. 175–189, 2019.

[47] Y. J. Jang, S. Jeong, and M. S. Lee, 'Initial energy logistics cost analysis for stationary, quasi-dynamic, and dynamic wireless charging public transportation systems', *Energies*, vol. 9, no. 7, p. 483, 2016.

[48] R. L. Vitale, 'Design and prototype development of a wireless power transmission system for a micro air vehicle (MAV)', PhD Thesis, Naval Postgraduate School, 1999.

[49] H. Liu, Q. Shao, and X. Fang, 'Modeling and optimization of class-E amplifier at subnominal condition in a wireless power transfer system for biomedical implants', *IEEE Trans. Biomed. Circuits Syst.*, vol. 11, no. 1, pp. 35–43, 2016.

[50] X. Li, C.-Y. Tsui, and W.-H. Ki, 'A 13.56 MHz wireless power transfer system with reconfigurable resonant regulating rectifier and wireless power control for implantable medical devices', *IEEE J. Solid-State Circuits*, vol. 50, no. 4, pp. 978–989, 2015.

[51] H. Zhang, F. Lu, H. Hofmann, W. Liu, and C. C. Mi, 'Six-plate capacitive coupler to reduce electric field emission in large air-gap capacitive power transfer', *IEEE Trans. Power Electron.*, vol. 33, no. 1, pp. 665–675, 2017.

[52] Q. Xu, D. Hu, B. Duan, and J. He, 'A fully implantable stimulator with wireless power and data transmission for experimental investigation of epidural spinal cord stimulation', *IEEE Trans. Neural Syst. Rehabil. Eng.*, vol. 23, no. 4, pp. 683–692, 2015.

[53] Y. Xu, Z. Huang, S. Yang, Z. Wang, B. Yang, and Y. Li, 'Modeling and characterization of capacitive coupling intrabody communication in an in-vehicle scenario', *Sensors*, vol. 19, no. 19, p. 4305, 2019.

[54] J. C. Schuder, 'High-level electromagnetic energy transfer through a closed chest wall', *IRE Internet Conv Rec*, vol. 9, pp. 119–126, 1961.

[55] G. Cochran, M. Johnson, M. Kadaba, F. Vosburgh, M. Ferguson-Pell, and V. Palmeiri, 'Piezoelectric internal fixation devices: A new approach to electrical augmentation of osteogenesis', *J. Orthop. Res.*, vol. 3, no. 4, pp. 508–513, 1985.

[56] N. Marati, A. K. Bhoi, D. Albuquerque, and A. Kalam, *AI Enabled IoT for Electrification and Connected Transportation*. Springer, 2022.

[57] U.-M. Jow and M. Ghovanloo, 'Modeling and optimization of printed spiral coils in air, saline, and muscle tissue environments', *IEEE Trans. Biomed. Circuits Syst.*, vol. 3, no. 5, pp. 339–347, 2009.

[58] M. M. Ahmadi and G. A. Jullien, 'A wireless-implantable microsystem for continuous blood glucose monitoring', *IEEE Trans. Biomed. Circuits Syst.*, vol. 3, no. 3, pp. 169–180, 2009.

[59] S. O'Driscoll, A. S. Poon, and T. H. Meng, 'A mm-sized implantable power receiver with adaptive link compensation', in *2009 IEEE International Solid-State Circuits Conference-Digest of Technical Papers*, IEEE, 2009, pp. 294–295.

[60] M. Yin and M. Ghovanloo, 'A flexible clockless 32-ch simultaneous wireless neural recording system with adjustable resolution', in *2009 IEEE international solid-state circuits conference-digest of technical papers*, IEEE, 2009, pp. 432–433.

[61] U.-M. Jow and M. Ghovanloo, 'Optimization of data coils in a multiband wireless link for neuroprosthetic implantable devices', *IEEE Trans. Biomed. Circuits Syst.*, vol. 4, no. 5, pp. 301–310, 2010.

[62] L. Andia, R.-F. Xue, K.-W. Cheng, and M. Je, 'Closed loop wireless power transmission for implantable medical devices', in *2011 International Symposium on Integrated Circuits*, IEEE, 2011, pp. 404–407.

[63] W. Wu and Q. Fang, 'Design and simulation of printed spiral coil used in wireless power transmission systems for implant medical devices', in *2011 Annual International Conference of the IEEE Engineering in Medicine and Biology Society*, IEEE, 2011, pp. 4018–4021.

[64] M. Zargham and P. G. Gulak, 'Maximum achievable efficiency in near-field coupled power-transfer systems', *IEEE Trans. Biomed. Circuits Syst.*, vol. 6, no. 3, pp. 228–245, 2012.

[65] S. Mutashar, M. A. Hannan, S. A. Samad, and A. Hussain, 'Analysis and optimization of spiral circular inductive coupling link for bio-implanted applications on air and within human tissue', *Sensors*, vol. 14, no. 7, pp. 11522–11541, 2014.

[66] O. Knecht, R. Bosshard, and J. W. Kolar, 'High-efficiency transcutaneous energy transfer for implantable mechanical heart support systems', *IEEE Trans. Power Electron.*, vol. 30, no. 11, pp. 6221–6236, 2015.

[67] S. Stöcklin, T. Volk, A. Yousaf, J. Albesa, and L. Reindl, 'Efficient inductive powering of brain implanted sensors', in *2015 IEEE Sensors Applications Symposium (SAS)*, IEEE, 2015, pp. 1–6.

[68] M. S. Heo, H. S. Moon, H. C. Kim, H. W. Park, Y. H. Lim, and S. H. Paek, 'Fully implantable deep brain stimulation system with wireless power transmission for long-term use in rodent models of parkinson's disease', *J. Korean Neurosurg. Soc.*, vol. 57, no. 3, p. 152, 2015.

[69] K. Yamaguchi, T. Hirata, and I. Hodaka, 'A general method to parameter optimization for highly efficient wireless power transfer', *Int. J. Electr. Comput. Eng.*, vol. 6, no. 6, p. 3217, 2016.

[70] S. Mehri, A. C. Ammari, J. Ben Hadj Slama, H. Rmili, and others, 'Geometry optimization approaches of inductively coupled printed spiral coils for remote powering of implantable biomedical sensors', *J. Sens.*, vol. 2016, 2016.

[71] P. Abiri *et al.*, 'Inductively powered wireless pacing via a miniature pacemaker and remote stimulation control system', *Sci. Rep.*, vol. 7, no. 1, p. 6180, 2017.

[72] T. Campi, S. Cruciani, V. De Santis, and M. Feliziani, 'EMF safety and thermal aspects in a pacemaker equipped with a wireless power transfer system working at low frequency', *IEEE Trans. Microw. Theory Tech.*, vol. 64, no. 2, pp. 375–382, 2016.

[73] S. H. Sung *et al.*, 'Flexible wireless powered drug delivery system for targeted administration on cerebral cortex', *Nano Energy*, vol. 51, pp. 102–112, 2018.

[74] J. Zhao, R. Ghannam, M. Yuan, H. Tam, M. Imran, and H. Heidari, 'Design, test and optimization of inductive coupled coils for implantable biomedical devices', *J. Low Power Electron.*, vol. 15, no. 1, pp. 76–86, 2019.

[75] Y. Palagani, K. Mohanarangam, J. H. Shim, and J. R. Choi, 'Wireless power transfer analysis of circular and spherical coils under misalignment conditions for biomedical implants', *Biosens. Bioelectron.*, vol. 141, p. 111283, 2019.

[76] A. Lakhdari, N.-E. M. Maaza, and M. Dekmous, 'Design and optimization of inductively coupled spiral square coils for bio-implantable micro-system device', *Int. J. Electr. Comput. Eng.*, vol. 9, no. 4, p. 2637, 2019.

[77] S. Bahrami, G. Moloudian, S. R. Miri-Rostami, and T. Björninen, 'Compact microstrip antennas with enhanced bandwidth for the implanted and external subsystems of a wireless retinal prosthesi', *IEEE Trans. Antennas Propag.*, vol. 69, no. 5, pp. 2969–2974, 2020.

[78] S. Çetin, Y. E. Demirci, and O. Büyükgümüş, 'Performance evaluation of a wireless charging converter for active implantable medical devices', *Mugla J. Sci. Technol.*, vol. 6, no. 2, pp. 11–17, 2020.

[79] N. Ha-Van, T. L. Vu, and M. T. Le, 'An efficient wireless power transfer for retinal prosthesis using artificial intelligent algorithm', in *2020 50th European Microwave Conference (EuMC)*, IEEE, 2021, pp. 1115–1118.

[80] A. I. Mahmood, S. K. Gharghan, M. A. Eldosoky, M. F. Mahmood, and A. M. Soliman, 'Wireless power transfer based on spider web–coil for biomedical implants', *IEEE Access*, vol. 9, pp. 167674–167686, 2021.

[81] A. Z. Zaki, T. G. Abouelnaga, E. K. Hamad, and H. A. Elsadek, 'Design of dual-band implanted patch antenna system for bio-medical applications', *J. Electr. Eng.*, vol. 72, no. 4, pp. 240–248, 2021.

[82] A. O. Kaka, M. Toycan, S. D. Walker, and D. Kavaz, 'Dual band, miniaturized, implantable antenna design with on-body antennas for wireless health monitoring', *Appl. Comput. Electromagn. Soc. J.*, vol. 35, no. 4, p. 443, 2020.

[83] J. Bao, S. Hu, Z. Xie, G. Hu, Y. Lu, and L. Zheng, 'Optimization of the coupling coefficient of the inductive link for wireless power transfer to biomedical implants', *Int. J. Antennas Propag.*, vol. 2022, pp. 1–12, 2022.

[84] T. P. van Nunen, R. M. Mestrom, and H. J. Visser, 'Wireless power transfer to biomedical implants using a class-e inverter and a Class-DE rectifier', *IEEE J. Electromagn. RF Microw. Med. Biol.*, 2023.

[85] S. R. Khan and G. Choi, 'Analysis and optimization of four-coil planar magnetically coupled printed spiral resonators', *Sensors*, vol. 16, no. 8, p. 1219, 2016.

[86] A. K. RamRakhyani and G. Lazzi, 'On the design of efficient multi-coil telemetry system for biomedical implants', *IEEE Trans. Biomed. Circuits Syst.*, vol. 7, no. 1, pp. 11–23, 2012.

[87] N. Korakianitis, G. A. Vokas, and G. Ioannides, 'Review of wireless power transfer (WPT) on electric vehicles (EVs) charging', in *AIP conference proceedings*, AIP Publishing, 2019.

[88] Z. Zhang and H. Pang, 'WPT for Low-Power Applications', 2023.

[89] S. R. Hui, 'Magnetic resonance for wireless power transfer', *IEEE Power Electron. Mag.*, vol. 3, no. 1, pp. 14–31, 2016.

[90] N. Kim, K. Kim, J. Choi, and C.-W. Kim, 'Adaptive frequency with power-level tracking system for efficient magnetic resonance wireless power transfer', *Electron. Lett.*, vol. 48, no. 8, pp. 452–454, 2012.

[91] S. Mekhilef, S. Faramarzi, R. Saidur, and Z. Salam, 'The application of solar technologies for sustainable development of agricultural sector', *Renew. Sustain. Energy Rev.*, vol. 18, pp. 583–594, 2013.

[92] A. Brecher, D. Arthur, and others, 'Review and evaluation of wireless power transfer (WPT) for electric transit applications', 2014.

[93] K. Kadem, 'Modélisation et optimisation d'un coupleur magnétique pour la recharge par induction dynamique des véhicules électriques', PhD Thesis, Université Paris-Saclay, 2020.

[94] A. Karalis, J. D. Joannopoulos, and M. Soljačić, 'Efficient wireless non-radiative mid-range energy transfer', *Ann. Phys.*, vol. 323, no. 1, pp. 34–48, 2008.

[95] N. Shinohara, 'Power without wires', *IEEE Microw. Mag.*, vol. 12, no. 7, pp. S64–S73, 2011.

[96] G. Rituraj, E. R. Joy, B. K. Kushwaha, and P. Kumar, 'Analysis and comparison of series-series and series-parallel topology of contactless power transfer systems', in *TENCON 2014-2014 IEEE Region 10 Conference*, IEEE, 2014, pp. 1–6.

[97] M. Abou Houran, X. Yang, and W. Chen, 'Magnetically coupled resonance WPT: Review of compensation topologies, resonator structures with misalignment, and EMI diagnostics', *Electronics*, vol. 7, no. 11, p. 296, 2018.

[98] M. Bouklachi, M. Biancheri-Astier, A. Diet, and Y. Le Bihan, 'HF coils design and shielding for a medical monitoring patch', 2018.

[99] P.-A. Gori, 'Transmission dynamique d'énergie par induction: application au véhicule électrique', PhD Thesis, Université Paris Saclay (COmUE), 2019.

[100] R. Bosshard, J. W. Kolar, and B. Wunsch, 'Accurate finite-element modeling and experimental verification of inductive power transfer coil design', in *2014 IEEE Applied Power Electronics Conference and Exposition-APEC 2014*, IEEE, 2014, pp. 1648–1653.

[101] H. Movagharnejad and A. Mertens, 'Design metrics of compensation methods for contactless charging of electric vehicles', in *2017 19th European Conference on Power Electronics and Applications (EPE'17 ECCE Europe)*, IEEE, 2017, p. P-1.

[102] E. G. Kilinc, C. Dehollain, and F. Maloberti, 'Design and optimization of inductive power transmission for implantable sensor system', in *2010 XIth international workshop on symbolic and numerical methods, modeling and applications to circuit design (SM2ACD)*, IEEE, 2010, pp. 1–5.

[103] L. Pichon, 'Electromagnetic analysis and simulation aspects of wireless power transfer in the domain of inductive power transmission technology', *J. Electromagn. Waves Appl.*, vol. 34, no. 13, pp. 1719–1755, 2020.

[104] M. R. Pahlavani and A. Shiri, 'Impact of dimensional parameters on mutual inductance of individual toroidal coils using analytical and finite element methods applicable to tokamak reactors', *Prog. Electromagn. Res. B*, vol. 24, pp. 63–78, 2010.

[105] A. Khaligh and S. Dusmez, 'Comprehensive topological analysis of conductive and inductive charging solutions for plug-in electric vehicles', *IEEE Trans. Veh. Technol.*, vol. 61, no. 8, pp. 3475–3489, 2012.

[106] W. Zhang and C. C. Mi, 'Compensation topologies of high-power wireless power transfer systems', *IEEE Trans. Veh. Technol.*, vol. 65, no. 6, pp. 4768–4778, 2015.

[107] R. R. Harrison, 'Designing efficient inductive power links for implantable devices', in *2007 IEEE International Symposium on Circuits and Systems*, IEEE, 2007, pp. 2080–2083.

[108] H. Ali, T. J. Ahmad, and S. A. Khan, 'Inductive link design for medical implants', in *2009 IEEE Symposium on Industrial Electronics & Applications*, IEEE, 2009, pp. 694–699.

[109] S. R. Khan, S. K. Pavuluri, and M. P. Desmulliez, 'Accurate modeling of coil inductance for near-field wireless power transfer', *IEEE Trans. Microw. Theory Tech.*, vol. 66, no. 9, pp. 4158–4169, 2018.

[110] C. Jiang, K. Chau, C. Liu, and C. H. Lee, 'An overview of resonant circuits for wireless power transfer', *Energies*, vol. 10, no. 7, p. 894, 2017.

[111] B. Fatima, B. Aimad, and N. Fares, 'Iterative Method Based Optimization of Wireless Power Transfer for Biomedical Implants', in *2023 International Conference on Advances in Electronics, Control and Communication Systems (ICAECCS)*, IEEE, 2023, pp. 1–6.

[112] 居村岳広, 'Wireless Power Transfer: Using Magnetic and Electric Resonance Coupling Techniques', *No Title*.

[113] M. Benzi and A. J. Wathen, 'Some preconditioning techniques for saddle point problems', *Model Order Reduct. Theory Res. Asp. Appl.*, pp. 195–211, 2008.

[114] A. Lambora, K. Gupta, and K. Chopra, 'Genetic algorithm-A literature review', in *2019 international conference on machine learning, big data, cloud and parallel computing (COMITCon)*, IEEE, 2019, pp. 380–384.

[115] O. Kramer and O. Kramer, *Genetic algorithms*. Springer, 2017.

[116] S. Mirjalili and S. Mirjalili, 'Genetic algorithm', *Evol. Algorithms Neural Netw. Theory Appl.*, pp. 43–55, 2019.

[117] J. Pierezan and L. D. S. Coelho, 'Coyote optimization algorithm: a new metaheuristic for global optimization problems', in *2018 IEEE congress on evolutionary computation (CEC)*, IEEE, 2018, pp. 1–8.

[118] V. J. Chin and Z. Salam, 'Coyote optimization algorithm for the parameter extraction of photovoltaic cells', *Sol. Energy*, vol. 194, pp. 656–670, 2019.

[119] H. H. Mostafa and A. M. Ibrahim, 'Performance investigation for tracking GMPP of photovoltaic system under partial shading condition using coyote algorithm', in *2019 21st International Middle East Power Systems Conference (MEPCON)*, IEEE, 2019, pp. 34–40.

[120] R. Venkatasatish and D. Chittathuru, 'Coyote Optimization Algorithm-Based Energy Management Strategy for Fuel Cell Hybrid Power Systems', *Sustainability*, vol. 15, no. 12, p. 9638, 2023.

[121] P. H. Winston, *Artificial intelligence*. Addison-Wesley Longman Publishing Co., Inc., 1984.

[122] A. Rehman and T. Saba, 'Evaluation of artificial intelligent techniques to secure information in enterprises', *Artif. Intell. Rev.*, vol. 42, pp. 1029–1044, 2014.

[123] M. O. Mendonça, S. L. Netto, P. S. Diniz, and S. Theodoridis, 'machine learning: Review and trends', *Signal Process. Mach. Learn. Theory*, pp. 869–959, 2024.

[124] I. M. Hassoon and S. A. Hantoosh, 'EDIBLE FISH IDENTIFICATION BASED ON MACHINE LEARNING', *Iraqi J. Comput. Inform.*, vol. 49, no. 2, pp. 62–72, 2023.

[125] Y. Meraihi, A. B. Gabis, S. Mirjalili, A. Ramdane-Cherif, and F. E. Alsaadi, 'Machine learning-based research for COVID-19 detection, diagnosis, and prediction: a survey', *SN Comput. Sci.*, vol. 3, no. 4, p. 286, 2022.

[126] K. Anwar, J. Siddiqui, and S. Saquib Sohail, 'Machine learning techniques for book recommendation: an overview', in *Proceedings of International Conference on Sustainable Computing in Science, Technology and Management (SUSCOM), Amity University Rajasthan, Jaipur-India*, 2019.

[127] Z. Ding, Y. Huang, H. Yuan, and H. Dong, 'Introduction to reinforcement learning', *Deep Reinf. Learn. Fundam. Res. Appl.*, pp. 47–123, 2020.

[128] K. Gurney, *An introduction to neural networks*. CRC press, 2018.

[129] Y. Lyu, Y. Niu, T. He, L. Shu, M. Zhuravkov, and S. Zhou, 'An Efficient Method for the Inverse Design of Thin-Wall Stiffened Structure Based on the Machine Learning Technique', *Aerospace*, vol. 10, no. 9, p. 761, 2023.

[130] L. Xu and Q. Yang, 'Deep electron cloud-activity and field-activity relationships', *J. Chemom.*, vol. 37, no. 8, p. e3503, 2023.

[131] S. Chim, J.-G. Lee, and H.-H. Park, 'Dilated skip convolution for facial landmark detection', *Sensors*, vol. 19, no. 24, p. 5350, 2019.

[132] Y. Wu and J. Feng, 'Development and application of artificial neural network', *Wirel. Pers. Commun.*, vol. 102, pp. 1645–1656, 2018.

[133] J. D. Kelleher, *Deep learning*. MIT press, 2019.

[134] G. Patra *et al.*, 'Deep learning methods for scientific and industrial research', in *Handbook of Statistics*, vol. 48, Elsevier, 2023, pp. 107–168.

[135] P. Sharma, 'Deep Learning and Neural Networks: Methods', 2023. doi: 10.59646/csebookc7/004.

[136] S. Badillo *et al.*, 'An introduction to machine learning', *Clin. Pharmacol. Ther.*, vol. 107, no. 4, pp. 871–885, 2020.

[137] Y. Huang, C.-Y. Huang, X. Li, and K. Li, 'A dataset auditing method for collaboratively trained machine learning models', *IEEE Trans. Med. Imaging*, 2022.

[138] K. Worden, G. Tsialiamanis, E. Cross, and T. Rogers, 'Artificial neural networks', in *Machine Learning in Modeling and Simulation: Methods and Applications*, Springer, 2023, pp. 85–119.

[139] Z.-H. Zhou, *Machine learning*. Springer nature, 2021.

[140] C. S. Nwankwo, M. K. Raji, and E. S. Oghogho, 'Application of data analytics techniques in analyzing crimes', 2018.

[141] D. W. Hosmer Jr, S. Lemeshow, and R. X. Sturdivant, *Applied logistic regression*. John Wiley & Sons, 2013.

[142] S. Suthaharan and S. Suthaharan, 'Decision tree learning', *Mach. Learn. Models Algorithms Big Data Classif. Think. Ex. Eff. Learn.*, pp. 237–269, 2016.

[143] S. J. Rigatti, 'Random forest', *J. Insur. Med.*, vol. 47, no. 1, pp. 31–39, 2017.

[144] A. Mammone, M. Turchi, and N. Cristianini, 'Support vector machines', *Wiley Interdiscip. Rev. Comput. Stat.*, vol. 1, no. 3, pp. 283–289, 2009.

[145] C. C. Aggarwal and others, *Neural networks and deep learning*, vol. 10. Springer, 2018.

[146] S. Ray, 'A quick review of machine learning algorithms', in *2019 International conference on machine learning, big data, cloud and parallel computing (COMITCon)*, IEEE, 2019, pp. 35–39.

[147] S. Cao, L. Wossnig, B. Vlastakis, P. Leek, and E. Grant, 'Cost-function embedding and dataset encoding for machine learning with parametrized quantum circuits', *Phys. Rev. A*, vol. 101, no. 5, p. 052309, 2020.

[148] S. Fu, Y. Tian, J. Tang, and X. Liu, 'Cost-sensitive learning with modified Stein loss function', *Neurocomputing*, vol. 525, pp. 57–75, 2023.

[149] F. Richoux and J.-F. Baffier, 'Automatic error function learning with interpretable compositional networks', *Ann. Math. Artif. Intell.*, pp. 1–29, 2023.

[150] A. Irie, K. Shimamura, A. Koura, and F. Shimojo, 'Importance of Adjusting Coefficients in Cost Function for Construction of High-Accuracy Machine-Learning Interatomic Potential', *J. Phys. Soc. Jpn.*, vol. 91, no. 4, p. 045002, 2022.

[151] K. Hsu, H. V. Gupta, and S. Sorooshian, 'Artificial neural network modeling of the rainfall-runoff process', *Water Resour. Res.*, vol. 31, no. 10, pp. 2517–2530, 1995.

[152] H. Demuth, M. Beale, and M. Hagan, 'Neural Network Toolbox (MATLAB), version 6, The MathWorks'. Inc, 2008.

[153] L. He, S. Zhao, X. Wang, and C.-K. Lee, 'Artificial neural network-based parameter identification method for wireless power transfer systems', *Electronics*, vol. 11, no. 9, p. 1415, 2022.

[154] F. Bennia, A. Boudouda, and F. Nafa, 'Optimal design of wireless power transfer coils for biomedical implants using machine learning and meta-heuristic algorithms', *Electr. Eng.*, pp. 1–16, 2024.